INFORMATION TO USERS

This manuscript has been reproduced from the microfilm master. UMI films the text directly from the original or copy submitted. Thus, some thesis and dissertation copies are in typewriter face, while others may be from any type of computer printer.

The quality of this reproduction is dependent upon the quality of the copy submitted. Broken or indistinct print, colored or poor quality illustrations and photographs, print bleedthrough, substandard margins, and improper alignment can adversely affect reproduction.

In the unlikely event that the author did not send UMI a complete manuscript and there are missing pages, these will be noted. Also, if unauthorized copyright material had to be removed, a note will indicate the deletion.

Oversize materials (e.g., maps, drawings, charts) are reproduced by sectioning the original, beginning at the upper left-hand corner and continuing from left to right in equal sections with small overlaps.

Photographs included in the original manuscript have been reproduced xerographically in this copy. Higher quality 6" x 9" black and white photographic prints are available for any photographs or illustrations appearing in this copy for an additional charge. Contact UMI directly to order.

UMI®

University of Alberta

Wake-Stabilized Diffusion Flames in Crossflow:

Application to the Efficiencies of Gas Flares

by

Matthew R. Johnson   ©

A thesis submitted to the Faculty of Graduate Studies and Research in partial fulfillment

of the requirements for the degree Doctor of Philosophy

Department of Mechanical Engineering

Edmonton, Alberta

Fall 2001

The author has granted a non-exclusive licence allowing the National Library of Canada to reproduce, loan, distribute or sell copies of this thesis in microform, paper or electronic formats.

The author retains ownership of the copyright in this thesis. Neither the thesis nor substantial extracts from it may be printed or otherwise reproduced without the author's permission.

L'auteur a accordé une licence non exclusive permettant à la Bibliothèque nationale du Canada de reproduire, prêter, distribuer ou vendre des copies de cette thèse sous la forme de microfiche/film, de reproduction sur papier ou sur format électronique.

L'auteur conserve la propriété du droit d'auteur qui protège cette thèse. Ni la thèse ni des extraits substantiels de celle-ci ne doivent être imprimés ou autrement reproduits sans son autorisation.

0-612-68950-6

Canada

University of Alberta

Library Release Form

Name of Author: Matthew R. Johnson

Title of Thesis: Wake-Stabilized Diffusion Flames in Crossflow:
Application to the Efficiencies of Gas Flares

Degree: Doctor of Philosophy

Year the Degree Granted: 2001

Permission is hereby granted to the University of Alberta Library to reproduce single copies of this thesis and to lend or sell such copies for private, scholarly or scientific purposes only.

The author reserves all other publication and other rights in association with the copyright in the thesis, and except as herein before provided, neither the thesis nor any substantial portion thereof may be printed or otherwise reproduced in any material form whatever without the author's prior written permission.

Matthew Johnson
#406, 11007-83 Avenue
Edmonton, Alberta
Canada   T6G 0T9

June 29, 2001

There is an art to science, and a science in art; the two are not enemies, but different

aspects of the whole.

Isaac Asimov (1920 - 1992)

That which we call sin in others, is experiment for us.

Ralph Waldo Emerson (1803 - 1882)

University of Alberta

Faculty of Graduate Studies and Research

The undersigned certify that they have read, and recommend to the Faculty of Graduate Studies and Research for acceptance, a thesis entitled Wake-Stabilized Diffusion Flames in Crossflow: Application to the Efficiencies of Gas Flares submitted by Matthew R. Johnson in partial fulfillment of the requirements for the degree of Doctor of Philosophy.

Larry W. Kostiuk

David J. Wilson

Robert K. Cheng

Warren B. Kindzierski

Brian A. Fleck

Date: JUNE 14, 2001

Abstract

This thesis presents a detailed experimental investigation of wake-stabilized diffusion flames in crosswind, which are fundamental to the applied problems of solution gas flaring. With over 1.4 billion m^3 of solution gas being flared and vented in Alberta annually and much more being flared worldwide, the relevance of this research is clear. To overcome the significant problems associated with studying emissions of open diffusion flames in a crosswind, a new measurement technique was developed. Flames were established at the exit of a burner tube that was mounted vertically in the test section of a closed-loop wind tunnel. The accumulation rates of the major carbon containing species in the products of combustion were tracked experimentally and used to calculate the carbon conversion efficiency. Efficiency measurements were conducted for a variety of different fuel types, stack diameters, and wind speeds. The results show that for any given fuel, increased crosswind speed (U_∞) adversely affects the conversion efficiency, while increased jet exit velocity (V_j) makes the flame less susceptible to the effects of crosswind. Consideration of buoyancy and momentum forces as defined by a Richardson Number successfully predicted the velocity dependency of the conversion inefficiency as being $U_\infty / V_j^{1/3}$ and correlated data for each of the fuels. Further experiments examined the importance of burner diameter, fuel composition and energy density, and ambient turbulence. Lowering the energy density of the fuel was found to have a profound, adverse effect on the measured inefficiency and results of this work have led to a change in the regulations governing flaring in the province of Alberta. Correlations for this effect have been found. Analysis of the combustion products showed that the

inefficiencies are primarily in the form of unburned hydrocarbons along with some carbon monoxide and not pyrolitic compounds. Photographic data shows a link between the flame burning in detached pockets and the measured inefficiencies. These results suggested that the observed inefficiencies could be a result of "fuel stripping" from the fuel jet before any combustion. Measurements with a single point fast flame ionization detector verified this hypothesis and showed that unburned fuel was ejected beneath the flame in highly intermittent and spatially variable bursts. Based on these results, a new fuel stripping mechanism for the inefficiencies of wake-stabilized diffusion flames in crossflow has been proposed.

Preface

This thesis is written in the paper-based format outlined by the Faculty of Graduate Studies and Research at the University of Alberta. Each of the Chapters 1, 2, 3, and 5 and sections of Chapter 4 have been published or have been submitted for publication in refereed journals. Chapter 1 provides an overview of solution gas flaring in Alberta, which is the practical problem motivating this research. Solution gas flares are described in detail and the concept of an efficiency to characterize combustion completion is introduced. The large variability among individual flare installations highlights the need to create a general understanding of these flows. Chapter 2 presents a detailed methodology that was developed to measure the carbon conversion efficiencies of diffusion flames in crosswind. The methodology uses a closed-loop wind tunnel, which was modified extensively to facilitate this research. Additional details of the efficiency measurements are described in Appendix A.

Chapter 3 presents detailed results of experimental measurements of the efficiency of low-momentum jet diffusion flames in crosswind. Several new results are described and consistent trends in the data are readily apparent. Initial attempts to correlate this data are presented which are successful is describing velocity dependencies of the flow. Chapter 4 is a detailed investigation of the parameters that affect the conversion efficiency of these wake-stabilized diffusion flames in crosswind. This chapter presents data from a variety of different experiments that highlight the complexity of the problem. Questions raised in this chapter point to the need to understand the mechanism responsible for the

measured inefficiencies of the flames. Chapter 5 presents data from a detailed series of experiments designed to determine the origins of the measured inefficiencies noted in chapters 3 and 4. The data show that the inefficiencies are due to the stripping of unburned fuel from the reaction zone by coherent structures in the flow field.

Acknowledgements

Anyone who has written a Ph.D. thesis, or who has seen someone through the years it requires to complete, knows that the realization of a Ph.D. is a long process that would not be possible without the assistance of others. I have been very fortunate to have had strong support of many people during the course of my research and for that I am very grateful.

Several people deserve special recognition for their invaluable contributions to my work. I wish to thank my supervisor Dr. Larry Kostiuk who, from the time I started my Ph.D., treated me as a research colleague and empowered me to pursue my own ideas while providing continual ideas, input, support, and supervision in a manner that could only be described as exemplary. I am also very grateful to my co-supervisor Dr. David Wilson whose knowledge and experience were invaluable resources and who in his role as a mentor has helped influence my career.

I am grateful for the assistance and input of Mr. Mark Ackerman whose experimental expertise was very valuable especially in the early stages of my work. The input of Drs. Doug Dale and David Checkel was also appreciated. Like all of the members of the Combustion and Environment Research Group, their cooperation and opinions were important resources. Although not officially connected with my research, Dr. Lorenz Sigurdson also deserves special mention for his enthusiastic input and advice with the finer aspects of vortex dynamics and coherent flow structures. The contributions of Dr.

Eric Bourguignon were also very much appreciated. As a post-doctoral fellow in our laboratory he shared in the development of the methodology that was ultimately used to measure combustion efficiency.

In the design and construction of the Combustion Windtunnel facility, several people made significant contributions. I am particularly indebted to Mr. Terry Nord for his meticulous work in building electronic circuits for various experimental apparatus. George Skinner shared in the struggles of constructing and installing numerous pieces of experimental apparatus and left behind many stories that have kept me amused during the long hours in the lab! The technical staff in the department of mechanical engineering also deserve recognition for their significant efforts in helping to redesign and construct the facility and its innumerable mechanical components.

I am particularly thankful for the assistance of my friends and colleagues on the Flare Research Project: Pascal Poudenx, Rob Prybysh, Glen Thomas, and Oleg Zastavniuk. In my capacity as a project engineer for the facility, I relied on these people on a daily basis to help keep experiments running and to continually redesign and reconfigure the facility for new experiments. Moreover, their willingness to help and their patience with my sometimes perfectionist ideals had a direct contribution to the success of my research.

Jim Spangelo of the Alberta Energy and Utilities board also deserves special mention. His assistance in providing background information on flaring in Alberta was especially helpful. As well, I would like to acknowledge the assistance of Jason Nichols, who as a

summer student in the lab spent many boring hours watching over somewhat tedious experiments for me.

During my tenure as a Ph.D. student, I was very fortunate to have had financial support in the form of scholarships from the Killam Trusts, the Natural Sciences and Engineering Research Council (NSERC), Luscar Ltd., Petro-Canada, and the Association of Professional Engineers Geologists and Geophysicists of Alberta (APEGGA). I am very grateful for the generosity of these organizations.

On a more personal note, I wish to thank Pat, Cheryl, Andrea, Cathy, Jeff, and Steve who have made sure I enjoyed life beyond the confines of my lab. In big ways and small ways they all contributed to my success and I am privileged to call them friends. I would be remiss if I did not also thank my friends in *Ensemble de la Rue*, who in pushing me to achieve new artistic heights never let me forget the big picture.

Finally, I would like to thank my parents who have supported me always.

Thank you all.

Table of Contents

CHAPTER 3

EFFICIENCIES OF LOW MOMENTUM JET DIFFUSION FLAMES IN

CROSSWINDS 70

CHAPTER 4

AN INVESTIGATION OF PARAMETERS THAT AFFECT CONVERSION EFFICIENCY OF WAKE-STABILIZED DIFFUSION FLAMES 100

List of Tables

List of Figures

List of Plates

Nomenclature

a, b, c, d	stoichiometric constants
A, B, C, etc.	arbitrary constants
A/D	analogue to digital
AEUB	Alberta Energy and Utilities Board
Avg. Vol.	average volume flared or vented monthly
C1, C2, C3, etc.	hydrocarbons with 1, 2, or 3 carbon atoms in each molecule
C7+	hydrocarbons with 7 or more carbon atoms in each molecule
C_2H_6	ethane
C_3H_8	propane
C_mH_n	mean composition of hydrocarbons in combustion products
CO	carbon monoxide
CO_2	carbon dioxide
C_xH_y	mean composition of unburned hydrocarbons
d_i	inner diameter of the burner tube
d_o	outer diameter of the burner tube (stack)
Dev. of Max.	deviation of the maximum from the mean in percent
DIAL	Differential Absorption Light
FFID	fast flame ionization detector
FTIR	Fourier Trasform Infra-Red
g	gravitational constant
GOR	gas / oil ratio

H_2S	hydrogen sulphide
HC	unburned hydrocarbons
HHV	higher heating value
I.D.	inner diameter
L	characteristic length
LDV	Laser Doppler Velocimeter
LHV	lower heating value
LHV_{mass}	lower heating value calculated on a mass basis
m	average number of carbon atoms in hydrocarbon molecule in products
$\dot{m}$	mass flow rate
$\dot{m}_f$	mass flow rate of fuel
M	molecular weight (kg/kmol)
Max. Vol.	maximum volume flared or vented in a month
N_2	nitrogen
$\dot{n}$	molar flow rate
O.D.	outer diameter
O_2	oxygen
P	pressure
$P(U_\infty)$	probability distribution of crosswind velocity in presence of ambient turbulence
PPM	parts per million
q_o	volume flow rate at the source
$Q_{combust}$	volume flow rate of air consumed by the flare for combustion

$Q_{emitted}$	volume flow rate of combustion products emitted by the flare
Q_{fuel}	volume flow rate of fuel entering the flare stack
Q'_{fuel}	volume flow rate of gaseous fuel entering the flare stack
$\overset{\cdot}{Q}_{fuel}$	volume flow rate of liquid fuel entering the flare stack
Q_{flare}	volume flow rate of gas entering the flare stack
Q_{in}	volume flow rate of air leaking into the wind tunnel
Q_{inert}	volume flow rate of inert compounds entering the flare stack
Q_{out}	volume flow rate of air leaking out of the wind tunnel
R	momentum flux ratio, $R = \dfrac{\rho_j V_j^2}{\rho_\infty U_\infty^2}$
R_{source}	radius of the source
R_{plume}	radius of the plume
r.m.s.	root mean square
Re	Reynolds number
Ri	Richardson number
SF_6	sulpher hexafluoride
slpm	standard litres per minute
SO_2	sulpher dioxide
St	Strouhal number
$\overline{St}$	mean Strouhal number
St. Dev.	standard deviation
T	temperature
T_{max}	maximum temperature in the plume

T_∞	ambient temperature
t	time
t'	time when the concentrations of accumulated species in the wind tunnel are near zero
t_{exp}	exposure time
t_o	time at start of efficiency experiement
$\overline{t_s}$	mean peak spacing
Tot. Vol.	total volume flared or vented in a year
U_∞	velocity of crossflowing air
$\overline{U_\infty}$	mean velocity of crossflowing air (relevant to turbulent crosswind)
V	volume of the wind tunnel
V_j	exit velocity of the flare gas
V_{flare}	exit velocity of the flare gas
X	mole fraction divided by absolute temperature
X_{CO_2}	mole fraction of CO_2 divided by absolute temperature
X_L	ratio of mass flow rates of liquids to gases in the flare stream
x	average number of carbon atoms in hydrocarbon molecule
x	x-axis (streamwise direction)
Y	mole fraction
y	y-axis (vertical direction)
z	z-axis (horizontal crosstream direction)
α	fractional split of carbon in CO versus CO + CO_2
γ'	ratio of gaseous moles of products to gaseous moles of fuel

γ''	ratio of liquid moles of products to liquid moles of fuel
η	carbon conversion efficiency
η_T	calculated carbon conversion efficiency in turbulent crosswind
$(1-\eta)$	carbon conversion inefficiency
ρ_∞	density of ambient air
$\Delta\rho$	difference between the density of the plume and density of ambient air
$\Delta\rho_o$	difference between the density of the plume and density of ambient air at source location
ρ_j	density of the fuel jet
$\dfrac{\rho''_{fuel,l}}{\rho''_{fuel,g}}$	ratio of density change when of liquid fuel evaporates
x	standard deviation
$[i]$	concentration of species i
'	denotes gas
''	denotes liquid

CHAPTER 1

A CHARACTERIZATION OF SOLUTION GAS FLARING

IN ALBERTA

A version of this chapter has been accepted for publication as

Johnson, M.R., Spangelo, J.L., and Kostiuk, L.W., Journal of the Air &

Waste Management Association, 2001, in press.

This paper was co-authored by myself, Jim Spangelo of the Alberta
Energy and Utilities Board (AEUB), and one of my supervisors. The data
used for this paper were the property of the AEUB, which is the
government agency that regulates flaring activities in the province of
Alberta. The creation of the database, data analysis, and writing of the
manuscript were principally my work. Jim Spangelo provided access to
raw data files for my analysis and was extremely helpful in providing
background information about upstream oil and gas activities to allow me
to properly interpret the data.

1.1 INTRODUCTION

Flaring is the process of disposing of unwanted flammable gases and vapours by burning

them in a flame in the open atmosphere. In a typical flare, air and fuel are not premixed

and the combustion occurs as a turbulent diffusion flame in a crosswind. The purpose of

a flare is to consume flammable gases and vapours in a safe, reliable, and efficient

1

manner while converting them through oxidation to a more desirable emission than simply venting the gases to the atmosphere. Flaring is used extensively in the energy and petrochemical industries. Worldwide, it is estimated that 101.9 billion cubic meters of gas were flared or vented in 1997. [1]

Many different designs and strategies for flaring have been developed to meet the widely different purposes and operating conditions that industry requires. In the petroleum industry flaring can be roughly categorized under one of three broad headings: emergency flaring, process flaring, and production flaring. Emergency flaring typically occurs at large facilities such as refineries and gas plants where the primary concern is for the safety of the plant personnel and protection of the plant infrastructure. When an emergency situation arises such as a fire, compressor failure, valve rupture, etc., large volumes of flammable gas may have to be disposed of in a matter of seconds. Under these conditions, flow rates of gas through a flare can be very high and exit velocities may approach sonic speed.

Process flaring may also occur at refineries, sour gas plants, and petrochemical plants. At these facilities, gases that leak past relief valves are shunted to a process flare for disposal. Unlike emergency flares, process flares burn almost continuously at relatively low flow rates. However, during startup and shutdown or during the evacuation or blowdown of process units, gas flow rates can be significantly higher. An excellent overview of process and emergency flaring is provided in Jones [2]. Brzustowski [3] discusses some of the technology applied to larger flares and reviews the various criteria used in the design of flares specifically with respect to flame shape and length.

2

Production flaring is a broad heading in itself and refers to all types of flaring that occur in various levels of the upstream petroleum industry during the production of oil and gas fields. Within this category, flares can vary significantly. During the initial development of a gas well, gas may be flared at very high flow rates for a period of a few days in what is known as well testing. Well test flares may be of comparable size to the emergency flares previously described. However unlike process and emergency flares, in most cases well test flares do not have significant engineering provisions for smoke suppression or enhanced flame stability.

Significant flaring can also occur during the initial development of an oil well when all associated gas may be flared for a period of time until the gas is "conserved". Within this context, "conserved" means the gases are collected and processed later to sales grade natural gas or used for fuel at the battery site. If gas volumes are uneconomical to conserve, all of the gas produced may continue to be flared for the life of the well. Typically, these continuous flares involve relatively low gas flow rates and subsequently low exit velocities compared to well test or emergency type flares. The primary contributor to continuous gas flaring in the upstream oil and gas industry is solution gas flaring which is the main interest of the paper.

1.1.1 Solution Gas Flares

The term "solution gas" is used to refer to the collection of gases that come out of solution when conventional and heavy oil is extracted from high pressure reservoir conditions and reduced to near atmospheric pressure. Once brought to the surface, the oil is separated from any associated water and solution gas at a facility known as an oil battery. At the battery site the oil is temporarily stored before being processed further. The water is re-injected into the reservoir of origin and the gases may be flared, vented, or conserved. To provide information on the scale of flaring and venting in Alberta, some overall volumes are presented below. Solution gas volumes referred to in this paper are gas volumes produced from oil or bitumen batteries. The origins of these data are discussed later in the paper when a more detailed analysis is provided.

In 1999, 94 % of the 23.7 billion m^3 of solution gas produced in Alberta was conserved, while the remainder was flared or vented. Figure 1.1 shows a breakdown of the total volumes of gas flared and vented in various sectors of the upstream oil and gas industry in Alberta. Specific amounts of flaring and venting in each sector are shown in Figure 1.2. In total 2.01 billion m^3 of gas were flared and vented in 1999. Of that total, 71 % (1.42 billion m^3) was flared and vented as solution gas at oil and bitumen batteries. Thus, solution gas flaring is the most significant contributor to flaring and venting in the upstream petroleum industry in Alberta. The sheer volume of solution gas being disposed of makes it a significant concern to industry, regulators, and the public.

4
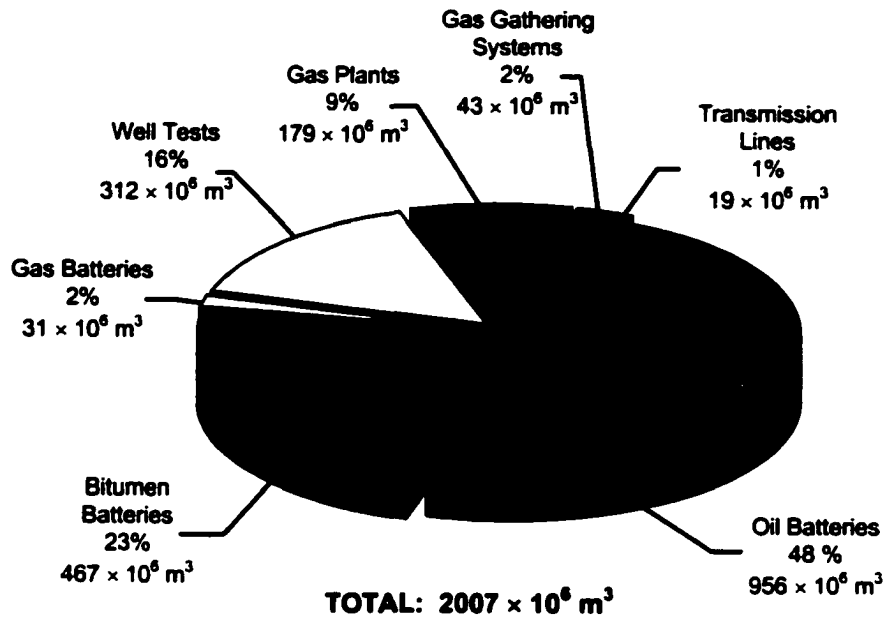
Figure 1.1: Volumes of gas flared and vented in Alberta in various sectors of the upstream oil and gas industry in 1999
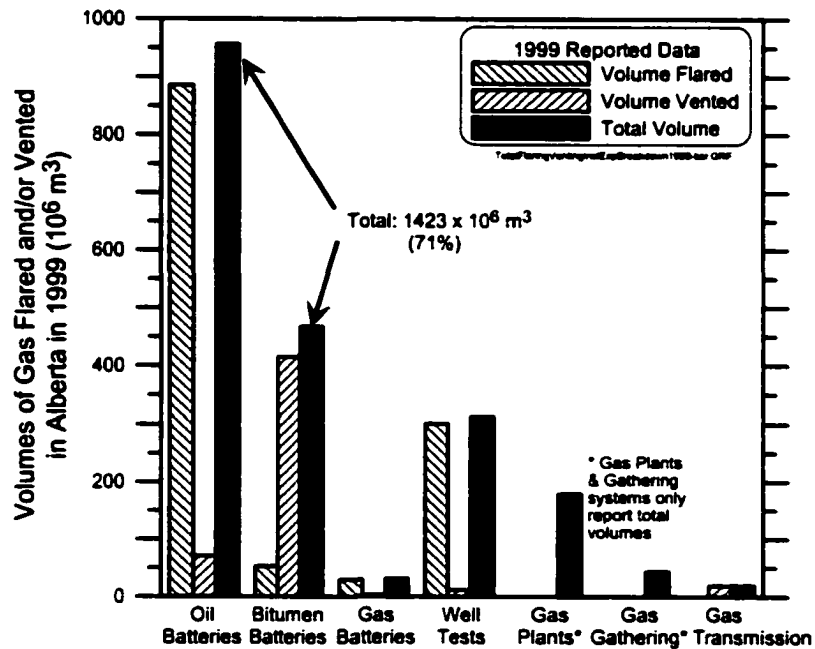
Figure 1.2: Relative amounts of gas flared and vented in various sectors of the upstream oil and gas industry in Alberta in 1999

5

Why is solution gas flared? In Alberta, the choice of whether to conserve or flare the solution gas at any particular battery site is part of the flare management framework administered by the Alberta Energy and Utilities Board (AEUB) [4]. At any given site, there are several reasons why flammable gases and liquids may be flared or vented and not conserved. These include: safety; high, low or intermittent gas flow; low energy density of the gas (low heating value); presence of hydrogen sulphide (H_2S) or other contaminants in the gas; proximity to available infrastructure; and economics. A recent study by Holford and Hettiaratchi [5] considered simple economics of six potential alternatives to solution gas flaring. These were: Low Pressure Gas Collection (clustering), Electrical Generation using Gas Turbines or Reciprocating Engines, Electrical Generation using "Mini-Turbines", Cogeneration, Re-injection of Gas with Produced Water, Oxidation (biological and physical), and collection and processing. Although potential economic reductions were identified at sites with large flare volumes, several significant barriers to implementation were also identified. Included among these barriers was the quality of available field data for making economic assessments. Successful implementation of any strategy to reduce flaring or to improve the performance of existing flares relies on accurate basic information with which a strategy can be developed. One of the goals of this paper is to better characterize solution gas flaring to aid in the improved management of solution gas flaring in Alberta.

1.1.2 Environmental Issues of Flaring and Venting

Environmental issues of gas flaring are generally described in terms of efficiency and emissions. The flare efficiency is a measure of the effectiveness of the combustion

6

process in fully oxidizing the fuel. In a typical solution gas stream, two different efficiencies may be relevant: the carbon conversion efficiency (also known as the combustion efficiency), which measures the ability of the flare to fully convert all hydrocarbons to carbon dioxide (CO_2); and the sulphur conversion efficiency, which measures a flares ability to convert H_2S to sulphur dioxide (SO_2). When inefficiencies occur, unburned fuel, carbon monoxide and other products of incomplete combustion (e.g., soot, volatile organic compounds, etc.) are emitted into the atmosphere. In the case of venting, both the carbon and sulphur based efficiencies drop to zero since none of the fuel is being converted to CO_2 or SO_2. If the flare stream contains methane, the unburned fuel represents an increase in greenhouse gas emissions since the global warming potential of methane is 21 times greater than that of CO_2 by mass [6] (7.7 times greater by volume). If the flare gas contains H_2S, any unburned fuel emissions are potentially toxic. As well, any combustion device that emits products of incomplete combustion can raise health concerns for animals and people.

1.2   DATA REPORTING

1.2.1   Gas Volume Data

In Alberta, operators of oil and gas batteries are required to complete production reports and submit them to the AEUB on a monthly basis. In addition to providing information on the amounts of oil, gas, and water received, produced and delivered, battery operators are required to report the volumes of gas flared and/or vented. Although AEUB guidelines do not specify how this gas is to be measured, Interim Directive 94-1 [7] states

7

that volumes of gas less than 500 m^3 are to be reported with 20 % uncertainty and volumes greater than this are to be reported with 5 % or better uncertainty. Smaller flaring and venting volumes are typically estimated by first measuring the gas/oil ratio (GOR) in the crude oil stream and then inferring the amount of gas flared or vented from the measured amount of oil produced. Larger volume sites may use orifice plates or other measurement devices.

The data presented in this paper have been derived from these monthly production reports, which are compiled and stored by the AEUB. A relational database was created to analyze these data under various criteria. Although since 1999, the AEUB has distributed parts of these data for public use, not all batteries are included in the publicly released data [8]. Data that are connected in any way to wells categorized as experimental are held confidential and are not published. This omission is deemed necessary to protect the economically sensitive production data from experimental wells. In 1999, 29 of the 8249 oil and bitumen battery sites in the province were classified as experimental. However, flaring and venting from these sites totalled 0.167 billion m^3, which represented 13 % over the 1.266 billion m^3 of gas that was flared and vented at non-confidential sites. It should be noted that the data presented in this paper are complete and include data from these confidential experimental batteries. (Confidentiality was maintained throughout data processing by not accessing any information on either battery locations or operators.)

8

Although most oil and bitumen well sites are physically tied into batteries that report production, flaring, and venting data to the AEUB, there are cases where collections of bitumen wells that are not physically connected, report data as a single entity. A single report for a collection of physically separated sites is known as a "paper battery". Although it is estimated that paper batteries make up 1.5 % of the total number of battery reports submitted to the AEUB, they account for 23.6 % of the solution gas flared and vented annually. The inclusion of paper batteries in the data is a significant complication that hinders data analysis. While it is generally assumed that wells in a paper battery are located within a small geographic region (typically within a few miles), this is not necessarily the case. The influence of paper batteries on the data will be discussed later in this paper.

1.2.2 Gas Composition Data

Unfortunately, battery operators are not currently required to report the composition of gas being flared and/or vented on an ongoing basis. Thus, there is no direct way to determine the composition of solution gas flared and vented in Alberta. The AEUB does keep a separate record of composition of solution gas measured at individual oil wells. Although operators are not required to measure composition at well sites, under current guidelines if the measurements are made, the operators are obliged to submit the data to the AEUB. A data file of 5614 solution gas analyses was obtained from the AEUB for use in this paper. This number of analyses represents approximately 11 % of the 51976 active and abandoned wells associated with solution gas batteries in the province.

9

Although these analyses are not a random sample of all of the wells in the province, they are currently the best available data to use in estimates of the composition of gases flared and vented in the Alberta.

An important compositional issue is the presence of hydrogen sulphide (H_2S) in the flare gas, which is a known toxic gas and a strong odorant. Since the well analysis data are not directly connected to the battery site data, it is necessary to consider an alternate approach to estimate the amount of H_2S being flared at battery sites. As part of the application to create a battery code for the purpose of production reporting, operators are currently obligated to indicate whether the gas is "sweet" or "sour" (a qualitative indicator of the presence of hydrogen sulphide (H_2S) in the gas). However, no guidelines are presently in place which define at what maximum level of H_2S the gas is to be deemed sour instead of sweet. Operators are also required to provide an estimate of the maximum H_2S concentration in the solution gas, but this maximum is not necessarily indicative of operating conditions at the time of approval. Moreover, during the operating life of a battery, as wells are added and removed, the composition of the flared and vented gas would be expected to change.

AEUB guidelines state that if there is more than 10 PPM H_2S in the solution gas at a battery, sour gas warning signs must be posted. If the signs are posted indiscriminately at sweet sites, companies may be subject to an enforcement process. As part of the battery inspection process, the AEUB will note whether a battery is sweet or sour based on the

10

posted signage and the inspector's knowledge of the area, although this is obviously not a quantitative measure of gas composition.

1.3 FLARING AND VENTING OF SOLUTION GAS IN ALBERTA

In 1999, there were approximately 8249 active oil and bitumen battery sites scattered throughout Alberta which produced a total of 59.4 million m^3 of oil and 23.7 billion m^3 of solution gas. Although most solution gas produced in Alberta is "conserved", approximately 6 % of these gases were flared or vented at the battery sites. In 1999, 3715 of these battery sites reported volumes of gas flared totalling 0.938 billion m^3 while 1346 reported venting of gas totalling 0.485 billion m^3. In total, there were 4499 oil and bitumen batteries in Alberta that reported flaring or venting during 1999 with a combined gas volume of 1.42 billion m^3. It is this number of flare sites and the volumes of gas being flared that make the process of solution gas flaring an environmental concern for the public and oil and gas producers.

1.3.1 Characteristics of Solution Gas Flares

It is extremely difficult to describe solution gas flares in terms of a common set of characteristics. Although operators of oil and bitumen batteries are required to report total volumes of gas flared at battery sites on a monthly basis, other data such as the composition of gas being flared, flare diameter, type of ignition system, type of liquid separation system, and composition of liquids in the separation system are not reported.

11

Furthermore, anecdotal evidence suggests that most of these parameters can vary widely from site to site.

Physical Characteristics. Although there is no single set of physical characteristics that describe or define solution gas flaring operations, certain common features are believed to exist in that the flare stack height for solution gas is of the order 10 m high and a common stack size is approximately 10 cm in diameter. Other important parameters such as the volume flow rate and velocity of the solution gas exiting from the flare stack (V_j) can vary widely. Moreover, gas flow rates to the flare may not be steady depending on the operation of the oil wells feeding the battery and the downstream operations of facilities such as a gas plant that may shutdown periodically. Variations in the mean wind speed (U_∞) at the site also continually alter the flaring conditions. The ratio of U_∞ / V_j could easily vary from zero to 25, which produces flames that are either upright or bent over horizontally, and can significantly affect the performance of the flare [9]. Furthermore, there is considerable variation in the design of the flare tip in terms of wind shrouds and automated ignition systems (e.g., electric spark or continual pilot) that are mounted around the exit of the flare stack.

Battery Size / Volume Distributions. Figure 1.3 shows a histogram of the number of oil and bitumen battery sites in Alberta sorted by their total volumes of gas flared and/or vented during 1999. In total, there were 4499 battery sites in Alberta that reported flaring and/or venting during that year. The logarithmic scale on the horizontal axis of the histogram highlights the large variability in flow rates among individual battery sites.

12

The disparity between the median volume flared or vented of approximately 60,300 m³/year and the mean volume of 316,200 m³/year emphasizes the skewness of the volume distribution.
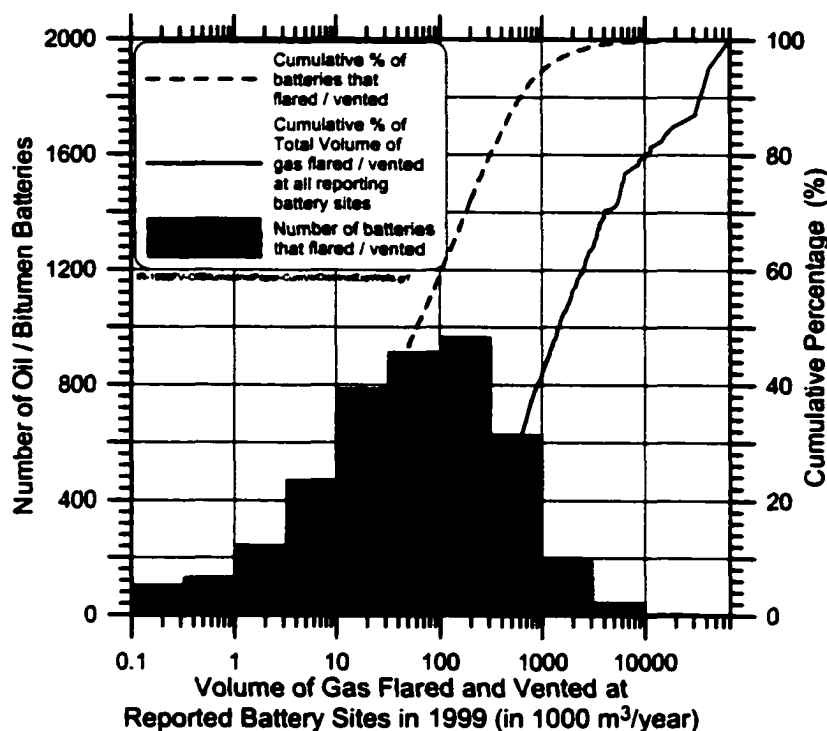
Figure 1.3: Distributions of gas volumes flared and vented at reported individual battery sites in Alberta in 1999

Also shown on Figure 1.3 are the cumulative distributions of both the number of battery sites and the total volumes of gas released at all sites sorted by the amount flared and/or vented at the battery sites. These cumulative distributions give an indication of the estimated size of the flaring operations at individual battery sites and illustrate the proportion of gas flared at these sites. For example, referring to the dashed line in Figure 1.3, it is apparent that 95 % of battery sites flare and vent less than 1,080,000 m³/year. Assuming this amount of gas was consumed in a continuously

13

operating flare, this would equate to an exit velocity of 4 m/s on a 10 cm diameter flare stack. Of course, most of these 95 % of battery sites flare amounts much less than 1,080,000 m³/year and would be expected to operate intermittently at higher and lower flow rates than their average flow rate. Thus, it is estimated that typical exit velocities for solution gas flares would be less than 6 m/s.

Although 95 % of battery sites in Alberta flare or vent less than 1,080,000 m³/year, the solid line on Figure 1.3 shows that these 95 % of batteries only generate 43.6 % of the total gas flared and vented at all battery sites. Alternatively stated, 5 % (or 225) of the battery sites in the province account for 56.4 % of the gas flared and vented at oil batteries in Alberta. This observation has significant implications for strategies to manage and mitigate solution gas flaring. If solutions were implemented at the largest 5 % of battery sites, this would affect more than 50 % of the gas flared and vented in Alberta annually. Unfortunately, the practicalities of such an implementation are not as simple as they might seem since the data contained in Figure 1.3 is biased by the inclusion of paper batteries.

Although there were only 98 paper batteries in 1999 that reported flaring and/or venting, these 98 groupings accounted for 23.6 % of the gas flared and vented in the province or 336.4 million m³. Thus, many of these largest 5 % of sites may not actually be physically connected as a single gas source. With this limitation in the data, it is difficult to address the issue of site to site variability in battery size or devise strategies for the management

14

of these gases. Therefore, it is useful to remove the paper batteries from the data, and study a reduced data set of batteries that are known to physically exist.

Figure 1.4, shows the same type of information as Figure 1.3, but only for physical battery sites (i.e., no paper batteries). There were a total of 4401 physical battery sites that reported flaring and/or venting in 1999 with a total gas volume of 1.09 billion m^3. The mean volume released at physical batteries was 246,900 m^3/year whereas the median volume was 58,700 m^3/year. Thus, the significantly skewed distribution noted in Figure 1.3 is still apparent. In fact, the cumulative distributions show quite similar trends as observed in Figure 1.3.
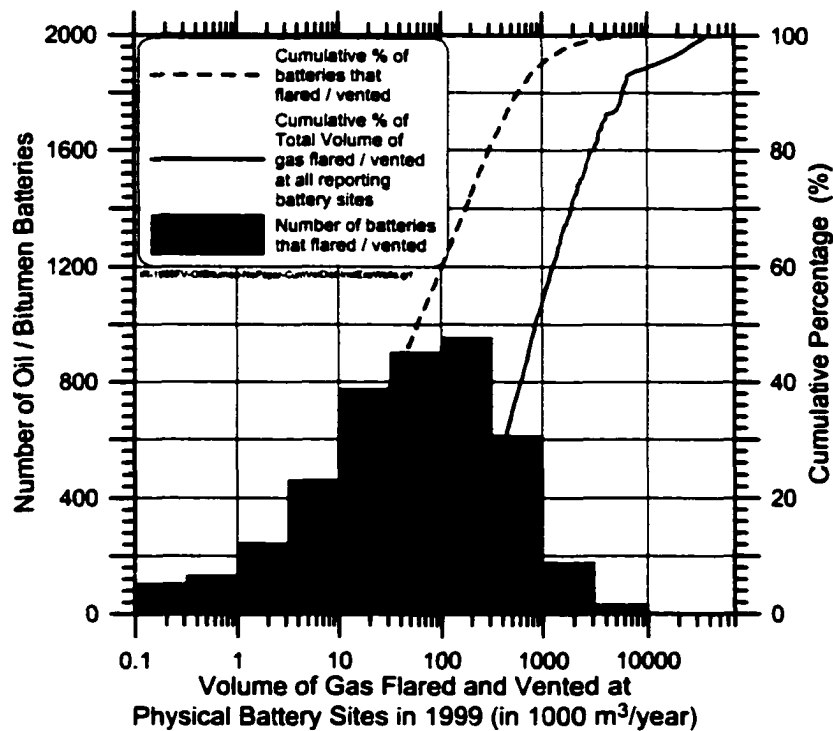
Figure 1.4: Distributions of gas volumes flared and vented at physical battery sites in Alberta in 1999. "Paper Batteries" have been separated out of the data.

15

From the dashed line in Figure 1.4, it is apparent that 95.2 % of the physical sites flare and vent less than 1,000,000 m^3 of gas per year. These same sites only generate 53.9 % of the gas flared and vented at physical batteries annually. Alternatively stated, the largest 5 % of the physical batteries (221 sites) flare and vent 47 % of the gas released at physical sites in the province which represents 35.7 % of the total solution gas flared and vented at all sites (including paper batteries) in the province. If one looks at the largest 20 % of physical sites (881 sites), it is apparent that these 20 % release 78.5 % of the gas at physical sites or 59.9 % of all the solution gas flared and vented in Alberta. Thus, the significance of these distributions with and without paper batteries is the same – if one were to attempt to mitigate problems associated with flaring, significant progress could be made by starting with the largest sites in the province.

Although, the decision to concentrate on the largest sites might seem obvious at this point, other important complications have the potential to limit the applicability of alternatives to flares. One such problem is the variability of the volume of gas flared or vented at individual sites over time. Figure 1.5 contains an array of bar graphs that show the volumes of gas flared and/or vented on a monthly basis at four individual physical battery sites. Although these sites were chosen so that their total annual volumes were of the same order as the mean annual volume for all physical sites of 247×10^3 m^3/year, they show starkly different trends. Batteries can flare or vent fairly steady volumes (5a), have a single anomalous month (5b), demonstrate erratic monthly volumes (5c) or have erratic volumes with the occurrence of zero reported volume in some months (5d). On each plot in Figure 1.5 the total, average, and maximum gas volumes are noted. As well,

16

the standard deviation of the monthly volumes and the deviation of the maximum, which is defined according to

$$Deviation\ of\ Maximum = \frac{Maximum\ Volume - Average\ Volume}{Average\ Volume} \times 100\% \qquad (1.1)$$

are reported.
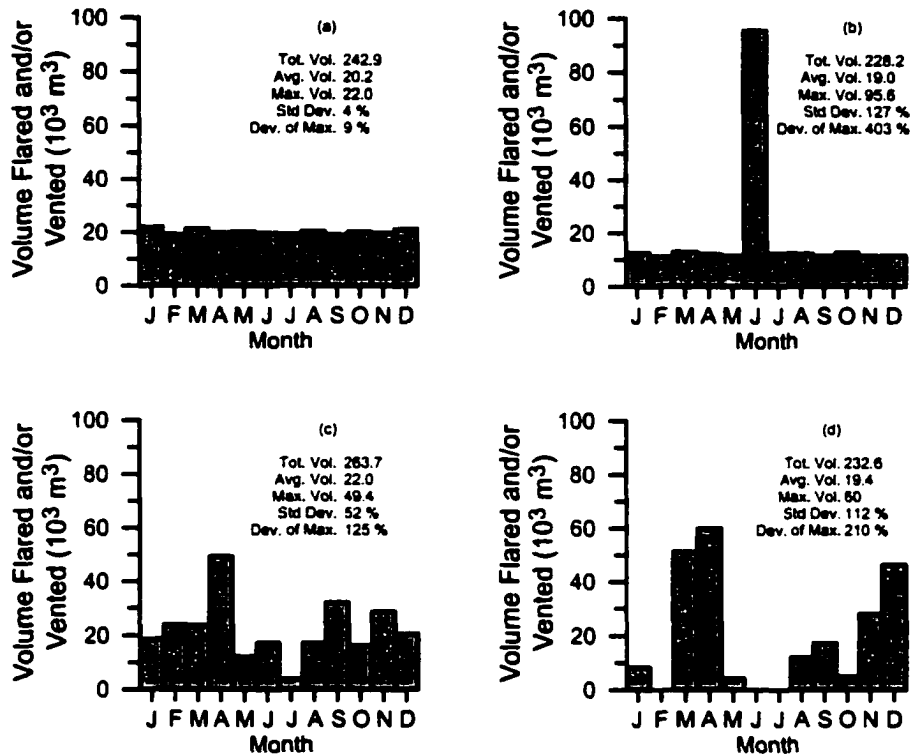
Figure 1.5: Examples of month to month variation in volumes of gas flared and vented as reported at individual battery sites

One of the primary engineering advantages of flares is their ability to handle wide ranges of gas flow rates on a single device. In industry terms this is often described as "turndown", the ratio of the maximum sustainable flowrate to the minimum flowrate required for operation. Typically, the turndown of a flare is limited only by flame stability, and may be 100:1 or greater. Unfortunately, most other technologies such as

17

internal combustion engines, turbines, and compressors have much narrower operating ranges. A typical turndown ratio for such a device might not be more than 2 or 3:1. In the context of flaring mitigation, this is a significant limitation. If a particular battery site has a relatively steady supply of gas, there may be many more possibilities to mitigate flaring than for a site with a highly variable gas supply.

While turndown ratios required to handle all the monthly gas volume at each site in Figure 1.5 could be presented, sites where the gas supply drops to zero in a given month (i.e. Figure 1.5d) would result in the turndown ratio going to infinity. Moreover, in a practical context if one was to pursue an alternative technology to flaring at a given site, one might be willing to size the technology so that the maximum gas flow rates could be handled with the trade-off of venting or flaring gas when the flow rates were too low. With this in mind, a more useful parameter to describe the variability of the gas flow at a battery site is the deviation of the maximum monthly volume, where sites with smaller deviations are more suitable to implementation of any steady flow devices. The standard deviation is also a useful statistic, but it is more difficult to interpret with respect to a turndown ratio.

The four plots in Figure 1.5 show varying degrees of variability in the monthly volumes of gas flared and/or vented. Figure 1.5a is an example from a site where the flow rate of gas being flared appears to be essentially continuous. The standard deviation of the monthly volumes is only 4 % and the deviation of the maximum is 9 %. On the criteria

18

of steady flowrate only, this site would be an example where alternate technologies might be applicable. By contrast, Figures 1.5b to 5d all have some significant variability.

The site in Figure 1.5b, appears to have operated fairly steadily for 11 months of the year, but in June 403 % more gas was flared or vented. Upon closer examination of Figure 1.5b one can determine that this battery normally conserves most of its gas. During the month of higher flaring, gas deliveries dropped suggesting that this may have due to downstream facilities being shutdown or for some other reason unable to handle the gas. In this example, 42 % of the gas flaring and/or venting during the year occurred in a single month. It would be difficult to apply an alternate technology with limited turndown in this situation or at other sites with similar monthly volume distributions.

Figures 1.5c and 5d show still different types of monthly distributions and appear to be almost random. The deviation of the maximum for the site in Figure 1.5c is 125 %, compared to the 210 % from Figure 1.5d. The data in Figure 1.5d have the added feature that the site appears not to have operated (or at least did not flare or vent) for three months of the year. It is difficult to hypothesize what of many factors may be influencing the operation of the sites in Figures 1.5c and 5d.

These four examples illustrate the wide variability that is apparent at solution gas battery sites. To characterize flaring and venting at battery sites in general terms, it is important to know what are the more prevalent types of monthly volume distributions; i.e. what are the relative numbers of steady and unsteady sites? Figure 1.6 shows a histogram of the

deviation of the maximum volumes for all 4401 physical battery sites. These results suggest that the deviation of the maximum monthly volume is less than 100 % for more than 40 % of sites. At the same time, the tail of the distribution suggests that many sites have significant monthly variability. However, there is no way to tell from this figure if the monthly variability in gas volume is connected to either small or large volume sites.

Monthly Variation in Volume of Gas Flared and/or Vented at Oil and Bitumen Battery Sites
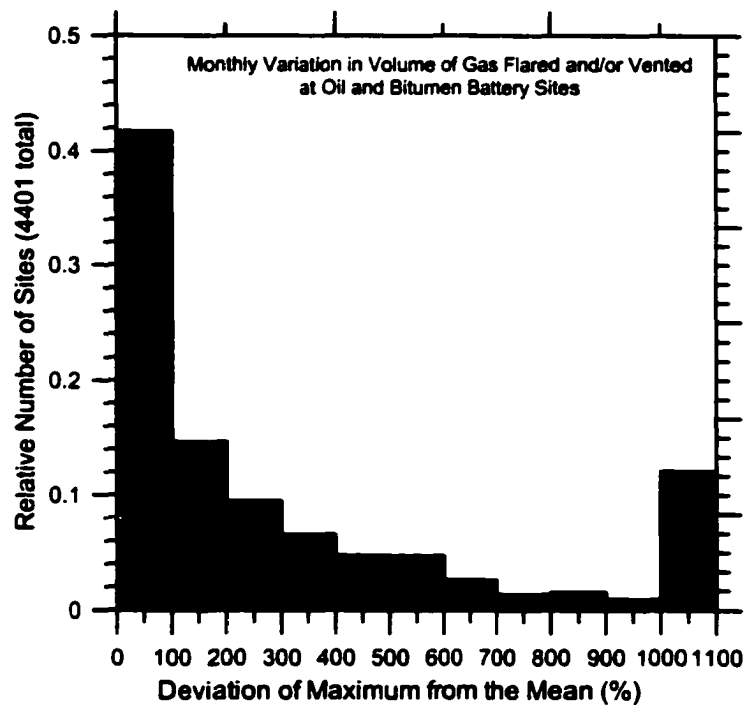
Figure 1.6: Distribution of the month to month variability in reported volumes of gas flared and vented at individual battery sites

Figure 1.7 shows an array of plots where the deviation of the maximum data from Figure 1.6 has been separated (conditioned) by total annual volume to match the size bins (width of the bars on the histogram) from Figure 1.4. In this manner, it is possible to test the influence of size of battery on the monthly variability in volumes flared and vented.

20
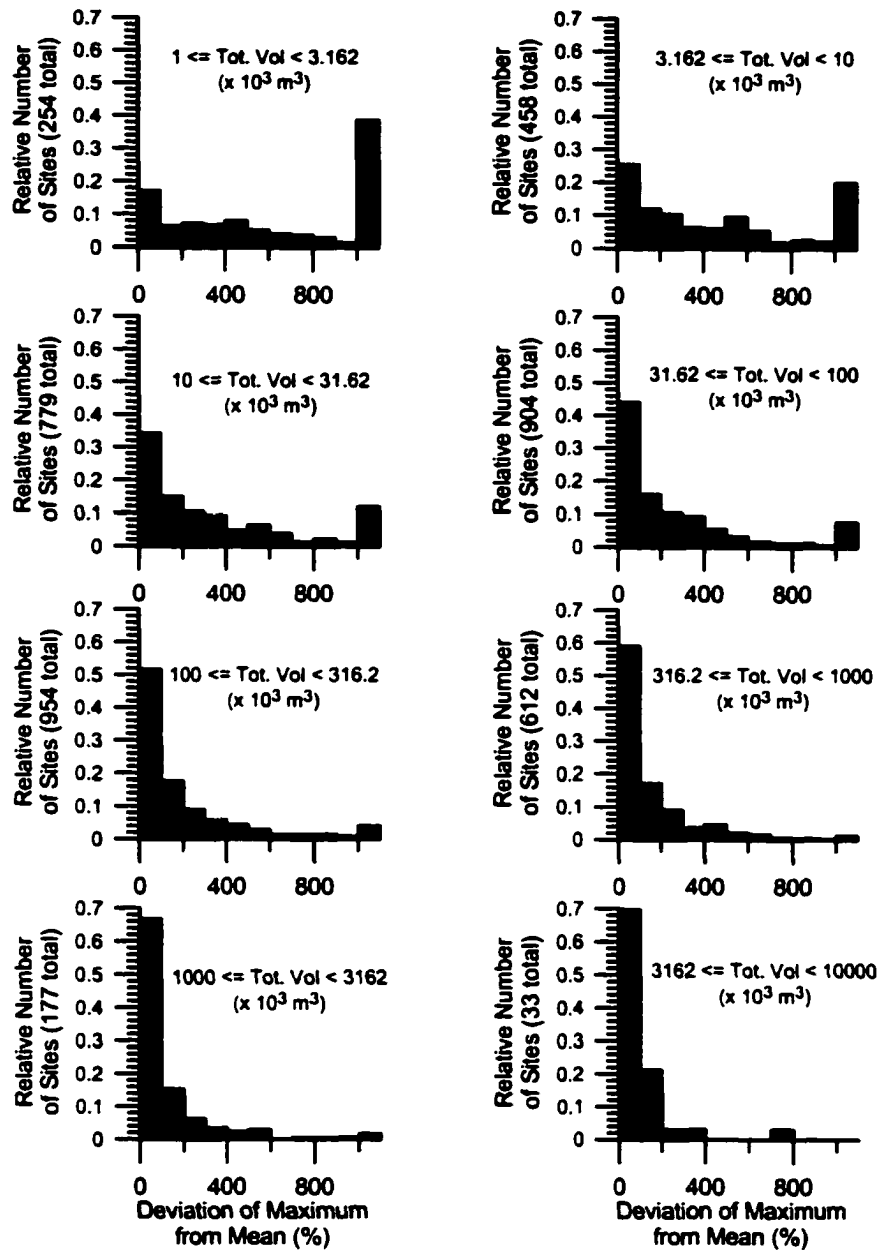
Figure 1.7: Variation in the month to month reported volumes of gas flared and vented at individual battery sites sorted by the size of the battery

From Figure 1.7, it is apparent that the monthly variability is strongly connected to the size of the battery. It is clear that the smaller size batteries have more monthly variability than the larger batteries. For example, less than 20 % of batteries with annual flare and

21

vent volumes between 1000 and 3162 m^3 have monthly distributions such that the deviation of the maximum is less than 100%. However, as the range of battery size is increased in successive plots, the proportion of sites with deviations of the maximum less than 100 % steadily increases to nearly 70 % for sites with annual volumes between 3,162,000 and 10,000,000 m^3. This result is significant since it suggests that larger battery sites are more likely to have steady volumes or gas flared or vented (at least as measured on a monthly basis). As discussed previously, these are the same sites that would need to be targeted first in any mitigation strategy for problems associated with flaring.

Composition of Solution Gases. Apart from the physical and environmental differences among battery sites, there are significant variations in the composition and phase of materials being flared and vented. Unfortunately, as described in the Data Reporting section, there is no prescribed reporting of composition analyses at individual battery sites. The AEUB does maintain a limited database of solution gas analyses from a selection of individual wells (i.e. basic gas phase composition of solution gas at individual oil wells), but these sites are generally removed from the battery sites which often flare a blend of gases from more than one well. However, these analyses represent the best currently available data on solution gas composition and are used here to provide the best possible insight into the composition gas being flared and vented at oil and bitumen battery sites in the Alberta.

22

Figure 1.8 shows a plot of the mean and maximum concentrations of major components found in solution gas at individual well sites. The most important observation to be made from this data is that there is significant variability in the relative concentrations of each of the major species contained in the solution gas. The notion of an average composition of solution gas is essentially irrelevant. Even methane (C1 hydrocarbons), which dominate the average concentration of the gas analyses at nearly 70 %, can vary greatly at individual wells. This variability is illustrated in Figure 1.9, which shows a histogram of C1 concentration for all 5614 solution gas analyses. As well, although the heavier hydrocarbons (C5, C6, C7+) are nearly negligible in the mean, at individual wells, their concentrations can be considerable.
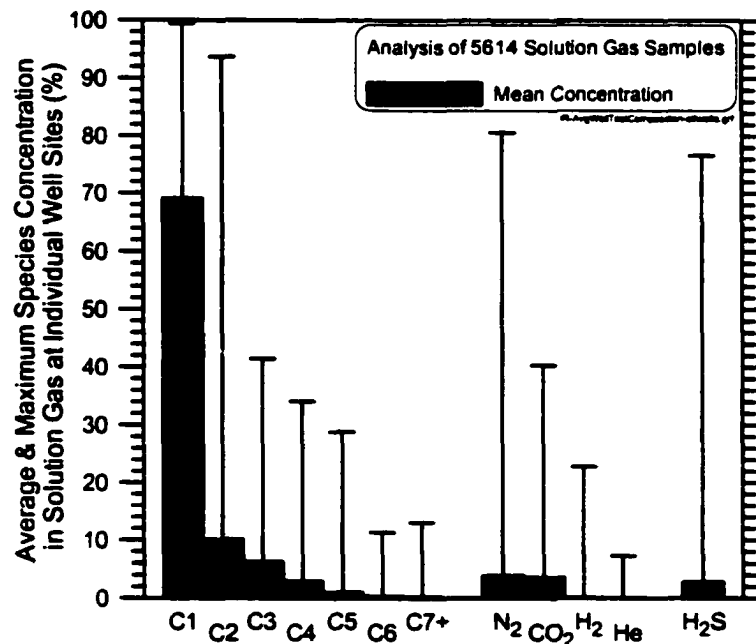
Figure 1.8: Analyses of solution gas at individual oil well sites in Alberta

23
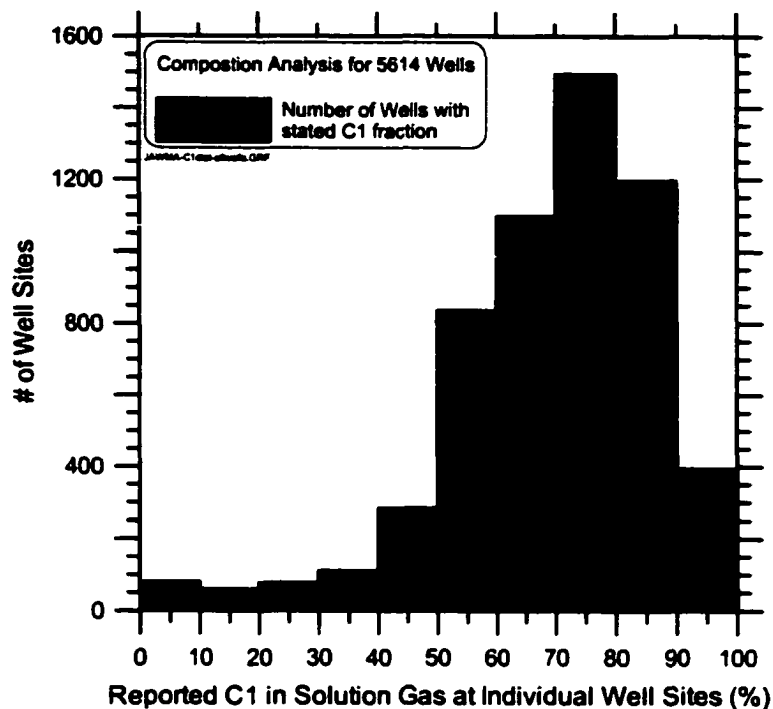
Figure 1.9: Histogram of C1 hydrocarbon concentration in solution gas at individual well sites in Alberta

These variations in composition are significant in terms of the potential uses for the solution gas and for the ability of the gas to be burned in a flare in a safe manner. Both the mass density (kg/m^3) and the energy density (MJ/m^3) of the flare stream are dramatically affected by the observed variations in composition. Assuming the composition of solution gas is alkane based, the range of mass densities for the data in Figure 1.8 calculated at 273 K and 1 atm is between 0.65 and 2.89 kg/m^3. The energy density (calculated as the higher heating value of the gas at 15 C and 1 atm) varies significantly from 4.9 to 133.7 MJ/m^3. As well, the presence of heavier hydrocarbons in the gases can dramatically affect the propensity of the gas to form soot when burned. The inert compounds carbon dioxide (CO_2) and nitrogen (N_2), which have mean concentrations around 4 %, can make up significant portions of the solution gas and at

24

higher concentrations could be expected to reduce the energy density of the gas. Research on the efficiencies of gas flares has shown that energy density can have a dramatic effect on flare performance [9].

Perhaps the most important component in distinguishing gas compositions at individual sites is the amount of hydrogen sulphide (H_2S), which may be present in the solution gas. Not only is H_2S a toxic component in solution gas, it can also lead to severe corrosion of metal parts that come into contact with gas containing H_2S or its combustion products. Figure 1.10 shows a histogram of H_2S concentration in the available solution gas analyses. Because there is wide variability in the samples, the horizontal axes of Figure 1.10 is shown with a logarithmic scale. Although 1848 (32.9 %) of the gas samples contained no H_2S, in some samples its concentration is quite significant.

In the context of flaring, gas that contains more than 10 PPM of H_2S is typically referred to as "sour" while gas with less than this amount are referred to as "sweet". Unfortunately there is no reliable way to connect the available composition data with the flaring and venting volume data from individual battery sites. Thus, it is not currently possible to reliably estimate the amounts of H_2S being flared and vented at solution gas batteries in Alberta. However, since this is an important issue to consider in a characterization of solution gas flaring, it is useful to make a qualitative estimate of the proportions of sweet and sour battery sites and gas volumes using AEUB site inspection data. Based on these data, it is estimated that 24 % of the battery sites in the province flare and/or vent gas that is sour. By correlating these qualitative labels with the volumes

25

of gas flared at individual sites, it is estimated that 36 % of the gas flared and vented in the province is sour.
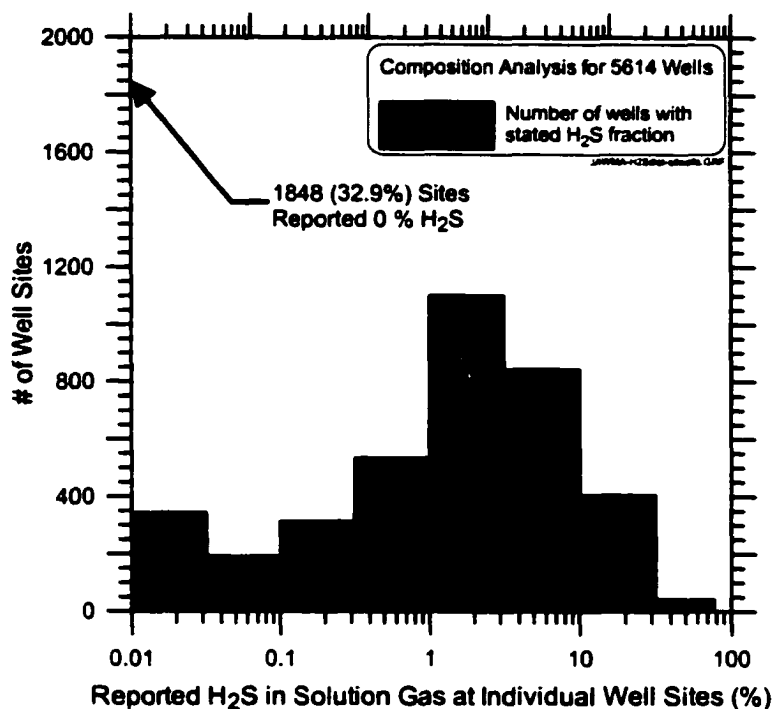
Figure 1.10: Histogram of H₂S concentration in solution gas at individual well sites in Alberta

Finally, it is generally accepted that some amount of liquids eludes the liquid knockout system and is carried to the flare in the form of liquid droplets entrained in the flare gases. However, field data on the composition, mass fraction, and size range of these liquid droplets do not exist. Given that solution gas is typically dissolved in an oil/water mixture in underground formations, it is probable that the entrained liquids are a mixture of brackish water and heavier hydrocarbons (C5 to C20) that would be expected to vary from site to site. Since the presence of entrained liquid droplets in the flare gases has the

26

potential to significantly affect flare performance, measurements need to be undertaken to assess the composition and quantity of these droplets in the field.

1.4 CONCLUDING REMARKS

In total, there were 4499 oil and bitumen batteries in Alberta that reported flaring or venting during 1999 with a combined gas volume of 1.42 billion m^3. This volume of gas represents approximately 71 % of all of the flaring and venting reported in the upstream oil and gas industry in Alberta. Despite the prevalence of solution gas flaring and venting and the implications of this practice for industry, regulators, and the public, the quality of currently available field data is poor. Data are complicated by the inclusion of "paper batteries" – collections of physically disconnected sites that are reported as a single "paper battery", which represent 23 % of the gas volumes flared and vented. As well, the composition of the gases being flared or vented at battery sites is currently not reported.

From analyzing the best available data, it is clear that solution gas flaring is neither well defined by a single set of operating parameters nor characterized by any single battery site. There is significant site to site variation in volumes of gas flared or vented, gas composition, and flare design. Concentrating only on oil and bitumen batteries that physically exist (i.e. ignoring paper batteries), it is apparent that the distribution of volumes of gas flared and vented at individual batteries is highly skewed with a mean volume of 246,900 m^3/year and a median volume of 58,700 m^3/year. Using this same data, it is apparent that 95% of these sites flare and vent less than 1,080,000 m^3/year of

27

solution gas. However, the remaining 5 % of physical batteries (221 sites), some of which handle more than 5,000,000 m³/year of gas, generate 35.7 % of the gas flared and vented annually at all oil and bitumen batteries in Alberta. Similarly, the largest 20 % of batteries (881 sites) flare and vent nearly 60 % of the solution gas flared and vented in the province. If one were to attempt to mitigate problems associated with flaring, significant progress can be made by focusing on the largest sites in the province.

An important characteristic of solution gas batteries is the monthly variability of the gas volume that is flared and/or vented. High variability in gas flow rate is a primary barrier for the successful implementation of alternative technologies to flaring. Although examples from individual sites show that some batteries have consistent monthly flare and vent volumes, others can deviate widely. Using the deviation of the maximum monthly volume from the average monthly volume, it was found that on average just over 40 % of sites could be considered "steady" (the deviation of the maximum from the average is less than 100 %). However, the variability in monthly flowrate was shown to correlate with the size of the battery, and larger batteries (larger annual flare and vent volumes) were shown to have a higher proportion of "steady" sites.

The current state of knowledge about the composition of gases being flared and vented in the province is much less complete. Using data from solution gas analyses at individual well sites as an indicator, it was shown that there is significant variability in the relative concentrations of each of the major species contained in solution gas. The notion of an average composition of solution gas is essentially irrelevant.

28

Perhaps the most important component in distinguishing gas compositions at individual sites is the amount of hydrogen sulphide (H_2S), which may be present in the solution gas. Unfortunately, since the available well analyses are generally removed from the battery sites which often flare a blend of gases from more than one well, it is not possible to make reliable quantitative estimates of the amounts of H_2S being flared and vented at solution gas batteries in the province. However, using AEUB site inspection data it is qualitatively estimated that 24 % of the battery sites in the province flare and/or vent gas that is sour (> 10 PPM H_2S). By correlating these qualitative labels with the volumes of gas flared at individual sites, it is estimated that 36 % of the gas flared and vented in the province is sour.

1.5 REFERENCES

1. Energy Information Administration (2000) *"International Energy Annual 1998"*, DOE/EIA-0219(98), Office of Energy Markets and End Use, U.S. Department of Energy, 250 pages.

2. Jones, H.R. (1973) *"Pollution Control in the Petroleum Industry"*, Noyes Data Corporation, Park Ridge, New Jersey, 322 pages.

3. Brzustowski, T.A. (1976) "Flaring in the Energy Industry", *Progress in Energy and Combustion Science*, 2, pp. 129-141.

4. Alberta Energy and Utilities Board (1999) *"GUIDE 60: Upstream Petroleum Industry Flaring Requirements"*, Alberta Energy and Utilities Board Guide Series, 1st Ed., 75 pages.

5. Holford, M.R. and Hettiaratchi, J.P. (1998) *"An Evaluation of Potential Technologies for Reducing Solution Gas Flaring in Alberta"*, Report to the Clean Air Strategic Alliance (CASA) Flaring Project Team, University of Calgary, Calgary, Alberta, 31 pages.

6. Houghton, J.T., Meira Filho, L.G., Callander, B.A., Harris, N., Kattenberg, A., and Maskell, K. (1996) *"Climate Change 1995: The Science of Climate Change"*, IPCC (Intergovernmental Panel on Climate Change), Cambridge University Press, Cambridge, U.K., 572 pages.

7. Alberta Energy and Utilities Board (1994) *"Interim Directive ID 94-1: Measurement of Oil, Gas, and Water Production"*, Alberta Energy and Utilities Board, Calgary, Alberta, January 18, 1994.

8. Alberta Energy and Utilities Board "Crude Oil and Crude Bitumen Batteries: Monthly Flaring, Venting and Production Data", *ST-60 series data files*, Calgary, Alberta.

9. Johnson, M.R. and Kostiuk, L.W. (2000) "Efficiencies of Low Momentum Jet Diffusion Flames in Crosswinds", *Combustion and Flame*, 123, pp.189-200.

CHAPTER 2

THE USE OF A CLOSED-LOOP WIND TUNNEL FOR MEASURING THE COMBUSTION EFFICIENCY OF FLAMES IN A CROSSFLOW

A version of this chapter has been published in Combustion & Flame as Bourguignon, E., Johnson, M.R., and Kostiuk, L.W., Combustion and Flame 119:319-334 (1999).

This paper was authored by Dr. Eric Bourguignon who was a post-doctoral fellow in our research group from September 1997 to August 1998, myself, and one of my supervisors. All three authors participated equally in developing the idea of using accumulation rates of major carbon containing species to measure the efficiency of jet diffusion flames in crossflow. After the mathematics of this approach were formalized, I was solely responsible for its implementation through installation of all instrumentation and writing software to automate data collection and processing. Since the publishing of this paper, I have continued to evolve, enhance, and refine the experimental methodology as described in Appendix A.

2.1 INTRODUCTION

The motivation for this work was to develop an experimental methodology to accurately measure the combustion efficiencies of open flames in a cross flow. This technique will

31

be applied to the study of the continuously operating flares used in the energy and petrochemical industries to burn unwanted combustible gases. Typical flare gases are hydrocarbon blends and may also contain hydrogen or sulfur based compounds such as hydrogen sulfide. The enthalpy of combustion of these gas mixtures can vary greatly depending on the relative amounts of inert gases such as carbon dioxide or nitrogen. Furthermore, these flare gas streams may contain liquids (e.g., water or hydrocarbon fuels) in the form of aerosols and may also contain small amounts of metals. In all cases, the goal of a continuously operating flare is to fully oxidize these streams to a safe, inert product mixture in a process that is ideally independent of the prevailing atmospheric conditions.

There has been a considerable amount of research conducted into flaring and the closely related topic of jet diffusion flames, either with or without a cross flow [c.f., 1-14]. The focus of these works has been primarily on stability limits, mechanisms of flame stabilization, size and shape of the flame, flame trajectory, local internal chemical structure of the flame, and emitted thermal radiation. In contrast, there has been a relatively small amount of work dealing with the emissions produced by flares. From a global perspective, the emissions of carbon dioxide and unburned hydrocarbons are well-known greenhouse gases. At the local level, the emission of hydrocarbons and oxides of nitrogen contribute to smog, and there is strong evidence that flares produce and emit a variety of toxic compounds [15].

32

A simple parameter that is used to characterize the emissions performance of a flare is its combustion efficiency. Previous studies have shown that the combustion efficiency of flares can be very high (>98%) over a wide range of flow rates and flare gas compositions as long as the flame remains stable [c.f., 16-22]. However, a recent study has found that solution-gas-flares (i.e. flares that burn the gases that come out of solution at a wellhead during the production of oil) can have efficiencies as low as 62% [15]. One parameter that has been identified as the potential cause of these lower combustion efficiencies is the cross flow velocity. A prior attempt to include the effects of wind was done by imposing a cross flow just above the end of the flare stack [21]. This flow arrangement, by not exposing the stack to the wind, excludes the possibility of the flame being caught in the recirculation region on the leeward side of the flare stack.

There are three methodologies typically employed to measure the combustion efficiency of flares: single point sampling, line of sight measurements, and plume collection. When working with flares in the open atmosphere, the efficiency is usually estimated from an analysis of the gases collected by a single aspirating probe placed nominally in the plume of the flare [15,18,19,21]. Atmospheric turbulence shifts the flame position so non-iso-kinetic sampling occurs across the plume and periods of sampling ambient air are frequent. Consequently, it is very difficult to relate formally the composition of the gases collected at the sample point to the mass of various compounds that are produced by the flare. It is important to note that these sampling techniques do not reference the composition of the flare gas stream and therefore cannot properly account for CO_2 in the fuel gas.

33

Line of sight measurement techniques that have been used for open atmospheric flares include passive Fourier Transform Infrared Radiation (FTIR) and Differential Absorption Light (DIAL) detection for in-situ, line-of-sight data collection [17]. It is important to note that these approaches do not attempt to calculate the efficiency based on all of the products of combustion.

In order to provide a more complete mass balance between reactants and products, some investigators have collected the entire plume coming off the flare [16,20,22,23]. The collected gases are mixed, sampled, and analyzed to calculate the overall efficiency of combustion. In cases where the entire plume is collected, the cross flow has been limited to very low, steady velocities to avoid complex plume collection systems.

The particular objective of this paper is to develop and validate the experimental methodology that will be used to investigate the impact of varying the flare rate, wind speed and fuel composition on the combustion efficiency. For simplicity, the case of flares that emit only gaseous products (i.e. non-sooting flames) is initially considered. Analyzing this case reveals that normal ambient concentrations of major species have a negligible effect on the calculated efficiency and allow the expressions developed for efficiency to be written in an explicit rather than an implicit form. In the final part of the paper, an extension to this approach is proposed for flames where the mass balance is complicated by non-gaseous combustion products (i.e. soot or condensate from heavy hydrocarbons).

34

2.2 COMBUSTION EFFICIENCY

The efficiency of a combustion process can be defined in a number of ways but is typically described as being either a combustion or a destruction efficiency [23]. Combustion efficiencies focus on the fully oxidized combustion products with the goal of completely oxidizing all of the fuel. In the case of hydrocarbon fuels, this means that all of the carbon in the fuel must end up as carbon dioxide and not as carbon monoxide, soot, or other hydrocarbons (e.g., aromatics, aldehydes, etc) in order to be 100% efficient. The combustion efficiency (η) used in this work is defined as the mass flow rate of carbon in the form of carbon dioxide produced by the flame, divided by the mass flow rate of carbon contained in the organic compounds of the flare stream. Although this definition could be better described as a carbon conversion efficiency, the term "combustion efficiency" is its traditional designation. Using $C_x H_y$ to describe a general hydrocarbon fuel or fuel blend, this mass based efficiency is:

$$\eta = \frac{Mass\ Flow\ Rate\ of\ Carbon\ in\ CO_2\ Produced\ by\ Flame}{Mass\ Flow\ Rate\ of\ Carbon\ in\ C_x H_y\ in\ the\ Flare\ Gas\ Stream} \qquad (2.1)$$

Since the analysis of combustion products is invariably based on concentration measurements, it is more convenient to express this same efficiency in terms of molar (volume) flow rates so that:

$$\eta = \frac{\dot{n}_{CO_2}}{x \cdot \dot{n}_{C_x H_y}} \qquad (2.2)$$

35

where $\dot{n}$ indicates molar flow rates and x is the number of carbons in C_xH_y. Implied in Eq. 2.2 is that the CO_2 being considered is only that produced by the flame and not that contained as part of the fuel stream.

2.3 EXPERIMENTAL METHODOLOGY AND FACILITY

To measure the molar production rates required to calculate the efficiency, the flares are burned in an enclosure. On-line gas analyzers are used to measure the time rate of change of concentrations of various species. These rates of increase in concentration are then interpreted as production rates by the flare. To provide a cross flow for the flare, the enclosure used for these experiments is a closed-loop wind tunnel.

The flare is located in the test section of the wind tunnel where the wind speed can be well controlled. Away from the test section of the tunnel, the products of combustion are mixed aggressively and thoroughly to allow gas sampling at a single point. By considering the details of the wind tunnel, a connection can be made between the rate of increase in concentration of a given species (e.g., CO_2, CO, etc.) and its production rate.

At first, compared to the simplicity of using an open-loop tunnel, the use of a closed-loop facility seems counterintuitive due the problem of recirculating product gases back through the flame. However, using an open tunnel requires measuring minute changes in composition of the large volumes of cross flow air that have been thoroughly mixed with the product gases. Only small changes in composition would occur, which would require

36

quantitative measurements of major combustion products to ppb accuracy relative to their ppm background concentrations. A variation on this open-loop approach would be to use a conical collector downstream of the flare to capture the entire plume. This approach is difficult to implement because the shape, location, and size of the plume vary greatly, especially when the flame is downwashed into the wake of the stack. Furthermore, when the cross flow is turbulent the flame and plume are buffeted randomly in the horizontal and vertical directions. Consequently, the collector size needs to be large and the products of combustion again become diluted below acceptable levels.

2.3.1 Test Facility

The closed-loop wind tunnel used in this work is shown in Figure 2.1. A contraction section upstream of the test section provides uniform laminar airflow across the flare with less than 1 % turbulence in the flow [24] (although turbulence generators may be added to the flow as necessary). The test section of the wind tunnel is 1.2 m high by 2.4 m wide by approximately 11 m long. This height of test section limits the size of flame that can be tested in this facility but the techniques developed here are applicable to larger facilities as well.

After the air passes through the test section it is drawn through the tunnel fan. The tunnel fan is driven by a variable speed 150 kW D.C. motor, which provides stable wind speeds in the test section from 0.2 to 35 m/s. The air is then discharged into the upper and plenum sections of the wind tunnel where six blowers are used to thoroughly mix the

37

product plume and tunnel air before the mixture is returned to the test section. These blowers are 60 cm diameter vane-axial fans driven by 0.56 kW motors at 1725 rpm and each displace 3.24m³/s of air at a mean velocity of 11.5 m/s. The thoroughness of this mixing was confirmed by continually injecting a tracer gas into the test section of the tunnel and monitoring its concentration at multiple locations after the mixing fans. The total internal volume of the wind tunnel is approximately 350 m³ and this provides 10 to 30 minutes of experimental running time before either oxygen depletion or build-up of combustion products begins to affect the experiments.
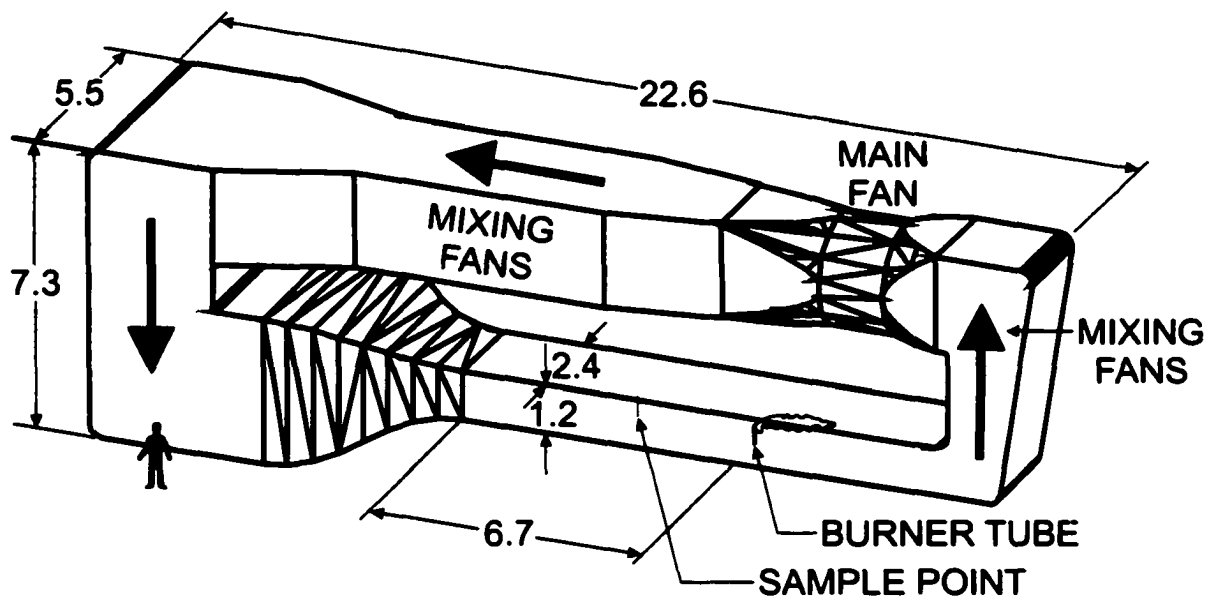
Figure 2.1: Schematic of the wind tunnel (All dimensions in meters)

The flares being tested are mounted 6.7 m from the leading edge of the test section. At this location the boundary layer of the wind tunnel is approximately 10 cm thick. Flare stacks ranging in size from 4 to 50 mm (outside diameter) can be tested. The flare used for this study was a jet diffusion flame created with a 25 mm outside diameter straight

38

pipe (internal diameter: 22 mm) that extended 40 cm into the tunnel. A 22 mm diameter, 12 mm deep perforated plate with symmetrically arranged, 3 mm diameter holes (65% flow blockage) was placed 35 mm upstream of the flare exit to ensure that the flow was turbulent. The flare gases (natural gas, methane, propane, and carbon dioxide) were supplied from compressed gas bottles. Calibrated mass flow controllers were used to create the required gaseous fuel composition and flow rate.

Concentrations of hydrocarbons, CO_2, CO, and O_2 are monitored with on-line gas analyzers. The unburned hydrocarbon gases are measured with flame ionization detectors with full-scale ranges of 4, 10, 40 100, 250, 1000, 2500, 10000 ppm. CO_2 and CO concentrations are measured with non-dispersive infrared analyzers. The available full-scale ranges for CO_2 measurements are 1000, 2500, 5000, 10000 ppm, while the ranges for CO are 200, 500, 1000, 2000 ppm. All of the analyzers have an uncertainty of ±1% of their full-scale reading. The temperature in the wind tunnel is measured with a 50 K range semiconductor temperature sensor that has an uncertainty in temperature measurement of ± 0.5 K. A Pitot tube placed next to the flare measures wind speed. All data are recorded at a sampling rate of 1 Hz.

2.3.2 Interpretation of Collected Data

Ideally, the wind tunnel would be sealed so that all the material produced by the flare would be captured within the tunnel for analysis. However, in practice, the wind tunnel leaks. Ambient air enters the wind tunnel, diluting the combustion products, and gases

39

within the wind tunnel leak out. A further complication that needs to be considered is that the products of combustion re-circulate in the tunnel. This recirculation exposes part of the unburned hydrocarbons in the tunnel to the flame (now as part of the combustion air) where they could be oxidized. The effects of leakage and "reburning" need to be accounted for in the species mass balance. Figure 2.2 models the wind tunnel as a constant pressure enclosure that exchanges gases with the surroundings where:

Q_{in} is the volume flow rate of ambient air into the tunnel,

Q_{out} is the volume flow rate of tunnel gases flowing out of the tunnel, and

P, T, ρ and Y are pressure, temperature, density, and mole fraction, respectively.

Ambient and tunnel conditions are identified with and without the subscript ∞, respectively, and the further subscript i is used to identify properties relating to a particular chemical species. The combustion products that recirculate through the flame are part of:

$Q_{combust}$, the volume flow rate of tunnel air involved in combustion.

40
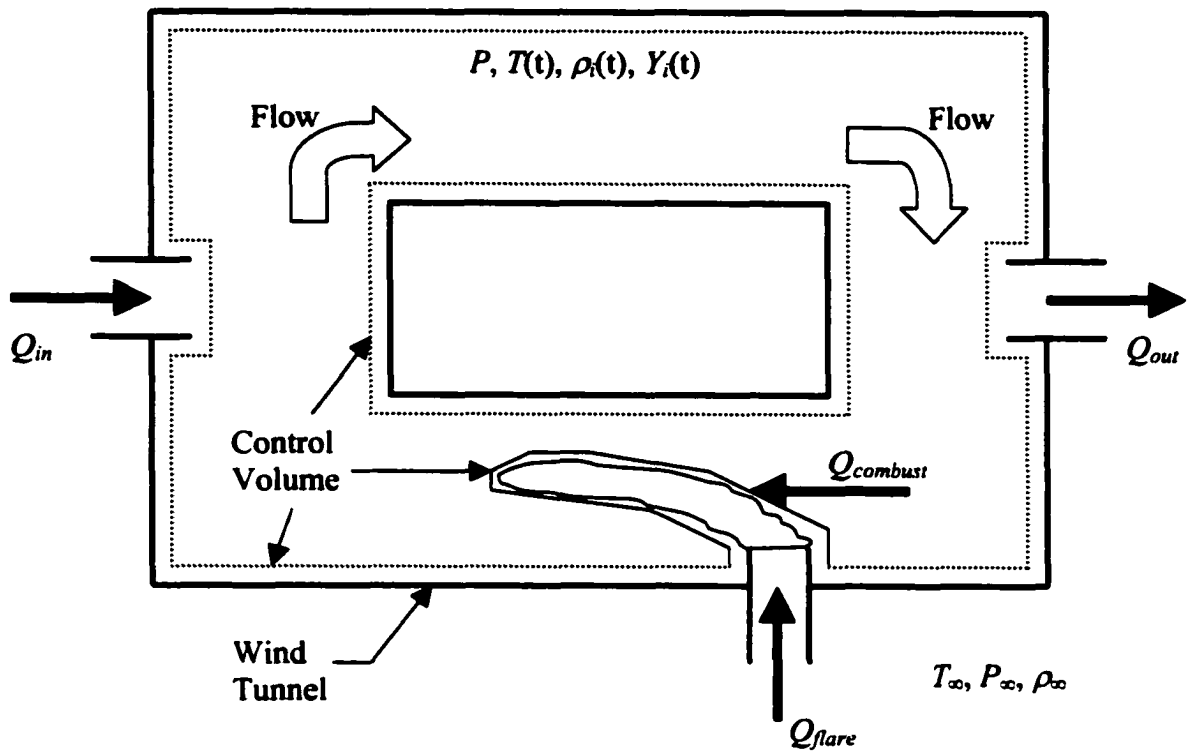
Figure 2.2: A model for the wind tunnel: A control volume is defined by the gases contained within the wind tunnel but not including the flame. Hence, the control volume exchanges gases with the ambient surroundings (Q_{in}, Q_{out}) and gases flow out of the control volume to participate in the combustion ($Q_{combust}$) and flow back into the control volume as products of combustion.

To perform a mass balance on the wind tunnel, it is convenient to consider a control volume defined by the air inside the wind tunnel, but not including the flame. This choice of control volume means that no chemical reactions occur inside the control volume and hence mass is only transported in and out of the control volume. In this situation, the rate of accumulation of mass of species i in the wind tunnel is given by:

41

$$\underbrace{V\frac{d}{dt}[\rho_i Y_i]}_{\text{Accumulation}} = \underbrace{\rho_i Y_{i,\infty} Q_{in}}_{\substack{\text{Transported}\\\text{in with}\\\text{infiltration of}\\\text{ambient air}}} - \underbrace{\rho_i Y_i Q_{out}}_{\substack{\text{Transported}\\\text{out with}\\\text{exflitration of}\\\text{tunnel air}}} + \underbrace{\rho_i Q_{i,emitted}}_{\substack{\text{Emitted into}\\\text{the control}\\\text{volume by}\\\text{combustion of}\\\text{flare gases}}} + \underbrace{\rho_i Q_{i,inert}}_{\substack{\text{Flow into}\\\text{tunnel as}\\\text{part of}\\\text{flare gas}}} \pm \underbrace{\eta \rho_i Y_{HC} Q_{combust}}_{\substack{\text{Net flow in}\\\text{or out due to}\\\text{combustion,}\\\text{where fuel mass}\\\text{originates from}\\\text{the air side}}} \quad (2.3)$$

where V is the tunnel volume and Y_{HC} is the mole fraction of hydrocarbons in the tunnel air. $Q_{i,emitted}$ is the volume flow rate of species i emitted into the wind tunnel by the flaring process where the fuel originates from the flare gas stream. $Q_{i,inert}$ is the volume flow rate of species i in the flare gases flowing into the wind-tunnel unaffected by combustion (this term is applicable for inert components only, e.g., CO_2). The last term of Eq. 2.3 (i.e. effects of re-burning) is modeled by assuming that the combustion of hydrocarbons entering with the combustion air burns with the same efficiency as hydrocarbons supplied via the fuel stream. While it is recognized that this is only a first order approximation, the importance of this assumption is shown to be negligible, as the mass fluxes associated with this term are extremely small as long as Y_{HC} remains small. The sign on the last term is negative if i is a reactant and positive if i is a product.

The total flow rate issuing from the flare is given by:

$$Q_{flare} = Q'_{fuel} + Q''_{fuel} + Q_{inert} \quad (2.4)$$

where Q'_{fuel} is the volume flow rate of gaseous fuel, Q''_{fuel} is the volume flow rate of liquid fuel, and Q_{inert} is the volume flow rate of inert gases.

42

The volume flow rates of gases exfiltrating and infiltrating the wind tunnel are not independent quantities and are related by:

$$Q_{out} = \left(\underbrace{Q_{in}}_{\substack{\text{Infiltration}}} + \underbrace{\gamma' Q'_{fuel}}_{\substack{\text{Molar imbalance}\\ \text{between the fuel}\\ \text{and products of}\\ \text{gaseous fuel}}} + \underbrace{\gamma'' \frac{\rho''_{fuel,l}}{\rho''_{fuel,g}} Q''_{fuel}}_{\substack{\text{Molar imbalance}\\ \text{and phase change}\\ \text{between the fuels}\\ \text{and products of}\\ \text{liquid fuels}}} + \underbrace{Q_{inert}}_{\substack{\text{Inert flow}\\ \text{in flare}\\ \text{stream}}} \right) \underbrace{\frac{T}{T_\infty}}_{\substack{\text{Heating of}\\ \text{the wind}\\ \text{tunnel}\\ \text{gases}}} \quad (2.5)$$

$$\underbrace{\phantom{Q_{out}}}_{\text{Exfiltration}}$$

where γ' and γ'' are coefficients that account for the number of moles of combustion products introduced into the tunnel relative to the number of moles of gaseous and liquid fuels, respectively, and $\dfrac{\rho''_{fuel,l}}{\rho''_{fuel,g}}$ accounts for the change in density as any liquid fuel evaporates.

Substituting Eq. 2.5 into Eq. 2.3 gives the mass balance for a particular species in the tunnel which is:

$$V \frac{d}{dt}[\rho_i Y_i] = \rho_i Y_{i,\infty} Q_{in} - \rho_i Y_i \left(Q_{in} + \gamma' Q'_{fuel} + \gamma'' \frac{\rho''_{fuel,l}}{\rho''_{fuel,g}} Q''_{fuel} + Q_{inert} \right) \frac{T}{T_\infty}$$

$$+ \rho_i Q_{i,emitted} + \rho_i Q_{i,inert} \pm \eta \rho_i Y_{HC} Q_{combust} \quad (2.6)$$

Although Eq. 2.6 is applicable at all times during the experiment, it is complex and involves terms that are difficult to measure (i.e. Q_{in} and $Q_{combust}$). This equation can be simplified by choosing a time, t', when the accumulated concentrations in the tunnel of species used in the efficiency calculation are small or approaching zero. By choosing this condition, the magnitude of the mass transport associated with the combustion air term

43

(i.e. the last term in Eq. 2.6) is negligible since Y_{nc} is small, and furthermore, $T \to T_\infty$, $Y_i \to Y_{i,\infty}$, $\rho_i \to \rho_{i,\infty}$. Thus, Eq. 2.6 becomes:

$$V \frac{d}{dt}[\rho_i Y_i]\bigg|_{t \to t'} = \rho_{i,\infty} Y_{i,\infty}\left(\gamma' Q'_{fuel} + \gamma'' \frac{\rho''_{fuel,l}}{\rho''_{fuel,g}} Q''_{fuel} + Q_{inert}\right) \\ + \rho_{i,\infty} Q_{i,emitted} + \rho_{i,\infty} Q_{i,inert} \tag{2.7}$$

Assuming ideal gas behavior, Eq. 2.7 becomes:

$$VT_\infty \frac{d}{dt}\left[\frac{Y_i}{T}\right]\bigg|_{t \to t'} = Y_{i,\infty}\left(\gamma' Q'_{fuel} + \gamma'' \frac{\rho''_{fuel,l}}{\rho''_{fuel,g}} Q''_{fuel} + Q_{inert}\right) + Q_{i,emitted} + Q_{i,inert} \tag{2.8}$$

which is the final expression for the mass balance for species i that can then be exploited experimentally to determine the efficiency of combustion.

In principle, everything in Eq. 2.8 is either known or measurable except for the volume flow rate of species i emitted into the tunnel as a result of the combustion of the flare stream (i.e. $Q_{i,emitted}$). If the species chosen for analysis was CO_2, then the flow rate of CO_2 emitted into the tunnel could be converted to its molar flow rate and the efficiency could be calculated from Eq. 2.2. In practice though, there are problems in accurately measuring the effective internal volume of a complex structure like a wind tunnel. Monitoring the concentration of a few species in the wind tunnel and solving a system of equations eliminates the need to know the tunnel volume.

44

2.4 FLARES WITH GASEOUS PRODUCTS OF COMBUSTION ONLY

An important specific case of flaring occurs when the material being flared creates only gas phase products (i.e. there is little or no soot formed by the flame and heavier hydrocarbons do not condense into their liquid phase). In this situation the combustion efficiency can be determined by a gas analysis of tunnel gases and Eq. 2.8 becomes:

$$VT_\infty \frac{d}{dt}\left[\frac{Y_i}{T}\right]_{t \to t'} = Y_{i,\infty}\left(\gamma' Q'_{fuel} + Q_{inert}\right) + Q_{i,emitted} + Q_{i,inert} \tag{2.9}$$

where for simplicity the flare stream is also restricted to being gaseous. The exclusion of liquid fuels from the flare stream does not affect the generality of this analysis and results in the same final expression. The global combustion equation for the major reacting species of a general hydrocarbon fuel is:

$$C_{x'}H_{y'} + aO_2 \to b\alpha CO_2 + b(1-\alpha)CO + cH_2O + dC_mH_n \tag{2.10}$$
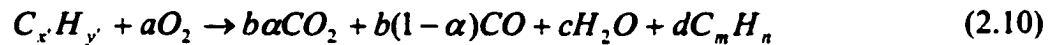
where C_mH_n represents the mean composition of all the unburned hydrocarbons in the products, and α and $(1-\alpha)$ give the fractional split between the CO_2 and CO formed. The stoichiometric coefficients for Eq. 2.10 as a function of combustion efficiency are shown in Table 2.1, and

$$\gamma' = b + c + d - a \tag{2.11}$$

45

Table 2.1: Expressions for the stoichiometric combustion coefficients

Stoichiometric Variable	Stoichiometric Coefficient
a	$x'\eta\left(1+\dfrac{1-\alpha}{2\alpha}\right)+\left[\dfrac{y'}{4}-\dfrac{x'}{4m}\left(1-\dfrac{\eta}{\alpha}\right)\right]$
b	$\dfrac{x'\eta}{\alpha}$
c	$\dfrac{y'}{2}-\dfrac{x'}{2m}\left(1-\dfrac{\eta}{\alpha}\right)n$
d	$\dfrac{x'}{m}\left(1-\dfrac{\eta}{\alpha}\right)$

Excluding the possibility of soot in the products allows a carbon balance to be achieved with detectors for CO_2, CO and hydrocarbons. In solving for efficiency through Eqs. 2.2, 2.9 and 2.11, there are three unknowns (tunnel volume, V, the molar split between CO_2 and CO, α, and the efficiency, η) and mass balance equations for the hydrocarbons, CO_2, CO are required in order to close the system of equations. From Eqs. 2.2 and 2.11, and Table 2.1, explicit expressions for the flow rate of species i as a result of combustion ($Q_{i,emitted}$) and the flow rate of i entering the tunnel without chemical reaction from the flare ($Q_{i,inert}$) can be written. Table 2.2 gives the expressions for $Q_{i,emitted}$ and $Q_{i,inert}$ that will be substituted into Eq. 2.9 for each species of interest, where $Y_{C_{x'}H_{y'}}$ and $Y_{CO_2,flare}$ are the volume fractions of hydrocarbons and CO_2 in the gaseous fuel, respectively.

It is not possible to determine the hydrocarbon gas concentration in the tunnel, $Y_{C_mH_n}$, from a concentration measurement using a FID. The FID, if calibrated with methane,

46

only gives an equivalent methane concentration, Y_{HC}. The relation usually employed to

connect the hydrocarbon gas concentration ($Y_{C_m H_n}$) and the FID reading (Y_{HC}) is

$$Y_{HC} = m Y_{C_m H_n}$$

(2.12)

which forces $m = 1$ in all of the expressions previously developed, although the

hydrocarbon concentration is measured to be at a proportionally higher amount which

maintains the carbon balance. This expression assumes a linear response from the FID

with respect to the number of carbon atoms in the hydrocarbons sampled from the tunnel.

Typical response factors for alkanes, alkenes and alkynes vary by less than 3% from the

response of methane. The uncertainty introduced into the calculated efficiency through

this assumption is tested as part of the sensitivity analysis that appears later.

Table 2.2: Expressions for the volume flow rates of species accumulating in the wind
tunnel and inert gases in the flare stream

i	$Q_{i, ambient}$	$Q_{i, inert}$
$C_m H_n$	$\dfrac{x'}{m}\left(1 - \dfrac{\eta}{\alpha}\right) Y_{C_{x'} H_{y'}} Q_{flare}$	N/A
CO_2	$\eta x' Y_{C_{x'} H_{y'}} Q_{flare}$	$Y_{CO_2, flare} \cdot Q_{flare}$
CO	$\dfrac{(1-\alpha)}{\alpha} \eta x' Y_{C_{x'} H_{y'}} Q_{flare}$	N/A

Finally, the mass balance equations for methane equivalent hydrocarbons, CO_2 and CO

can be written from Eq. 2.9 and Table 2.2 as

47

$$\frac{VT_\infty}{Q_{flare}}\frac{d}{dt}\left[\frac{Y_{HC}}{T}\right]_{t\to t'} = -Y_{C_{x'}H_{y'},\infty}\left(\gamma Y_{C_{x'}H_{y'}} + Y_{inert}\right) + x'\left(1-\frac{\eta}{\alpha}\right)Y_{C_{x'}H_{y'}} \qquad (2.13)$$

$$\frac{VT_\infty}{Q_{flare}}\frac{d}{dt}\left[\frac{Y_{CO2}}{T}\right]_{t\to t'} = -Y_{CO2,\infty}\left(\gamma Y_{C_{x'}H_{y'}} + Y_{inert}\right) + \eta x' Y_{C_{x'}H_{y'}} + Y_{CO2,flare} \qquad (2.14)$$

$$\frac{VT_\infty}{Q_{flare}}\frac{d}{dt}\left[\frac{Y_{CO}}{T}\right]_{t\to t'} = -Y_{CO,\infty}\left(\gamma Y_{C_{x'}H_{y'}} + Y_{inert}\right) + \frac{(1-\alpha)}{\alpha}\eta x' Y_{C_{x'}H_{y'}} \qquad (2.15)$$

Due to the coupling between the unknowns (η, V and α), no explicit expression could be obtained for the efficiency. Hence, the efficiency is determined using an iterative process.

2.4.1 Sample Results

Experiments were conducted with technical grade methane at flare rates and wind speeds that would produce relatively high and low efficiency flares as a result of the cross flow. The momentum flux ratio, R, is used to characterize the flow and is defined as:

$$R = \frac{\rho_{flare}V_{flare}^2}{\rho_\infty U_\infty^2} \qquad (2.16)$$

where V_{flare} and U_∞ are the mean velocity of the flare at its exit and of the air in the wind tunnel, respectively. Table 2.3 summarizes the experimental operating conditions.

During an experiment, the concentrations of hydrocarbons, CO_2 and CO are monitored in time as shown in Figure 2.3. At the beginning of the experiment, before the flare is lit,

48

the measured concentrations are steady and represent the background concentrations. After starting the flare there is a series of transient mixing events that occur before the tunnel's longitudinal mixing becomes stationary. As the flare burns, the concentrations of hydrocarbons, CO_2 and CO rise due to combustion and the gases warm in the wind tunnel. The variation of the temperature is shown in Figure 2.4 and is typically only a few Kelvin.

Table 2.3: Experimental conditions and efficiency results

Experimental Designation	Fuel Flow Rate (SLPM)	Cross flow (m/s)	Momentum Ratio	Efficiency by Eqs. 2.13-2.15 (%)[a]	Efficiency by Eq. 2.17 (%)[a]
A	60	10	0.24	97.1805	97.1799
B	50	12	0.16	91.7867	91.7850

[a] – number of significant digits are included to demonstrate how insensitive calculated efficiency is to background concentrations

The variation in the ratio of concentration over temperature is plotted in Figure 2.5. Fitting a line to the resulting curves provides a measure of $\frac{d}{dt}\left(\frac{Y_i}{T}\right)\Big|_{t\rightarrow t'}$ for each species that is required in Eqs. 2.13-2.15 and allows the combustion efficiency to be calculated as in Table 2.3. The shape of $\frac{d}{dt}\left(\frac{Y_i}{T}\right)$ correlates very well with a straight line, which validates the assumption that species mass fluxes other than that produced by the flame are small (i.e. the re-burning term in Eq. 2.6 can be neglected). Furthermore, the straight line removes any ambiguity of when to chose t'. Over the duration of the tests, it was observed that the O_2 concentration in the tunnel was reduced from 21% to 20.6% but this is not considered significant.

49
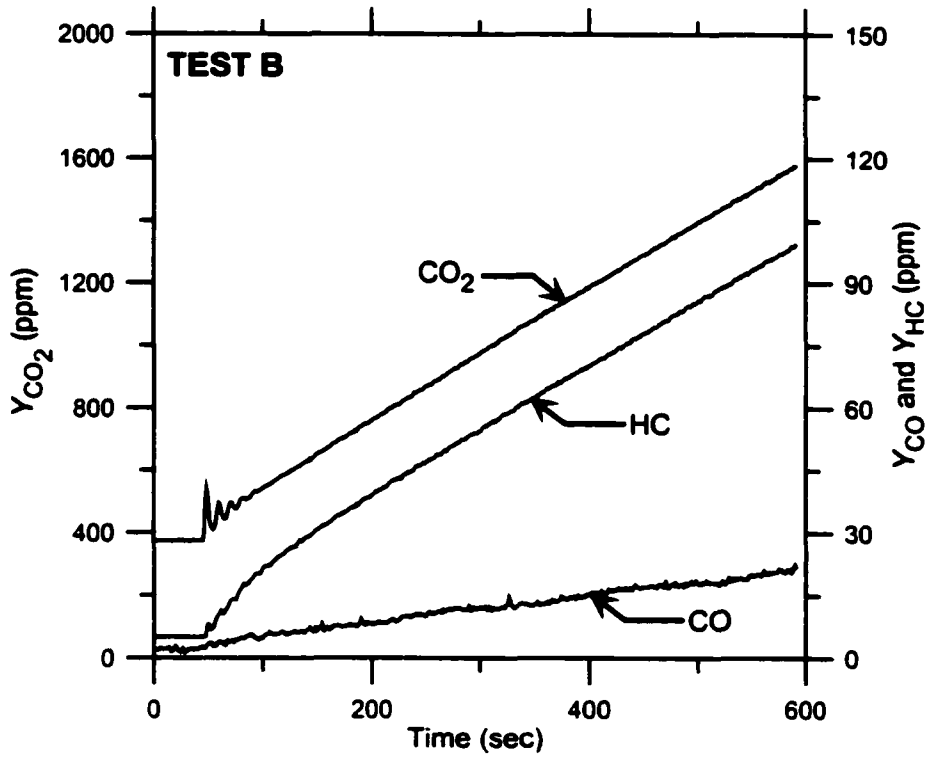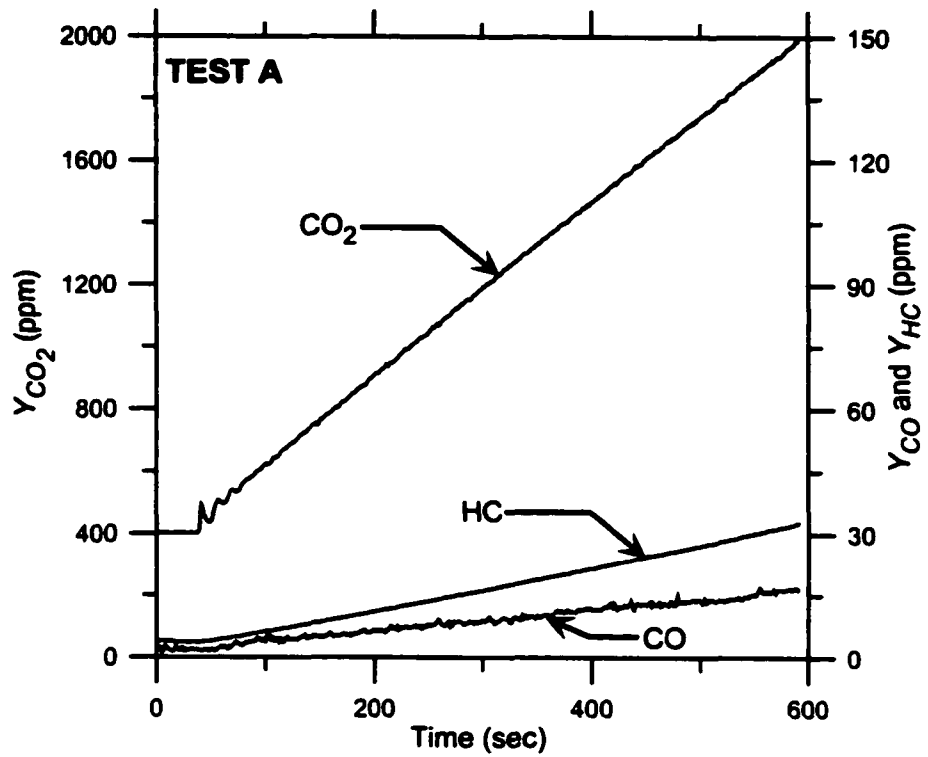
Figure 2.3: Measured concentrations of CO_2, CO, and hydrocarbons in the wind tunnel during experiments A and B

50
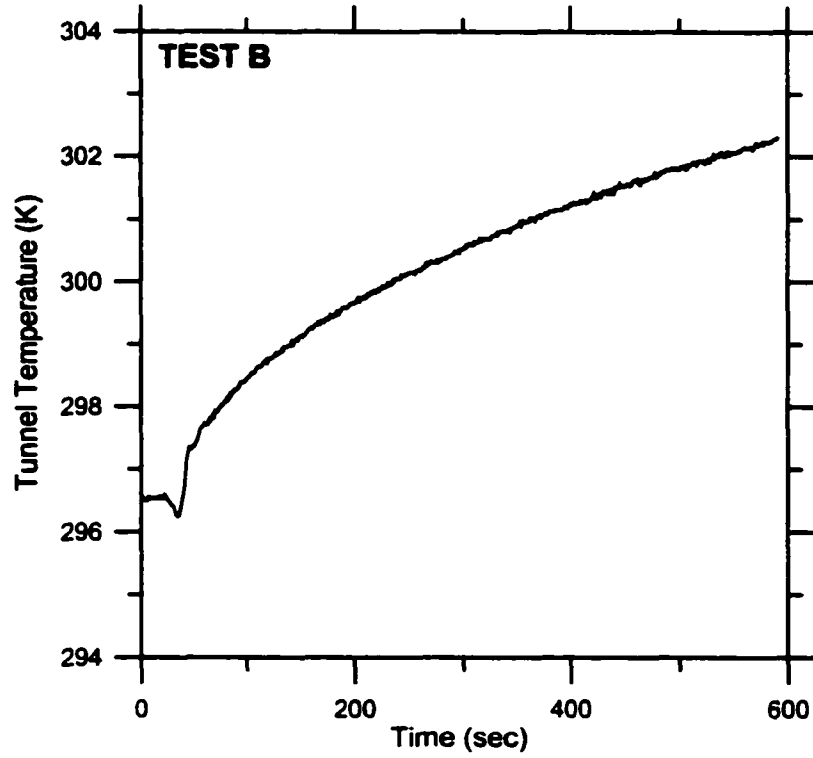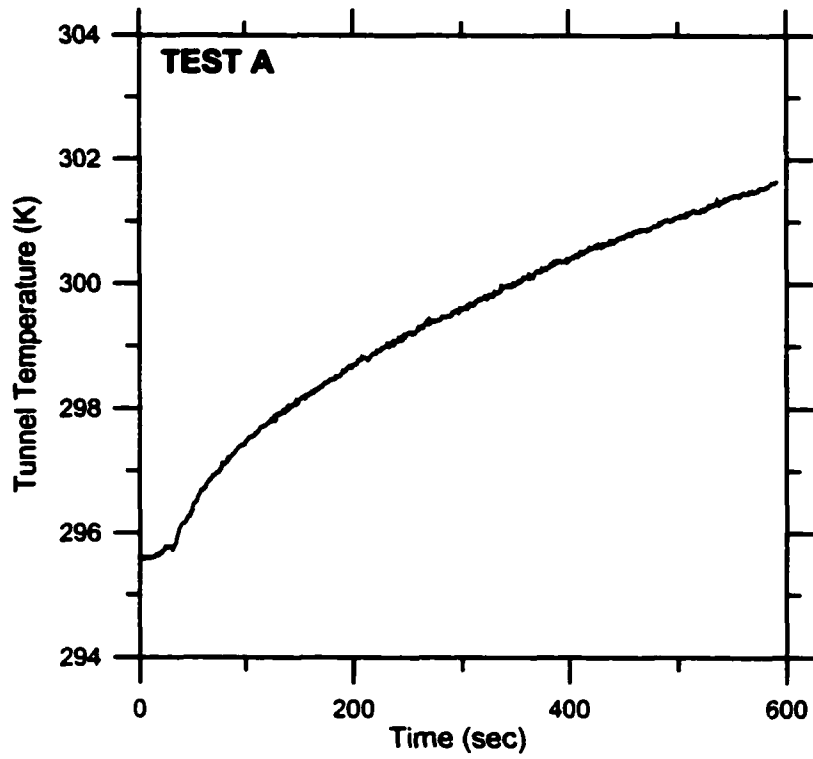
Figure 2.4: Measured temperature in the wind tunnel during experiments A and B.

51
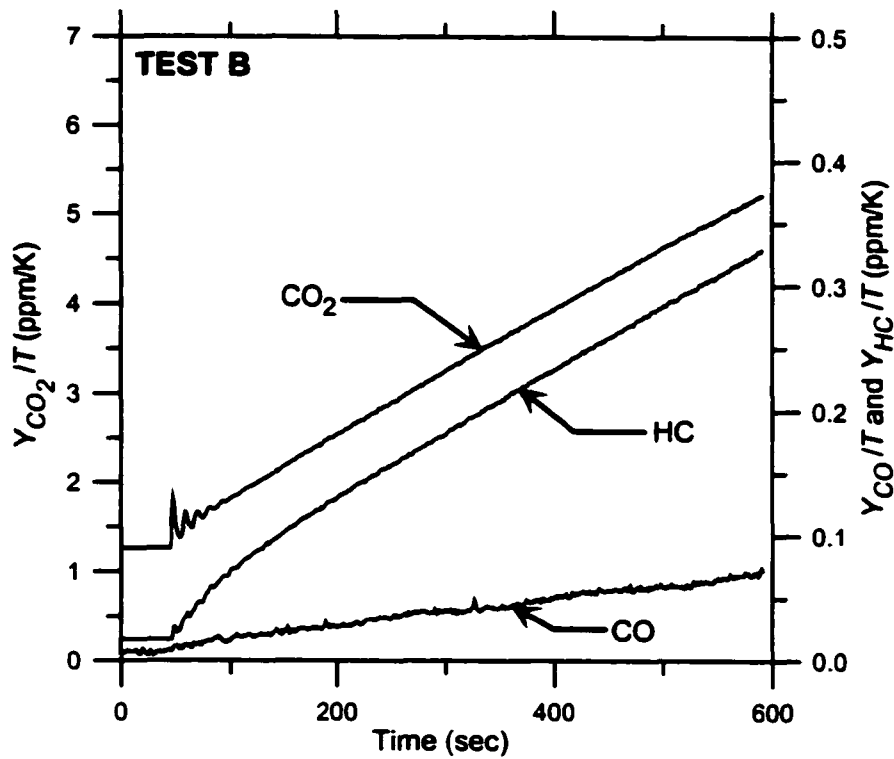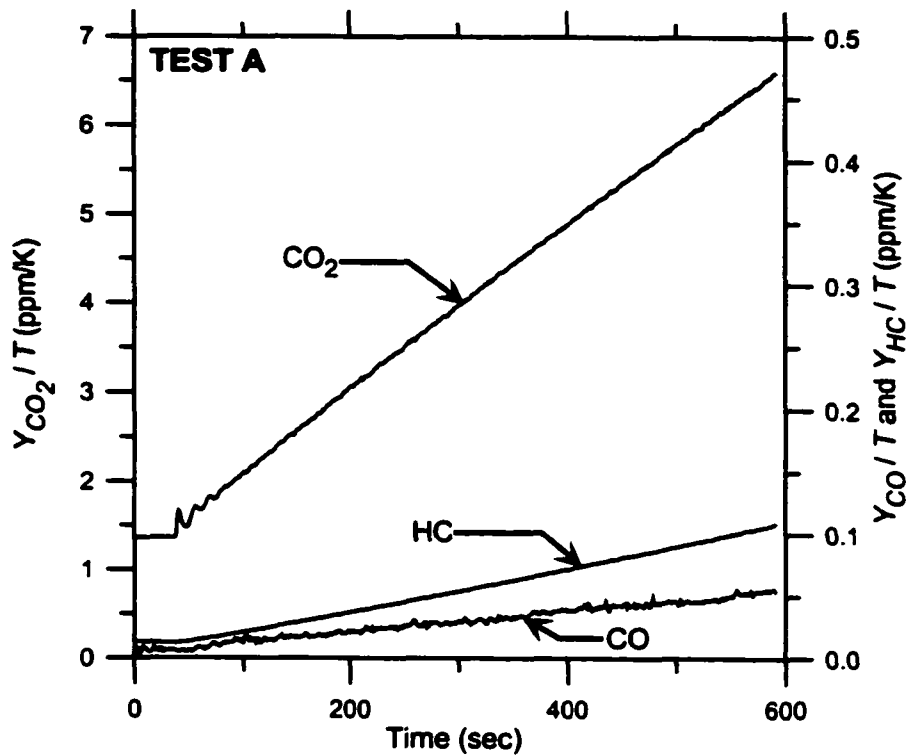
Figure 2.5: Ratio of the concentrations of CO_2, CO, and hydrocarbons divided by temperature for experiments A and B.

52

2.4.2 Background Sensitivity

Inspection of Eqs. 2.13-2.15 shows that if the background ambient concentration of hydrocarbons, CO_2 and CO could be ignored then this system of equations becomes greatly simplified. Figure 2.6 shows the error introduced into the efficiency due to an error in the background concentrations. Of interest is the error in the calculated efficiency when $Y_i/Y_{i,\infty} = 0$, i.e. when no background concentrations are included in the efficiency calculation. For the three species, the error created by setting their background concentrations to zero changes the measured efficiency by less than 0.015%. Hence, the influence of the background concentrations on the efficiency calculation can be considered negligible.

53
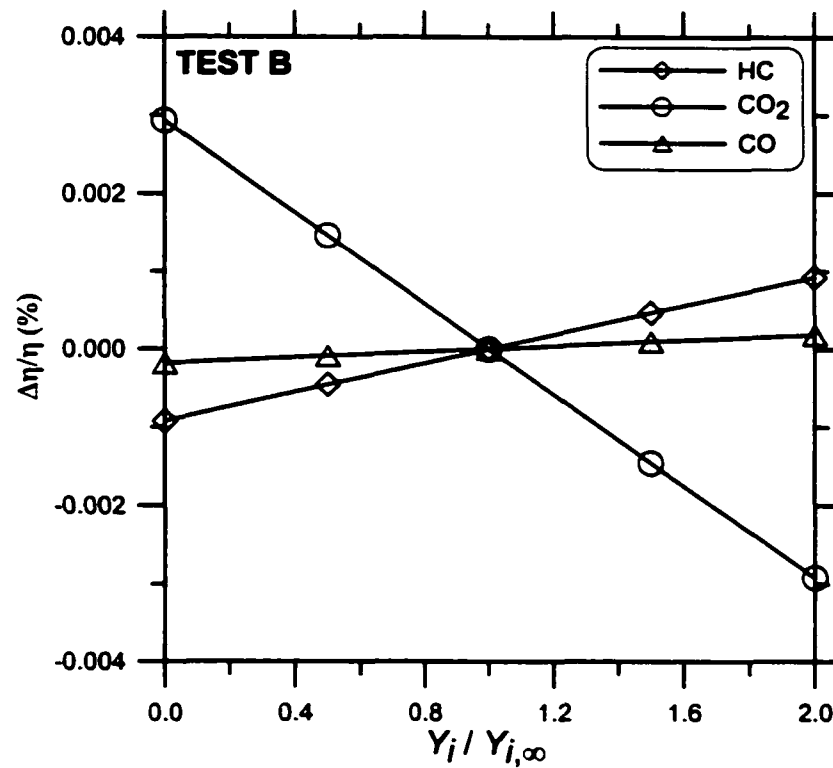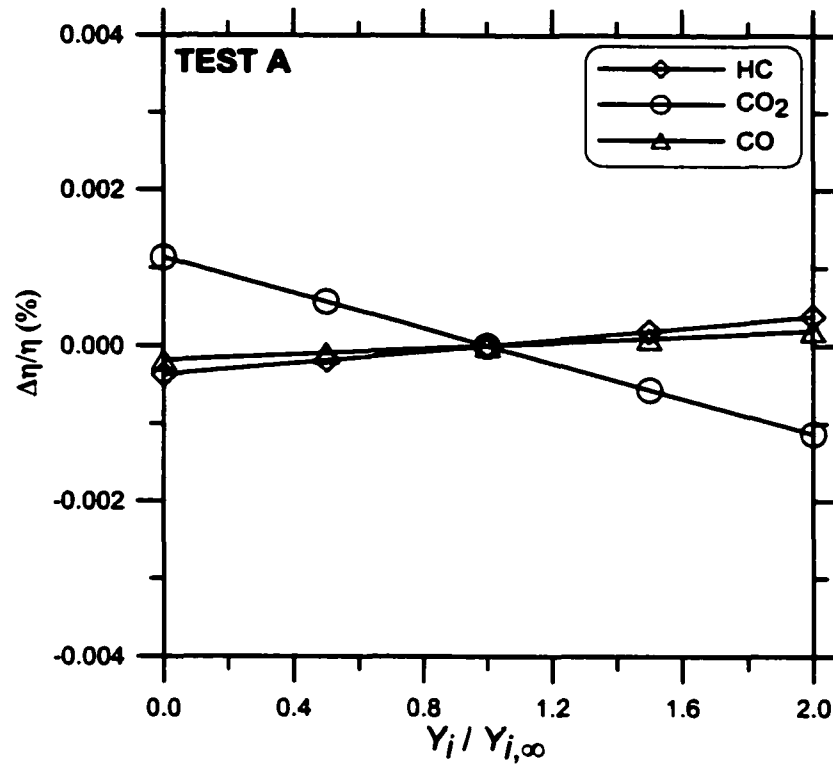
Figure 2.6: Percentage error introduced into the calculated efficiency by altering the background concentration for experiments A and B.

54

2.4.3 Simplified expression for efficiency

Since the background concentrations have a negligible effect on the calculated efficiency, the species mass balances, Eqs. 2.13-2.15, can be simplified as:

$$\eta = \frac{\dfrac{B}{(A+C)} - \dfrac{Y_{CO_2,flare}}{x'Y_{C_{x'}H_{y'}}}}{\left[1 + \dfrac{B}{(A+C)}\right]} \tag{2.17}$$

where

$$A = \frac{d}{dt}\left[\frac{Y_{HC}}{T}\right]_{t \to t'}, \qquad B = \frac{d}{dt}\left[\frac{Y_{CO_2}}{T}\right]_{t \to t'}, \text{ and} \qquad C = \frac{d}{dt}\left[\frac{Y_{CO}}{T}\right]_{t \to t'}. \tag{2.18}$$

This simplified expression for the efficiency depends on the temperature, the fraction of CO_2 in the flare gas, the fuel composition, and the rate of change in concentration of hydrocarbons, CO_2 and CO. Table 2.3 shows the values of the combustion efficiency for the two tests calculated using Eq. 2.17 to compare with the values calculated using the implicit expressions that include ambient background concentrations of the three relevant species.

2.4.4 Expected Uncertainty of Efficiency Measurements

An uncertainty analysis of Eq. 2.17 was performed based on the instrumentation used to measure the concentrations of hydrocarbon, CO_2 and CO, and the composition of the flare stream. The calculated uncertainty for a 99% confidence interval was shown to be 0.063 and 0.15 percent of the quoted efficiency for test conditions A and B, respectively.

55

These uncertainties are very small and provide confidence that the combustion efficiency can be measured accurately with this methodology. It should be noted that the uncertainties are small in this case because the flare gas stream composition is known accurately. Six hundred data points over ten minutes of testing were used to calculate the slopes of Y_i/T and the analyzers were operated in their most appropriate ranges for each test.

2.4.5 Sensitivity Study of Efficiency Measurements

As part of confirming that this approach to measuring efficiency is robust, it is important to show that the calculated efficiencies are not highly sensitive to errors in measured quantities. To determine this sensitivity, a small variation from the measured values of each variable in Eq. 2.17 was applied systematically and the effects observed. Table 2.4 lists the quantities measured as part of determining the efficiency of the two reported experiments.

Table 2.4: Measured parameter values for each experiment

Measured Parameter	Test A	Test B
Slope A (ppm/K·s)	1.83328×10^{-4}	5.05345×10^{-4}
Slope B (ppm/K·s)	9.23538×10^{-3}	6.83666×10^{-3}
Slope C (ppm/K·s)	8.46613×10^{-5}	1.06519×10^{-4}
$Y_{CO2, flare}$	5×10^{-5}	5×10^{-5}
$Y_{Cx'Hy'}$	0.98	0.98
x'	1.0016	1.0016

56

2.4.6 Sensitivity to Measured Slopes

Slope sensitivity has been tested by independently altering the magnitude of the variables A,B and C over a range of +/-20% from the measured value. Figure 2.7 shows the variation in the calculated efficiency relative to the efficiency based on the actual measured quantities. It can be seen that the calculated efficiency is most sensitive to the measurement of the slope associated with the CO_2 concentration. However, in all cases, the impact of incorrectly estimating any of the individual slopes does not produce an unacceptably large error in the calculated efficiency. One of the sources of error in the measurement of Y_{HC}/T results from using FIDs and the need for them to respond linearly with the number of carbon atoms in the hydrocarbon molecules. Since the expected error in this response is only a few percent, this sensitivity analysis shows that the error in the calculated efficiency will be less than 0.1%.

2.4.7 Sensitivity to CO₂ in Flare Gases

The technical grade methane used for the experiments contains very little CO_2 (<500ppm) but typical flare gases (natural gas or plant gases) may contain several percent of CO_2 in their mixture. Figure 2.8 shows the error introduced into calculated efficiency by artificially adding CO_2 relative to experiments conducted with no CO_2. It is important to note that lower efficiency flares (Test Case B), because they produce less CO_2, are more sensitive to not properly accounting for the CO_2 in the flare stream. For Test B the

57

artificial inclusion of 1% CO_2 in the flare gas produces a 1% error in the calculated efficiency and the calculated efficiency is linearly sensitive to the CO_2 in the fuel.

2.4.8 Sensitivity to Fuel Composition

The error introduced into the calculated efficiency due to an error in the mean carbon number (x') in the fuel is essentially zero ($<10^{-4}$ %) for variations in x' of +/-20% from the actual value. The reason for such insensitivity to knowing the hydrocarbon fuel gas composition can be seen in examining Eq. 2.17. The parameter x' only appears in the calculation of efficiency as a product with the volume fraction of CO_2 in the flare gases. Since these experiments were conducted with very little CO_2 in the flare gases, x' would be expected to have no influence on the calculated efficiency.

The sensitivity analysis is summarized in Figure 2.9, and shows errors introduced into the calculated efficiency for a 5% error in the measured slopes of hydrocarbons, CO_2 and CO, and the inclusion of 5% CO_2 in the flare gas stream. Eliminated from this comparison, because their magnitudes are essential zero, are the effects of accounting for background concentrations and x'. The calculated efficiency is most sensitive to the measurement of CO_2, for both its rate of accumulation and its concentration in the flare gases.

58
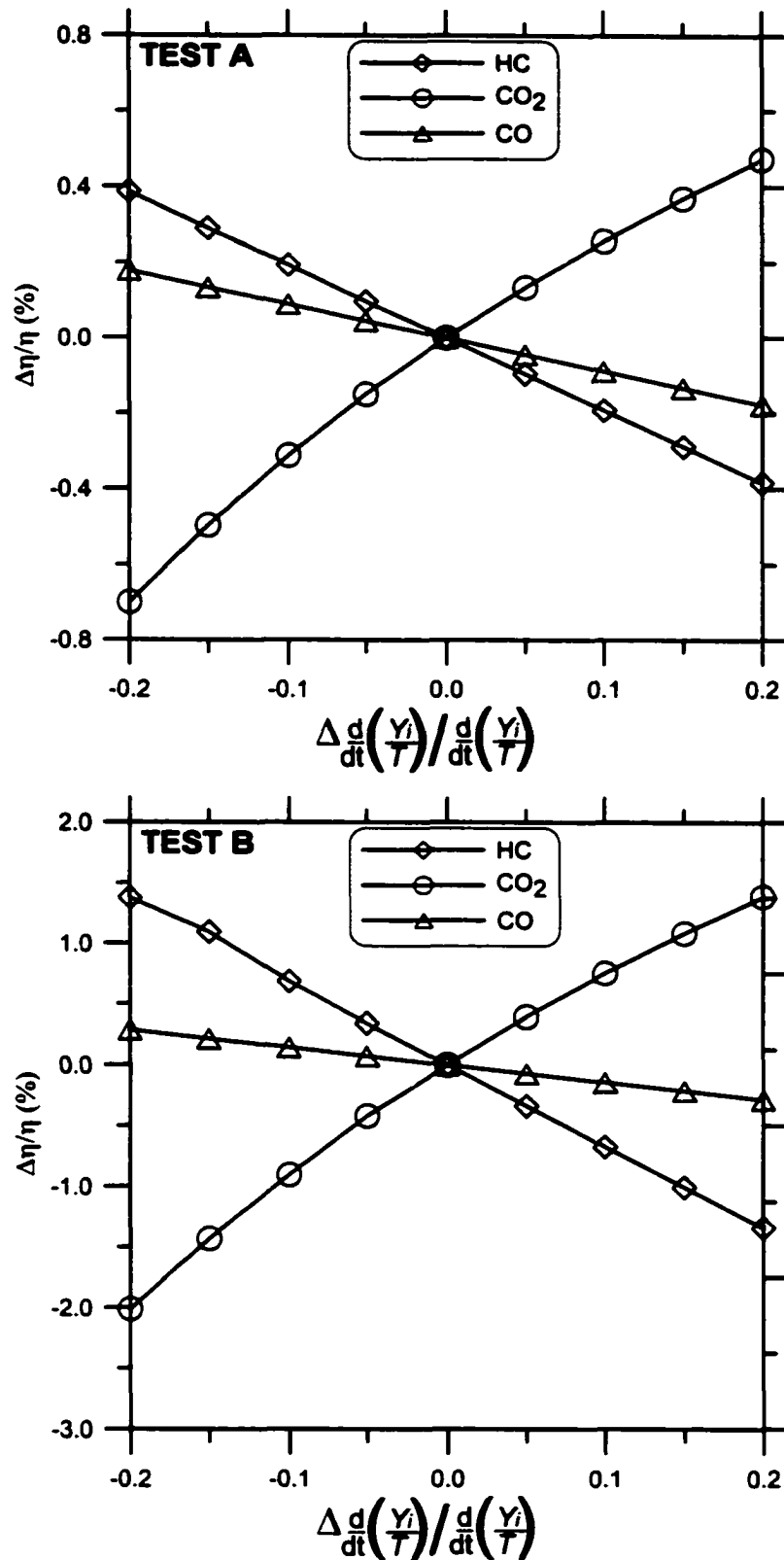
Figure 2.7: Percentage error introduced into the calculated efficiency as a result of altering the measured slope for experiments A and B.

59
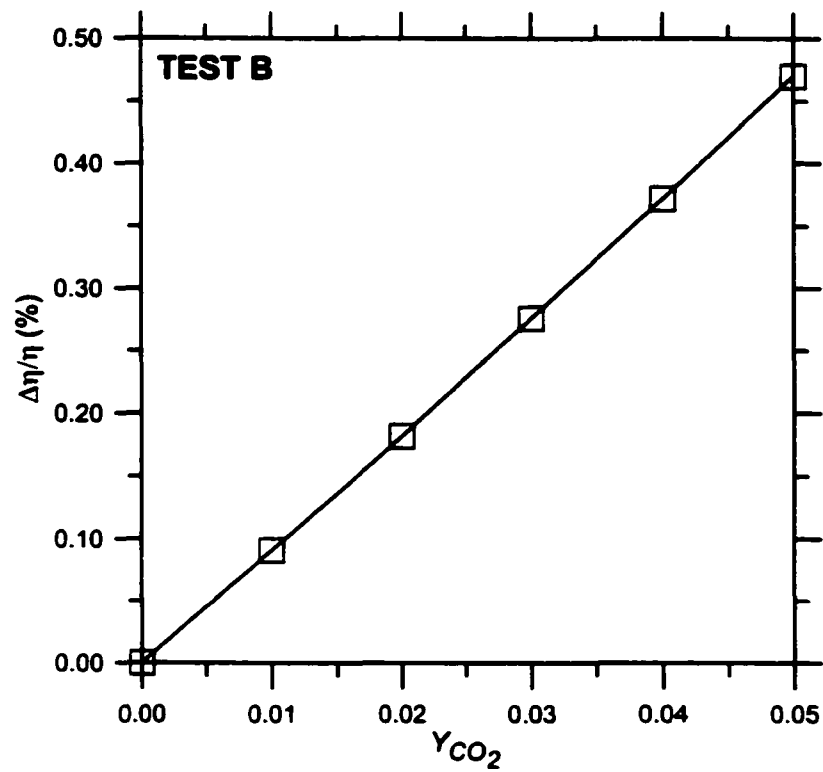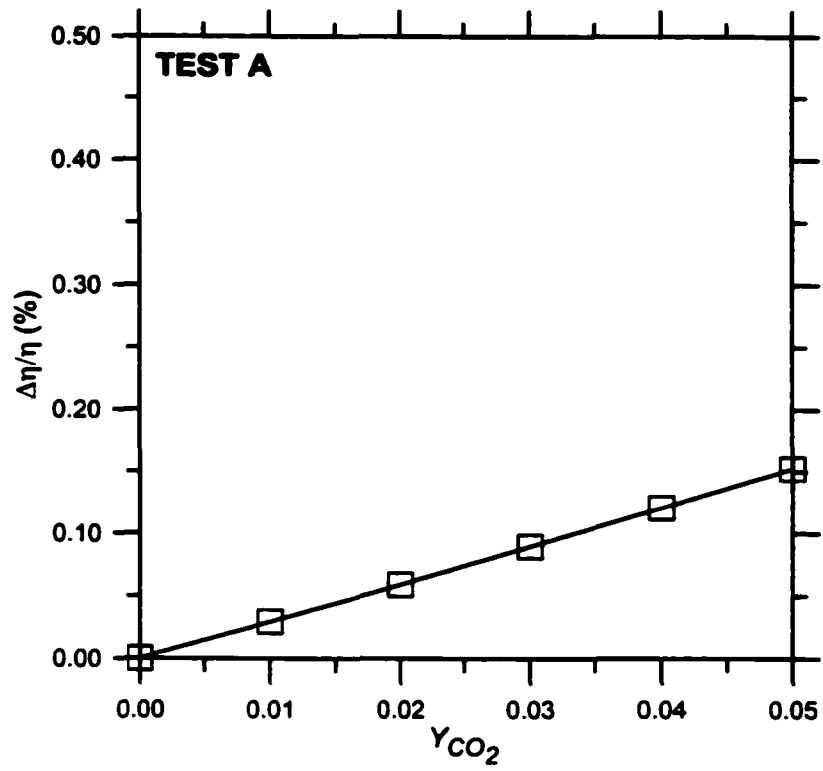
Figure 2.8: Percentage error introduced into the calculated efficiency as CO_2 concentration in the flare gases is artificially changed for experiments A and B.

60

TEST A

TEST B
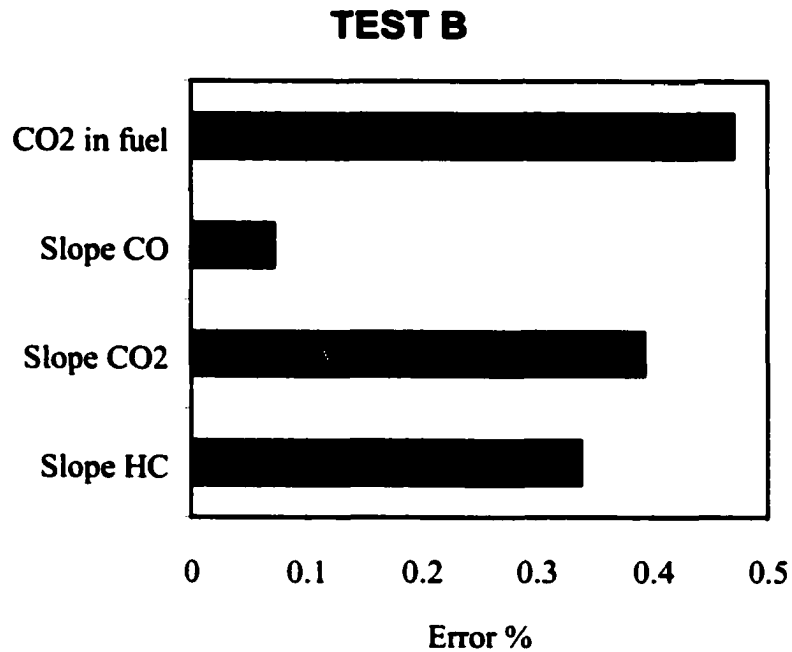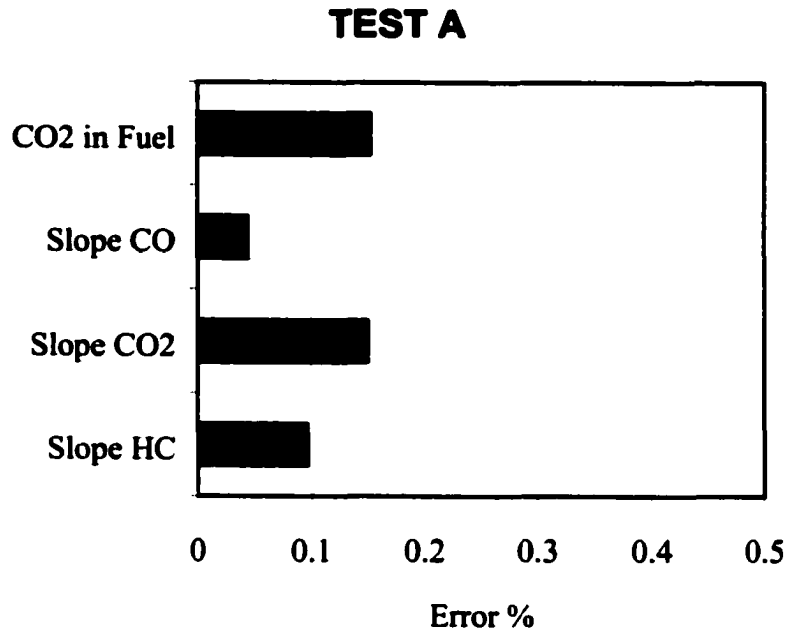
Figure 2.9: Comparison of the magnitudes of error introduced into the calculated efficiency as a result of a 5% variation in the measured slopes and the inclusion of CO_2 in the fuel gases for experiments A and B.

61

The methodology described above for measuring combustion efficiency is currently being used to quantify the relationships between V_{flare}, U_∞, flare gas composition (e.g., methane, propane and the addition of CO_2) and efficiency. The results of this series of tests will be presented elsewhere. This methodology is restricted to flares that produce only small amounts of soot so that a carbon mass balance in the wind tunnel can be based on the measurement of gaseous hydrocarbons, CO_2 and CO. The following section proposes an extension to this methodology that can be used when not all of the carbon can be accounted for in this way.

2.5 FLARES WITH SOOT AND INCLUSION OF LIQUID FUELS

Using a FID measurement to account for the carbon not oxidized by the flame becomes increasingly uncertain as soot is produced or heavier hydrocarbons condense after cooling. In these situations the mass balance for hydrocarbons is no longer a useful equation to help solve for the flare efficiency. To overcome this problem a mass balance equation based on a separate inert tracer gas (e.g., Sulphur Hexafluoride, SF_6) that is injected in the tunnel during the flare experiment can be used to close the system of equations. Using this approach also eliminates the need to monitor the accumulation of CO in the tunnel since all that is considered is the mass of carbon that does not become CO_2. In principle, this approach appears simpler than the method presented for non-sooting flares but it does require the measurements of mass flow rates and compositions of the fuel and tracer gas streams injected into the tunnel. These measurements need to be done accurately in order not to introduce large errors into the calculated efficiency.

Considering the liquid component of the gaseous flare stream as an organic compound with mean formula $C_{x''}H_{y''}$ and a molecular weight of $M_{C_{x''}H_{y''}}$, then the efficiency definition (Eq. 2.2) can be rewritten as:

$$\eta = \frac{Mass\ Flow\ Rate\ of\ Carbon\ in\ CO_2}{Mass\ Flow\ Rate\ of\ Carbon\ in\ (C_{x'}H_{y'} + C_{x''}H_{y''})} \tag{2.19}$$

or in molar flow rates as

$$\eta = \frac{\dot{n}_{CO2}}{x'\dot{n}_{C_{x'}H_{y'}} + x''\dot{n}_{C_{x''}H_{y''}}} \tag{2.20}$$

where x'' is the mean number of carbons in the liquid fuel. Defining the ratio of the mass flow rates of liquid to gas in the flare stream as

$$X_L = \frac{\dot{m}_{C_{x''}H_{y''}}}{\dot{m}_{C_{x'}H_{y'}}} \tag{2.21}$$

and the ratio of molecular weights as

$$M = \frac{M_{C_{x''}H_{y''}}}{M_{C_{x'}H_{y'}}} \tag{2.22}$$

allows Eq. 2.20 to be rewritten as

$$\eta = \frac{\dot{n}_{CO2}}{\dot{n}_{C_{x'}H_{y'}}\left(x' + x''\dfrac{X_L}{M}\right)} . \tag{2.23}$$

Following the same approach as Eqs. 2.13-2.15, the mass balance equations for CO_2 and SF_6 become

$$VT_\infty \cdot B = \eta\left(x' + x''\frac{X_L}{M}\right)Y_{C_{x'}H_{y'}} Q_{flare} + Q_{flare} Y_{CO_2,flare} \tag{2.24}$$

63

$$VT_\infty \cdot \frac{d}{dt}\left[\frac{Y_{SF6}}{T}\right]_{t \to t'} = Q_{SF6} .$$ (2.25)

Defining D as:

$$D = \frac{d}{dt}\left[\frac{Y_{SF6}}{T}\right]_{t \to t'}$$ (2.26)

then the flare efficiency can be explicitly written by combining Eqs. 2.23-2.26 as

$$\eta = \frac{1}{\left(x' + x''\frac{X_L}{M}\right)Y_{C_{x'}H_{y'}}}\left(\frac{B}{D}\frac{Q_{SF6}}{Q_{flare}} - Y_{CO_2,flare}\right) .$$ (2.27)

Experimental data is currently not available to examine the sensitivity of Eq. 2.27 to the various measured quantities and therefore this proposed methodology has not been fully validated. Inspection of Eq. 2.27 shows that it is now necessary to measure the mass flow rate of fuel and tracer gas streams to calculate the combustion efficiency. A preliminary analysis of this equation shows that these mass flows need to be measured to an uncertainty of the same magnitude as the uncertainty desired in the combustion efficiency.

2.6 CONCLUSIONS

The need to measure accurately the combustion efficiency of flares in a cross flow has required the development of a new experimental approach. The methodology developed here uses a closed-loop wind tunnel to create the cross flow and to capture all of the products of combustion. The work presented deals mostly with the situation when the

64

combustion products are gaseous and little or no soot is formed. In this case, a carbon balance based on measuring the accumulation rates of hydrocarbons, CO_2 and CO in the tunnel are used to calculate the combustion efficiency. Problems of leakage from the tunnel and re-burning due to the recirculation of gases are accounted for in the mass balances. To test the accuracy and robustness of this technique, two results from experiments with methane jet diffusion flames are presented. One of these flames has a high combustion efficiency (97%) and the other is forced to be lower (91%) by the imposition of a stronger cross flow. The expected uncertainty is shown to be less than 0.1% for these two cases. A sensitivity analysis shows that the most important measurements involve tracking the accumulation of CO_2 in the tunnel and knowing the CO_2 concentration as part of the flare stream. Errors of 5% in either of these measurements produce an error in the calculated efficiency of the order of 0.4%. Therefore, this methodology is shown to been an accurate and robust approach to measuring the combustion efficiency in these flows.

Also presented is a proposed extension to this methodology that will allow the combustion efficiency of sooting flames to be calculated. This method is based on monitoring only the CO_2 produced by the flame but requires an inert tracer gas to be injected during the test to account for leakage from the tunnel and difficulties in measuring the effective tunnel volume. This proposed methodology was not tested for accuracy or measurement sensitivity, but due to the increased number of variables that need to be measured, its accuracy is not expected to be as good as the carbon balance method.

2.7 REFERENCES

1. American Petroleum Institute (1990) *"Guide for Pressure-Relieving and Depressuring Systems"*, Recommended Practice 521, 3rd Edition, The American Petroleum Institute, Washington, 106 pages.

2. Bilger, R.W. and Beck, R.E. (1974) "Further Experiments on Turbulent Jet Diffusion Flames", *Fifteenth Symposium (International) on Combustion*, The Combustion Institute, Pittsburgh, pp. 541-552.

3. Buch, K.A., Dahm, J.A., Dibble, R.W., and Barlow, R.S. (1992) "Structure of Equilibrium Reaction Rate Fields in Turbulent Jet Diffusion Flames", *Twenty-Fourth Symposium (International) on Combustion*, The Combustion Institute, Pittsburgh, pp. 295-301.

4. Brzustowski, T. (1976) "Flaring in the Energy Industry", *Progress in Energy and Combustion Science*, Vol. 2, pp. 129-141.

5. Everest, D.A., Feikema, D.A. and Driscoll, J.F. (1996) "Images of the Strained Flammable Layer Used to Study the Liftoff of Turbulent Jet Flames", *Twenty-Sixth Symposium (International) on Combustion*, The Combustion Institute, Pittsburgh, pp. 129-136.

6. Galant, S., Grouset, D., Martinez, G., Micheau, P. and Allemand, J.B. (1984) "Three-Dimensional Steady Parabolic Calculations of Large Scale Methane Turbulent Diffusion Flames to Predict Flare Radiation Under Cross-Wind Conditions",

66

Twentieth Symposium (International) on Combustion, The Combustion Institute, Pittsburgh, pp. 531-540.

7. Gollahalli, S.R., Brzustowski, T.A. and Sullivan, H.F. (1975) "Characteristics of a Turbulent Propane Diffusion Flame in a Cross-Wind", *Transactions of the Canadian Society for Mechanical Engineering*, Vol. 3, No. 4, pp. 205-214.

8. Kalghagi, G.T. (1981) "Blow-Out Stability of Gaseous Jet Diffusion Flames. Part I: In Still Air", *Combustion Science and Technology*, Vol. 26, pp. 233-239.

9. Kalghatgi, G.T. (1981) "Blow-Out Stability of Gaseous Jet Diffusion Flames. Part II: Effects of Cross Wind", *Combustion Science and Technology*, Vol. 26, pp. 241-244.

10. Kalghatgi, G.T. (1982) "Blow-Out Stability of Gaseous Jet Diffusion Flames. Part III: Effects of Burner Orientation to Wind Direction", *Combustion Science and Technology*, Vol. 28, pp. 241-245.

11. Kalghatgi, G.T. (1983) "The visible Shape and Size of a Turbulent Hydrocarbon Jet Diffusion Flame in a Cross-Wind", *Combustion and Flame*, Vol. 52, pp. 91-106.

12. Kalghatgi, G.T. (1984) "Lift-Off Heights and Visible Lengths of Vertical Turbulence Jet Diffusion Flames in Still Air", *Combustion Science and Technology*, Vol. 41, pp. 17-29.

13. Muniz, L. and Mungal, M.G. (1997) "Instantaneous Flame-Stabilization Velocities in Lifted-Jet Diffusion Flames", *Combustion and Flame*, Vol. 52, pp. 91-106.

14. Pitts, W.M. (1988) "Assessment of Theories for the Behavior and BlowOut of Lifted Turbulent Jet Diffusion Flames", *Twenty-Second Symposium (International) on Combustion*, The Combustion Institute, pp. 809-812.

15. Strosher, M. (1996) *"Investigation of Flare Gas Emissions in Alberta"*, Alberta Research Council Report to Environment Canada, Alberta Energy and Utilities Board, and Canadian Association of Petroleum Producers, Calgary, Alberta, Canada, 145 pages.

16. Kramlich, J.C., Heap, M.P., Pohl, J.H., Poncelet, E., Samuelsen, G.S. and Seeker, W.R. (1984) *"Laboratory Scale Flame-Mode Hazardous Waste Thermal Destruction Research"*, U.S. EPA Report Number EPA600/2-84-06, Washington, D.C., 151 pages.

17. Kuipers, E.W., Jarvis, B., Bullman, S.J., Cook, D.K. and McHugh, D.R. (1996) *"Combustion Efficiency of Natural Gas Flares; Effect of Wind Speed, Flow Rate and Pilots"*, Internal Report, Shell Research and Technology Thorton and British Gas Research Centre, 13 pages.

18. Lee, K.C. and Whipple, G.M. (1981) *"Waste Gas Hydrocarbon Combustion in a Flare"*, Union Carbide Corporation, South Charleston, West Virginia.

19. Palmer, P.A. (1972) *"A Tracer Technique for Determining the Efficiency of an Elevated Flare"*, E.I. duPont de Nemours and Co., Wilmington, Delaware.

20. Pohl, J.H, Lee, J. and Payne, R. (1986) "Combustion Efficiency of Flares", *Combustion Science and Technology*, Vol. 50, pp. 217-231.

21. Siegel, K.D. (1980) "*Uber den Umsatzgrad von Facelgas in Raffinerie-Hochfackeln*" (Degree of Conversion of Flare Gas in Refinery Flares), Ph.D. Dissertation, University of Karlsruhe, Germany.

22. Soelberg, N.R. (1983) "*Evaluation of the Efficiency of Industrial Flares: Influence of Gas Composition*", U.S. EPA Report Number 600/2-83-070, Washington, D.C., 119 pages.

23. Joseph, D., Lee, J., McKinnon, C., Payne, R. and Pohl, J. (1983) "*Evaluation of the Efficiency of Industrial Flares: Background – Experimental Design – Facility*", U.S. EPA Report Number 600/2-83-070, Washington, D.C., 375 pages.

24. Wilson, D.J. (1979) "Wind Tunnel Simulation of Plume Dispersion of Syncrude Mildred Lake Site", Environmental Research Monograph, Syncrude Canada, 198 pages.

CHAPTER 3

EFFICIENCIES OF LOW MOMENTUM JET DIFFUSION FLAMES IN CROSSWINDS

This work was co-authored by one of my supervisors and myself. This work was solely my work, while the writing of the manuscript was conducted jointly.

3.1 INTRODUCTION

A diffusion flame burning in a crosswind is a basic combustion problem that has many applications. A common application occurs in the energy and petrochemical industries where this configuration is relevant to gas flaring – the process of disposing of unwanted flammable gases by burning them in a flame in the open atmosphere. In 1996, approximately 115 billion cubic meters of natural gas were flared or vented by these industries worldwide [1]. Since methane has a 21 times greater global warming potential than the carbon dioxide produced from its combustion (on a mass basis) [2], it is important that the combustion be as complete as possible. The level of combustion

70

completion of these flames is quantified by the ratio of carbon-mass originally in the hydrocarbon fuel to the carbon-mass in the produced carbon dioxide. This carbon mass balance across the flame is often referred to as the "combustion efficiency" of the flame.

Published research on the combustion efficiencies of jet diffusion flames burning in an open environment is limited. In a prominent study by Pohl *et al.*, gaseous hydrocarbon fuels issued from 0.076 to 0.305 m diameter vertical pipes and burned in near quiescent conditions [3]. The entire plume of combustion products was collected, sampled and analyzed to calculate the combustion efficiency. They concluded that if the flames were stable (which was a function of the exit velocity and heating value of the fuel gases), the efficiencies were greater than 98%. Other investigators introduced wind that blew perpendicular to the fuel jet as another experimental parameter [4,5]. Siegel [4] subjected his 0.7 m diameter flare to mild crosswinds and, through multi-point sampling found efficiencies greater than 99%. However, his apparatus only applied the wind to the flame above the stack and not to the stack itself. This flow configuration would not have created vortex shedding from the stack or a low-pressure region in the wake of the stack, which have an important influence in the overall flow field [c.f. 6,7]. Kuipers et al. [5] used passive Fourier Transform Infrared and Differential Absorption Light Detection techniques to remotely analyze the plume of a 0.6 m diameter flare burning primarily methane in the open environment. They found efficiencies greater than 99%, but commented that lower momentum jets may have reduced efficiencies when exposed to a crosswind.

71

In contrast to the works described above, Strosher [8] reported field measurements of a 0.1 m diameter solution gas flare where the products of combustion were sampled from a single aspirating probe. (Solution gas is the gas that comes out of crude oil when the oil pressure is dropped from reservoir pressure to ambient conditions.) The composition of the gas was found to be dominated by C_1 to C_6 hydrocarbons (94%). During this series of tests, where a photograph shows the flame partially trapped in the wake of the stack, the efficiencies were reported in the range of 70%.

Several researchers have also investigated jet diffusion flames in crosswinds where the interest has not been on the efficiency of combustion. Kalghatgi [9,10] developed correlations for blow-off limits; Birch et al. [11] considered the problem of jet ignitability; and Askari et al. [12] measured and modeled the concentration field of a natural gas jet. All of these researchers conducted their experiments in a regime where the fuel jet to crosswind momentum flux ratio (R) defined as

$$R = \frac{\rho_j V_j^2}{\rho_\infty U_\infty^2}$$

was 6 to 2633, where ρ is density, V and U are velocities, and the subscripts j and ∞ designate the fuel jet and ambient fluids, respectively. Momentum ratios in this range typically produce lifted flames, which differ significantly from the low momentum jets studied here.

Flows with relatively low jet-momentum compared to the crosswind momentum have also been studied [13-15] and produce "burner-tube, wake-stabilized" flames that are

72

relevant to continuously operating gas flares [8]. The velocity and concentration fields in this situation are complex, and the flame may manifest itself in one of several semi-distinct modes. In all cases, the flowfields of wake-stabilized flames are dominated by the presence of a standing vortex on the downstream side of the burner tube. The occurrence of wake-stabilized flames is not solely a function of R and may also depend on the flow conditions when the flame is ignited.

This paper will report results of measured combustion efficiencies of steady, low-momentum, jet diffusion flames in a crosswind. Data are presented on the effects of jet exit velocity, crosswind speed, and fuel type on the efficiency of combustion. A correlation based on buoyancy and momentum flux is presented that shows the relative importance of jet exit velocity and wind speed on the efficiencies of these flames. Short and long exposure photographic images are also presented that show that the types of flames created in these tests though different in color, have important similarities to those of Huang and Wang [14] even though they are scaled up by a factor of four. These images also provide insight into the mechanism of the breakdown in combustion efficiency at higher crosswind speeds.

3.2 EXPERIMENTAL METHODOLOGY

The experiments were conducted in a large closed-loop wind tunnel shown schematically in Figure 3.1. The internal volume of the tunnel is approximately 350 m³. A 150 kW DC motor drives a 3 m diameter fan that is capable of producing stable crosswinds of

73

between 0.4 and 35 m/s. Arrays of turning vanes are employed at each of the four ninety degree bends in the tunnel to maintain the integrity of the mean flow. A series of three fine mesh screens and a 6.3:1 area ratio convergent nozzle produce a near uniform plug flow in the 2.44 m wide by 1.22 m high test section that follows. In the vertical section downstream of the flame and in the upper section of the tunnel, a series of six supplementary mixing fans are used to ensure that the plume of combustion products is fully mixed into the wind tunnel air before sampling. A hotwire probe (0.004 mm diameter) was used to characterize the velocity field in the test section. Figure 3.2 shows representative mean velocity profiles along the axes of symmetry of the test section, at the stack location for a crosswind speed of 8 m/s. The velocity is essentially uniform between the boundary layers, which are approximately 12 cm thick at this position. The r.m.s. turbulent velocity fluctuation in the core flow was found to be consistently less than 0.4 % except at low wind speeds (<2 m/s) where this intensity rises to about 1.8%. Filtering has shown that this increase is a result of small, low frequency (<0.2 Hz) oscillations of the mean wind speed, which are associated with the control circuitry of the wind tunnel fan and not turbulence.

74
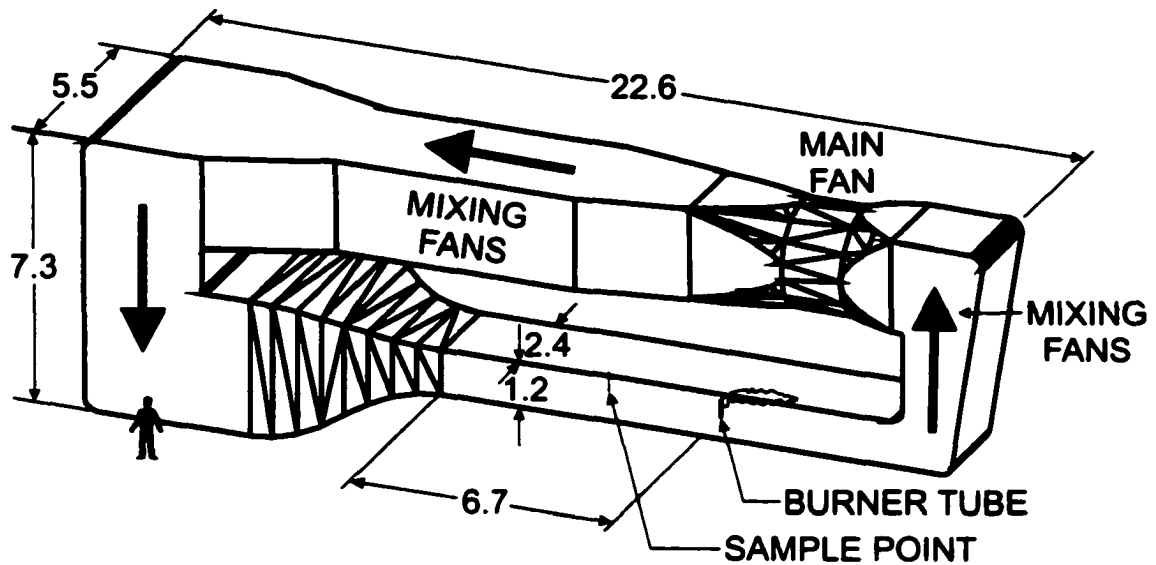
Figure 3.1: Schematic of closed-loop wind tunnel facility (All dimensions in meters)

For the data presented in this study, the diffusion flames were established at the exit of a 24.6 mm O.D. (22.1mm I.D.) pipe that extended between 30 and 85 cm into the wind tunnel. The height of the stack was varied to locate any flame outside the boundary layers of the tunnel walls. A 65% blockage ratio perforated plate "turbulence plug" with 3 mm diameter holes was placed inside of the pipe three pipe diameters upstream of the exit. The purpose of this plug is to create velocity profiles similar to turbulent pipe flow one would expect in full-scale industrial flares, independent of the actual flow velocity in the laboratory scale flares. Laser Doppler velocimetry was used to characterize the exit flow conditions of the burner tube. Figure 3.3 shows profiles of the mean velocity and turbulence intensity 5 mm above the exit of the burner tube for a mean jet velocity (V_j) of 2 and 4 m/s. The characteristic velocity, V_j, is the volume flow rate of fuel at ambient conditions divided by the inside area of the burner tube. Sales grade natural gas (95.2% CH_4, 2.1% C_2H_6, 1.7% N_2, 0.8% CO_2, 0.2% other) and sales grade propane (97.7% C_3H_8, 1.8% C_2H_6, 0.5% other) were used as fuels.

75
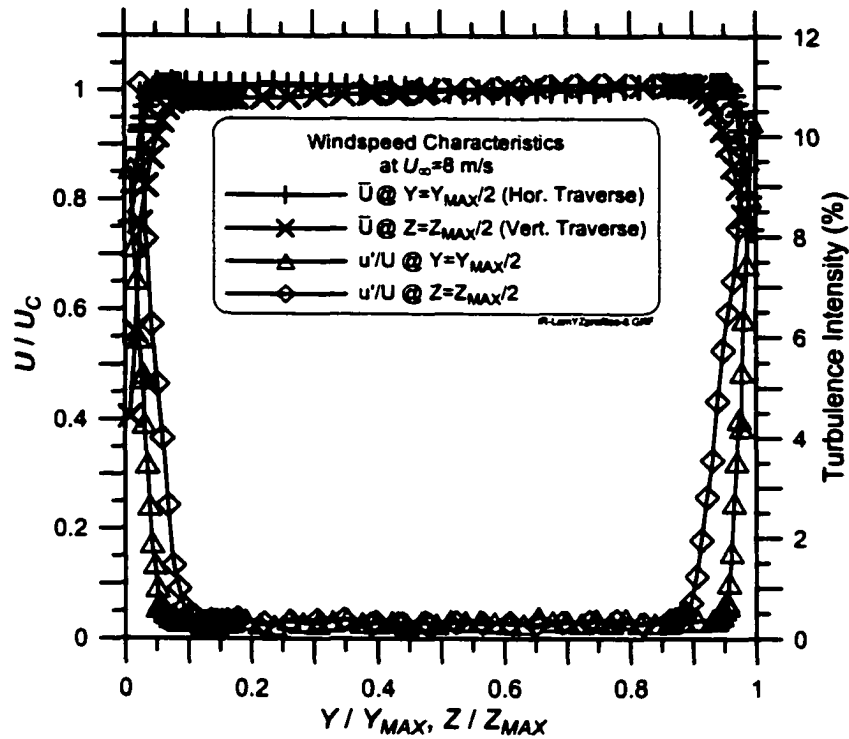
Figure 3.2: Horizontal and vertical traverses of mean velocity and turbulence intensity across the test section of the wind tunnel. U_C is the mean velocity at the center of the traverse.
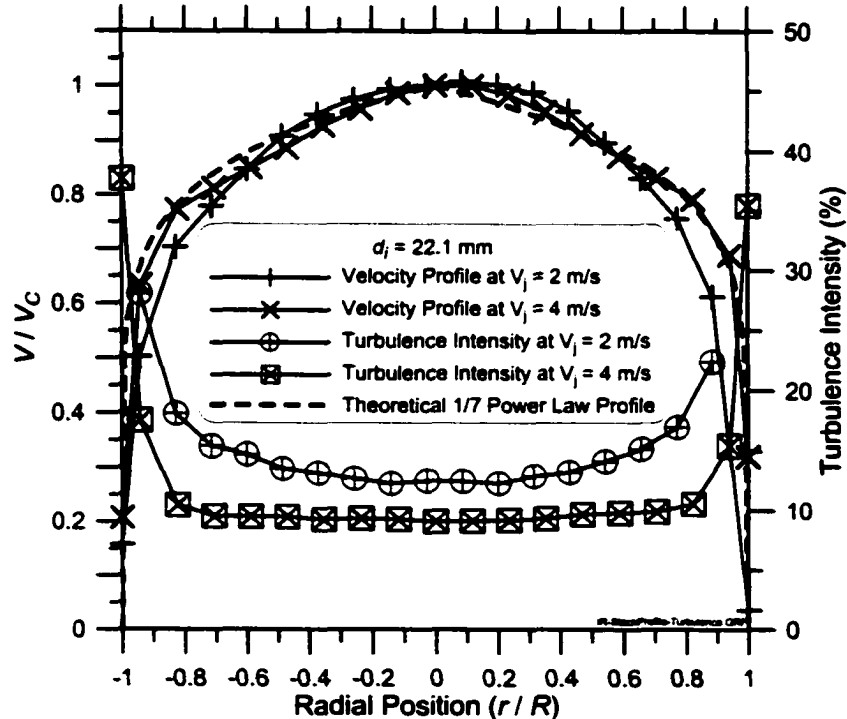
Figure 3.3: Mean velocity and turbulence intensity measured 5 mm above the exit plane of the burner tube. V_C is the mean velocity at the center of the traverse.

76

Photographs of the flames were taken using a 35 mm camera with 1600 a.s.a. color slide film. To acquire images of the natural gas flames, a 50 mm lens was used that had a maximum aperture size corresponding to f = 1.6. This large aperture was necessary to capture the low luminosity natural gas flames. To accommodate the longer propane flames, a 20 mm lens (maximum aperture size f = 2.8) was used. During the development process the film was "pushed" to 6400 a.s.a. for the natural gas flames and to 3200 a.s.a for the propane flames.

The methodology for calculating the combustion efficiency of the flames has been discussed in detail previously [16] and will only be briefly reviewed here. By using a closed-loop wind tunnel, the products of combustion were contained and mixed into the air stream before sampling. Concentrations of the major carbon-containing species, carbon dioxide (CO_2), carbon monoxide (CO), and unburned hydrocarbons (HC), were continually monitored using a suite of online gas analyzers. Figure 3.4 shows time traces of the concentrations of these species in the wind tunnel during a typical experiment.

77
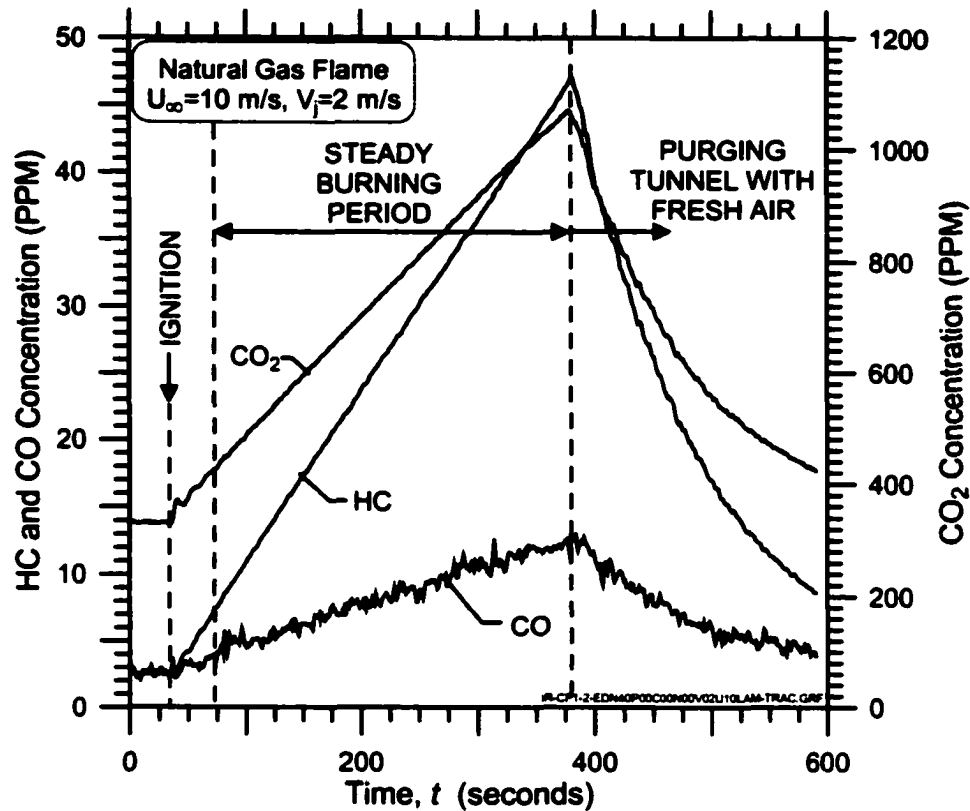
Figure 3.4: Measured concentrations of major carbon containing species in the wind tunnel during a typical experiment and tunnel purge cycle

Prior to ignition, the tunnel was filled with fresh air ($[CO_2]\sim350$ ppm, $[HC]\sim3$ ppm, and $[CO]\sim3$ ppm). The fuel flow was set and in Figure 3.4, ignition occurred at $t\sim30$ s, and following a brief startup transient, steady burning continued to $t\sim375$ s. At this point the fuel was shut off and after a brief delay the tunnel gases were purged with fresh air to begin the next test. The rates of accumulation of these species during the steady burning period were used to calculate a mass balance for the combustion process based on the mass of carbon in each species. The combustion efficiency (η) of the flame is defined as

$$\eta = \frac{mass\ accumulation\ rate\ of\ carbon\ in\ the\ form\ of\ CO_2\ produced\ by\ the\ flame}{mass\ flow\ rate\ of\ carbon\ entering\ the\ flame\ in\ the\ form\ of\ hydrocarbon\ fuel}$$

78

where, the denominator of this expression is calculated from the sum of the accumulation rates of CO_2, CO and unburned hydrocarbons, and therefore leakage from the tunnel is inherently accounted for in the mass balance. As discussed in [16], this definition of efficiency neglects the mass of soot in the combustion products which is shown to be a reasonable assumption for the fuels studied here based on measurements of soot production in [3, 17].

The wind tunnel is sufficiently large that, during a typical 5 to 10 minute test, the concentration of HC in the tunnel remains small (<250 ppm) and the effects of reburning are completely negligible [16]. This technique of tracking the accumulation rates of each species to calculate a carbon mass balance permits very accurate measurements of the efficiency. Typically, the experimental error in the measured combustion efficiency is less than 0.5% absolute. To emphasize the increase in emission produced by the flare the results are presented in terms of the combustion inefficiency ($1-\eta$).

3.3 RESULTS AND DISCUSSION

3.3.1 Visual Observations

Figure 3.5 show a series of short and long exposure photographs of what are in general highly luminous propane flames in a crosswind. Comparable images of natural gas flames are shown in Figure 3.6. While the long exposure photographs show the overall position and size of the flame, the short exposure images provide an interesting insight

79

into the various fluid mechanic structures in the flow as the shear layer vorticies are made visible by the flame. The diameter of the stack used in the current work is about four times larger than that used in previous studies [13-15] and there are significant similarities and differences between the flames at these two scales. In general, the average shape and structure of the flames at these two scales are quite comparable as discussed below. The fact that these similarities exist over a factor-of-four change in diameter is encouraging for the feasibility of modeling simple flares over a wide range of scales. The external cold-flow Reynolds number (Re) for this 24.6 mm diameter flare ranges from 1570 to 25,120 as the crosswind is increased from 1 m/s to 16 m/s, which is in the regime of laminar boundary layer separations. The next expected transition of the external flow regime will not occur until Re reaches $\sim 5 \times 10^5$ where the stack boundary layer becomes turbulent. As an example, this transition occurs at 16 m/s when the stack diameter is 470 mm and hence puts many industrial flares in the same external flow regime as the laboratory flares being tested here.
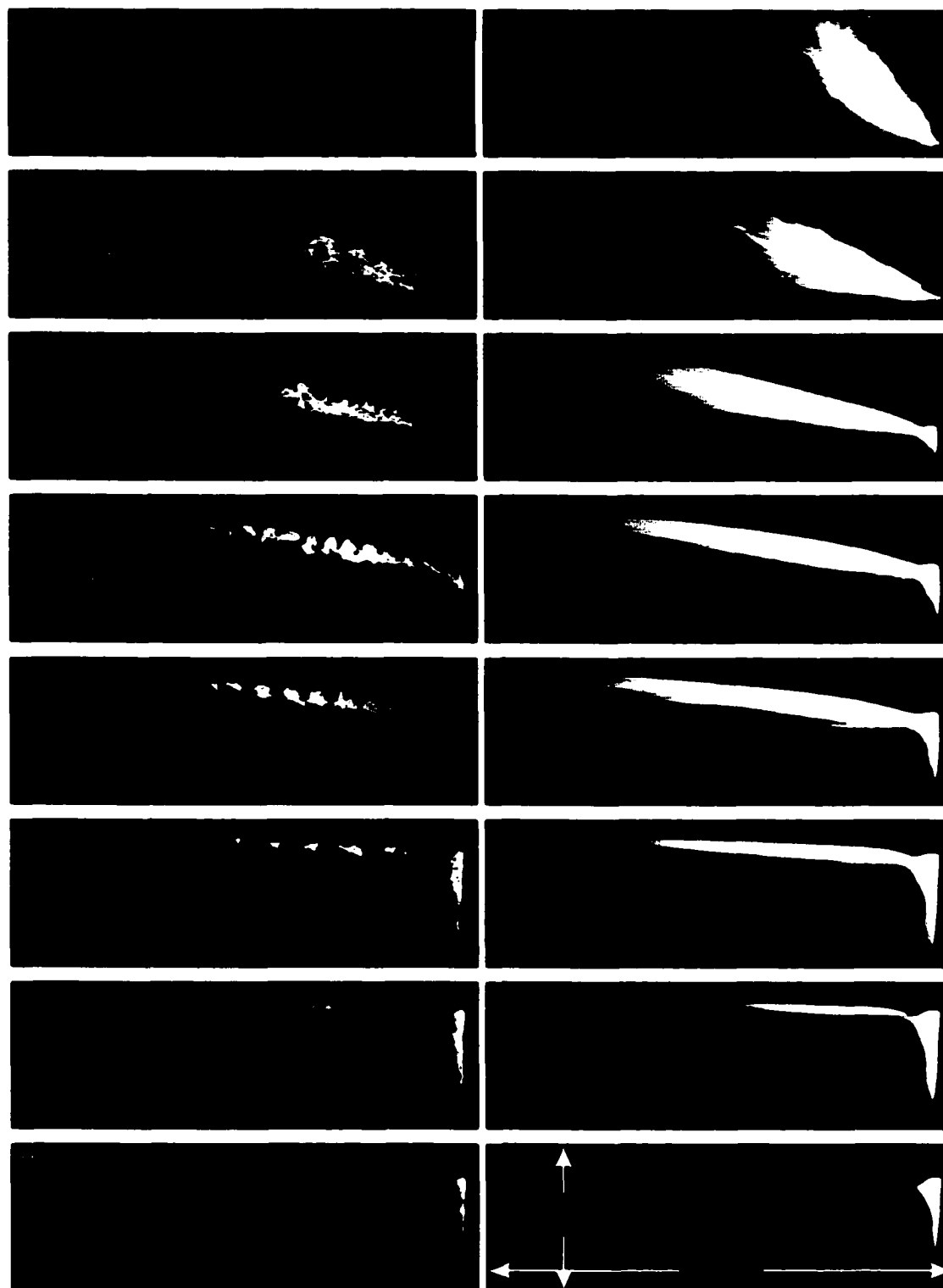
Figure 3.5: Short and long exposure photographs of propane flames in a crosswind

81
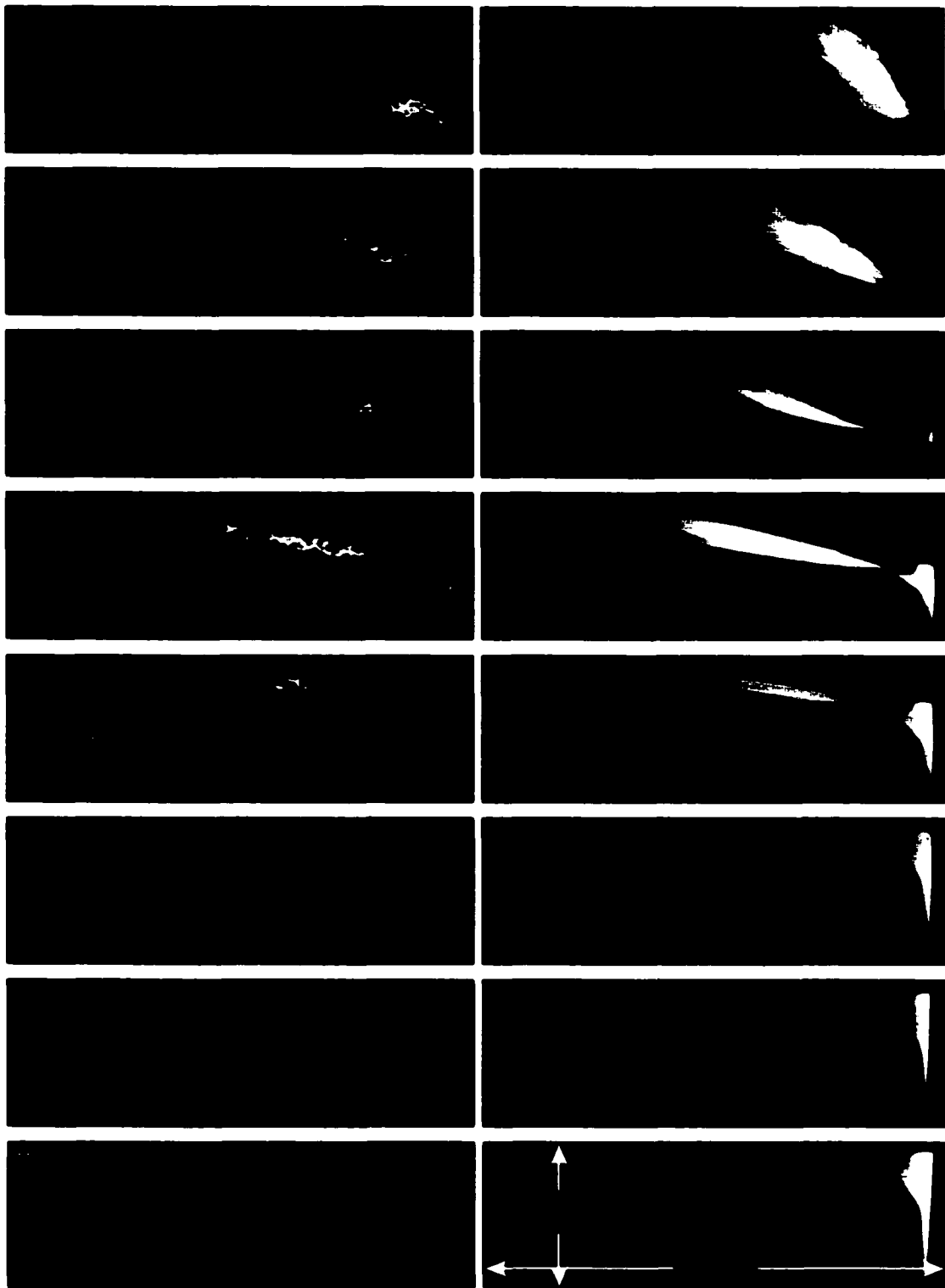
Figure 3.6: Short and long exposure photographs of natural gas flames in a crosswind where the conditions have been chosen to match the momentum flux ratios in Figure 3.5.

82

At the higher momentum flux ratios shown in Figure 3.5 (e.g., $R = 5.78$) the propane flame exists above the stack and is highly radiative. As the crosswind velocity is increased and R is reduced to 1.32 the onset of "downwash" occurs as a portion of the burning gases verge on being drawn into the low-pressure region on the leeward side of the stack. While not readily apparent in the photographs, at this and lower momentum flux ratios the shear layer between the propane fuel and the air changes such that the upper portion becomes a non-reacting mixing layer, akin to a lifted flame, as shown schematically in Figure 3.7. At one quarter of this scale, visual observations of propane flames show that a similar transition to a downwashed flame occurs at a slightly higher momentum ratio ($R \sim 3.5$) [13].

As R is further reduced, the three-zone flame structure described by Gollahalli and Najundappa [15] becomes apparent for the current burner size. As sketched in Figure 3.7, a planar stationary vortex attached to the burner tube defines the first zone; the long axisymmetric tail of the flame forms the second zone; and the junction that connects these two main parts of the flame defines the third zone. While the recirculating vortex may not be clearly defined in photographs, it is easily apparent to the naked eye when the flame is in motion. This recirculation zone grows down the tube as R is reduced, and may extend 30 diameters or more down the leeward side of the stack.

For the images presented here, the jet exit velocity of the fuel, V_j, was held constant at 2 m/s and the crosswind speed, U_∞, was varied from 1 to 27 m/. Thus, for a given fuel type, this fixes the mass flow rate of fuel. Also, noted on each of the images is the

83

combustion efficiency (discussed in detail later) and for most of the flames only a small fraction of the fuel is not consumed. Therefore, for all but the very low values of R, the size of the flames shows qualitatively where the same mass of fuel is consumed in the different flame modes. Previous images [13-15], fixed U_∞ and varied V_j, which alters the bulk flow rate of fuel and is a contributing reason for changing flame size and shape. Initially the effect of the crosswind is to increase the overall length of the flame. However, after reaching its peak length between $R = 0.15$ and $R = 0.084$, the flame shortens with further increases in wind speed. This maximum length corresponds with the appearance of detached pockets of combustion, which are apparent in the short exposure photographs. By contrast, as illustrated in the photographs, the width of the flame decreases monotonically with increased wind speed. Ultimately, at very low R, the main tail of the flame is extinguished and only the recirculating vortex of zone 1 remains of the original three zone flame.
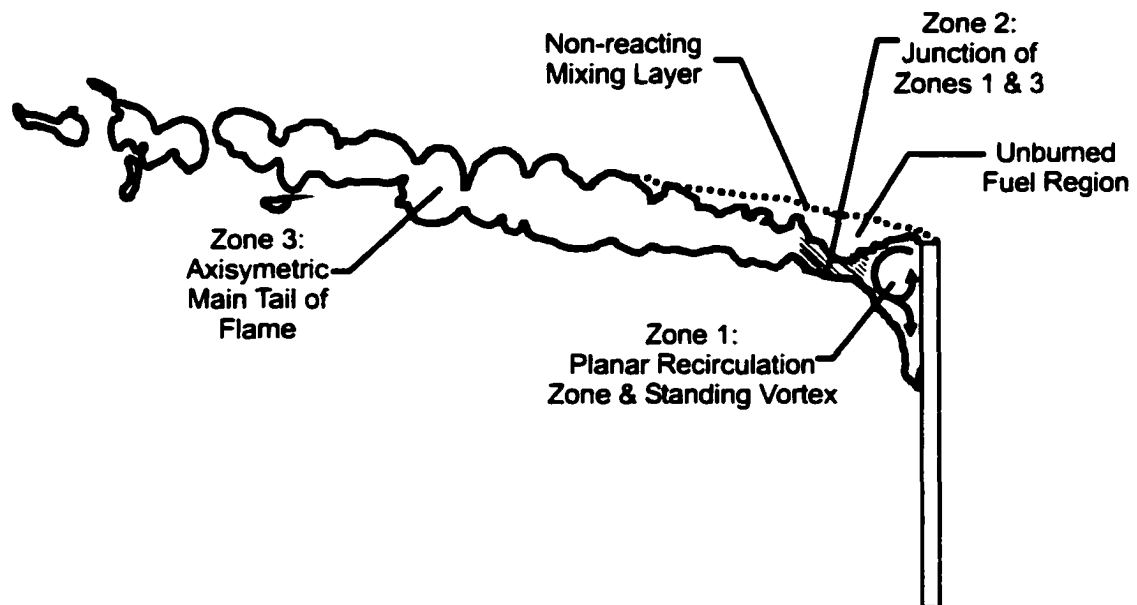
Figure 3.7: Sketch of flow structures in a low-momentum jet diffusion flame in a crosswind

84

Gas chromatographic analyzes of the unburned hydrocarbons collected in the tunnel show they have a very similar volume fraction distribution as the hydrocarbon fuel stream (i.e., hydrocarbon emissions from natural gas flares are primarily methane while emissions from propane flares are primarily propane). These results suggest that inefficiencies of the flare are mainly due to a portion of the fuel being stripped from the flare stream prior to the flow reaching any flame zone to burn these gases. This stripping mechanism is supported by the local extinctions observed in the short duration photographs as a result of intense mixing with air that dilutes the fuel beyond its lean limit. This notion of a lean-limit extinction for low-momentum flames in a crosswind has also been proposed in [15].

While the average structure of these flames shown in Figure 3.5 are quite similar to that of the smaller scale propane flames previously described [13-15], the color of the flames are noticeably different. The current images do not show the blue flames observed by Huang and Chang [13] despite the fact the fuel used in both studies was propane. To verify this observation, tests were conducted in the current facility on an identical 6.4 mm burner tube to that described in [13]. At this smaller scale, the blue regions in the flame were again apparent. The reasons for this difference are unclear at this time but may be associated with the mixing processes between the fuel jet and the air very near the jet exit.

Figure 3.6 shows images of natural gas flames with the same approximate value R and the same fuel jet exit velocity as the propane flames in Figure 3.5. In general these

85

flames were much less luminous and they are shorter in length since less oxygen needs to be entrained into the flame to burn equal volumes of fuel. This difference in flame length is more pronounced than the photographs and the change of scale of the images should be noted. Despite the differences in flame color and length, the flow structures of the natural gas flames are essentially the same as the propane flames. These images are the first side by side comparison of wake-stabilized flames combusting two different fuels.

The shapes and positions of the flames for the two fuel types are qualitatively related to the momentum ratio, R, as suggested by [18, 19], but important changes in structure do not coincide at fixed values of R. For example, the maximum flame length of both the propane flames and the natural gas flames occurs in the vicinity of R=0.15, but the extinction of the tail region of the flame (zone 2) occurs at a much higher momentum ratio (R=0.021) for the natural gas flames than the propane flames (R=0.0085). It seems apparent that R alone is not sufficient to account for the visual differences between the propane and natural gas flames.

3.3.2 Efficiency Measurements

Figure 3.8 shows the measured combustion inefficiencies (1-η) of low-momentum propane flames in a crosswind. These results demonstrate that the crosswind has a strong effect on the inefficiency of the combustion with a dependence that is approximately cubic. At relatively low wind speeds the inefficiencies are quite low ($< 0.25\%$), but as the crosswind is increased the inefficiency rises dramatically. There is an apparent

86

breakpoint in the propane curves in the vicinity of 2% inefficiency, after which the combustion efficiency degrades extremely rapidly with further increases in the wind speed. Figure 3.8 also shows that combustion efficiency depends on the mean fuel jet exit velocity, V_j. Higher velocity fuel jets are less sensitive to the effects of crosswind. For example, at $U_\infty = 12$ m/s, the 1 m/s propane jet has an inefficiency of 6% whereas for the 2 m/s propane jet, the inefficiency is only 1%.
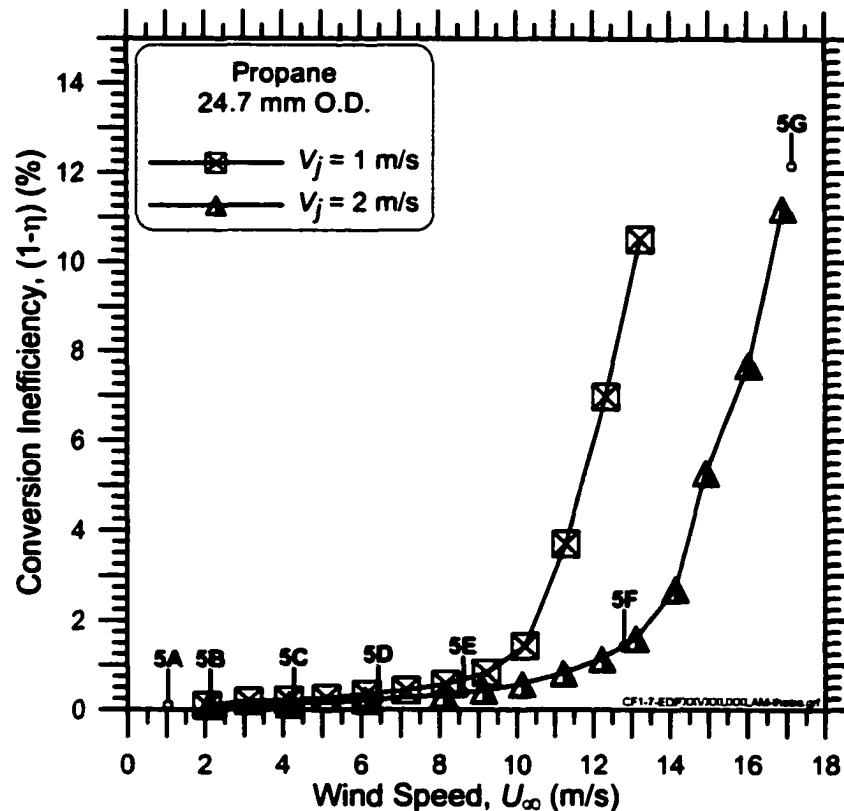
Figure 3.8: Inefficiency curves for propane flames that show a strong dependency on crosswind and the effects of altering the exit velocity of the jet. Points 5A-5G relate to images A through G in Figure 3.5.

The inefficiency curve for $V_j = 2$ m/s in Figure 3.8 reference the photographs of Figure 3.5 to connect the physical appearance of the flame with the measured inefficiency.

From these results it seems that in order to provoke significant inefficiencies, the crosswind must be of a magnitude to create detached flame pockets over the length of the flame and the onset of the disappearance of the tail region of the flame. Simply having a flame bent over with the windward side of the flame detached from the stack or having the flame base trapped in the recirculating flow in the wake of the stack is not sufficient to cause significant inefficiencies.

Inefficiency curves for the natural gas flames are shown in Figure 3.9. The shapes of these curves are very similar to those of the propane flames in Figure 3.8 and show the same approximately cubic dependence of inefficiency on wind speed. Although the "break point" in the curves also takes place at an inefficiency of approximately 2%, the ensuing rise in inefficiency is not as severe. Still, the natural gas flames are much more susceptible to the effects of crosswind than the comparable propane flames. For a natural gas flame with a jet exit velocity of 2 m/s at a crosswind speed of 11 m/s, the inefficiency is 11% whereas a propane flame under these same conditions has an inefficiency of only 0.8%. Referring to the photographs in Figure 3.6, it is again apparent that significant inefficiencies occur only after the flame is burning in detached pockets. Taken collectively, the analysis of the unburned hydrocarbons, the series of photographs, and the shape of the inefficiency curves all support the idea that the inefficiencies are caused by fuel stripping and/or local extinction.

It is worth noting that the data in Figure 3.9 for $V_j = 3$ and 4 m/s shows a slightly different shape than the other combustion inefficiency curves. At lower crosswind speeds

88

$(2 < U_\infty < 7$ m/s) these curves flatten out at ~1% inefficient. These measurements are "real" in that the measurement technique is still reliable at these levels and the data are repeatable. At these exit velocities the flame is near the transition from a rim stabilized flame to a lifted flame and may therefore result in a second source for fuel stripping at lower velocities that is not available in lower jet velocities. In the current experimental set-up it is difficult to validate this hypothesis since higher exit velocities of either natural gas or propane produce flames that impinge on the ceiling of the tunnel and are too large to test.
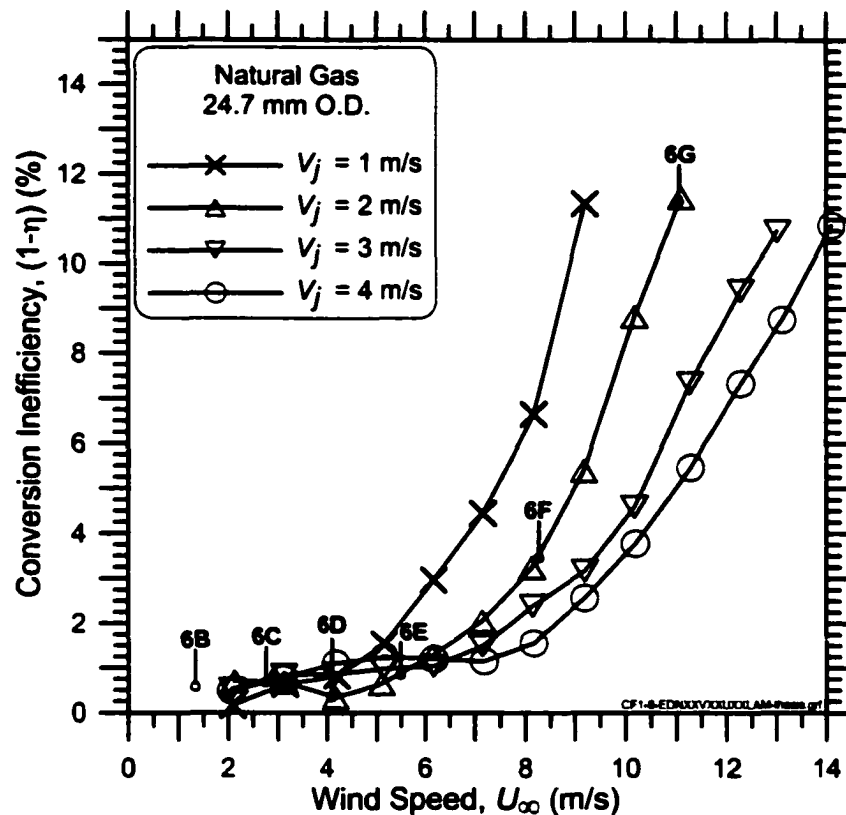
Figure 3.9: Inefficiency curves for natural gas flames. Points 6B-6G relate to images B through G in Figure 3.6.

Initial attempts to model the combustion efficiencies of these flares involved trying to connect geometric similarities in the mean flame shape to the measured inefficiencies. The photographic images presented here and other works [13-15,18, 19] suggest that the momentum flux ratio (R) between the fuel jet and air stream is important in determining the flame shape. Unfortunately, the inefficiency data do not collapse with respect to R since the magnitude of inefficiency shows a significantly greater dependency on U_∞ than V_j, where as R weights these velocities equally.

An alternate force balance worth considering that may play a role in these flows is characterized by a Richardson Number (Ri), which is a ratio of momentum to buoyancy forces. Comparing the mass of air to the mass of fuel involved in combustion, the air stream is the dominant momentum in the flow and the Richardson Number is expressed as

$$Ri = \frac{g(\Delta\rho/\rho_\infty)L}{U_\infty^2}$$

(3.1)

where g is the gravitational constant, L is a characteristic length scale of the flow and $\Delta\rho$ is the local density difference between two streams. It should be emphasized that Richardson Numbers are well defined for non-reacting flows, but in the case of wake-stabilized flames air is entrained into both the cold jet and the hot products (see Figure 3.7). Having more than one density difference to consider creates an ambiguity regarding which $\Delta\rho$ is appropriate. To help correlate the inefficiency data, Ri needs to be recast in a form that replaces $\Delta\rho$ with the mean exit velocity of the fuel jet. This manipulation is done by returning to the simplified case of a non-reacting plume as

90

shown in Figure 3.10. As the plume is advected downstream it entrains air, which reduces the density difference between the plume and the ambient air, and the cross-stream dimension of the plume increases. At the source location the conditions are set by the initial flow rate ($q_O = \pi V_j R_{source}^2$) and an initial density difference ($\Delta\rho_O$). At any downstream location, where the jet velocity has become indistinguishable from U_∞ (i.e., once the plume is fully bent over), the flow rate through the cross-section of the plume is

$$q = \pi U_\infty R_{plume}^2 .$$
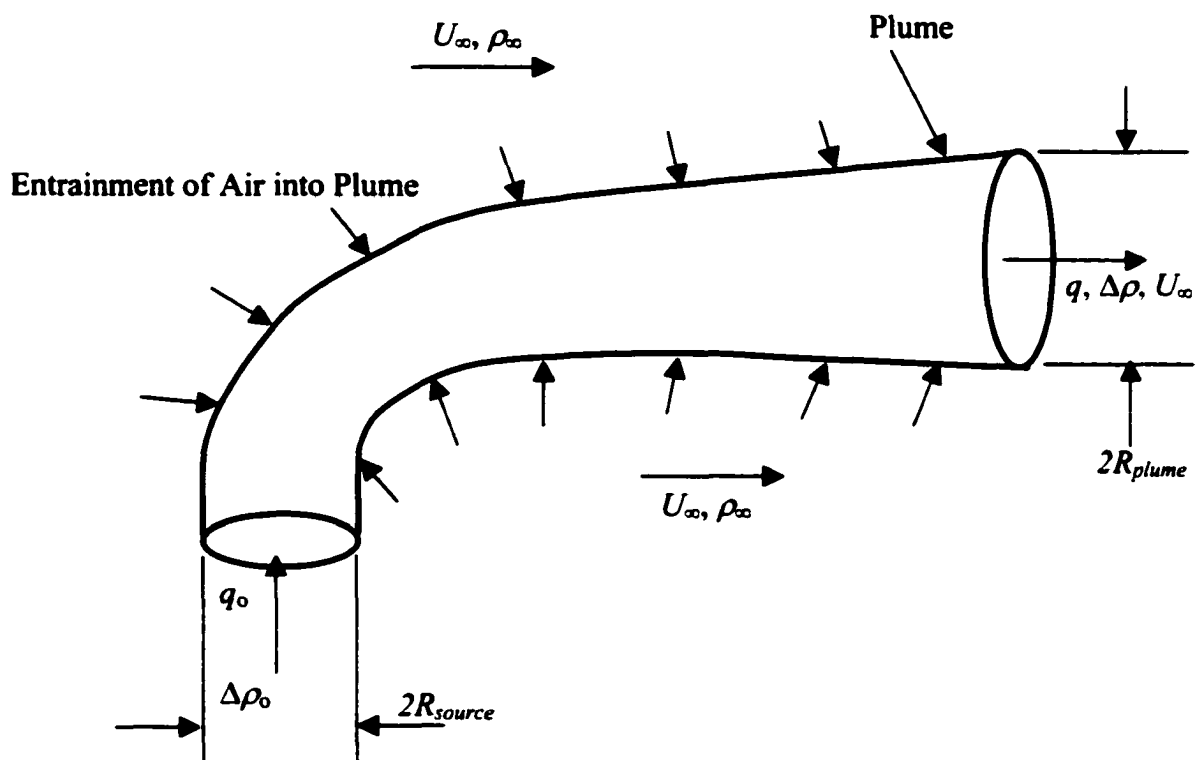
Figure 3.10: Sketch of the entrainment of ambient air into a bent over, non-reacting plume.

Conservation of mass requires that $q_o \Delta \rho_o = q \Delta \rho$ when the flow is at constant pressure

and the local density difference in Eq. 1 can be replaced by

$$\Delta \rho = \frac{V_j R_{source}^2}{U_\infty R_{plume}^2} \Delta \rho_o \qquad (3.2)$$

and the Richardson Number becomes

$$Ri = g \frac{V_j}{U_\infty^3} \frac{\Delta \rho_o}{\rho_\infty} \left(\frac{R_{source}}{R_{plume}} \right)^2 L \qquad (3.3)$$

This form of the Richardson Number now explicitly relates the jet exit velocity to the air

velocity and reduces the density difference to a single value. Terms relating to physical

scaling (R_{source}, R_{plume}, and L) have become more complex and contain information on

how the plume size is affected by combustion. For our purposes here, the valuable part

of the analysis is the explicit velocity dependency suggested by the ratio of buoyancy to

momentum forces. In that light, the predicted velocity dependency, if the combustion

efficiency was strongly connected to the interaction of buoyancy and momentum, can be

expressed as

$$\eta \propto \frac{U_\infty}{V_j^{1/3}} \qquad (3.4)$$

where this form of the velocity ratio is chosen to maintain the same general shape of

inefficiency curve as presented in Figures 3.8 and 3.9. Figure 3.11 shows that the

inefficiency data for the natural gas and propane flames are effectively collapsed for each

of the fuels through the use of this $U_\infty / V_j^{1/3}$ parameter. The collapsing of the data by

this parameter lends some credibility to the importance of buoyancy and momentum in

these flows, but important features are not accounted for in this approach. For example,

92

the inefficiency curves of the two fuels are different and those differences need to be better understood.

Initially, it was proposed that density was the most important difference between methane and propane that needed to be considered. With the model of fuel stripping being the likely cause of the inefficiency, it was felt that methane could be more easily stripped from the flow because of its lower density and result in higher inefficiencies. Attempts to collapse the data for the two fuels by ratios of density differences with respect to air (i.e., $\Delta\rho_{o,propane}/\Delta\rho_{o,methane}$) or simple ratios of densities suggested by Ri or R, respectively, do not work. Further attempts to use densities associated with the product gas temperature also fail to bring the data from the two fuels together because methane and propane have very similar product densities.

To further understand the full range of physical processes that participate in setting the combustion inefficiency, Figure 3.11 includes data from a fuel stream created by blending 60% propane with 40% CO_2 at three exit velocities. CO_2 was chosen as the diluent to maintain the same fuel jet density as pure propane. As a result, this blended fuel has the same cold flow density difference as propane and the same momentum flux as propane for the same exit velocities. Despite these similarities, Figure 3.11 shows this blended fuel stream is more susceptible to the effects of the crosswinds than pure propane.

93
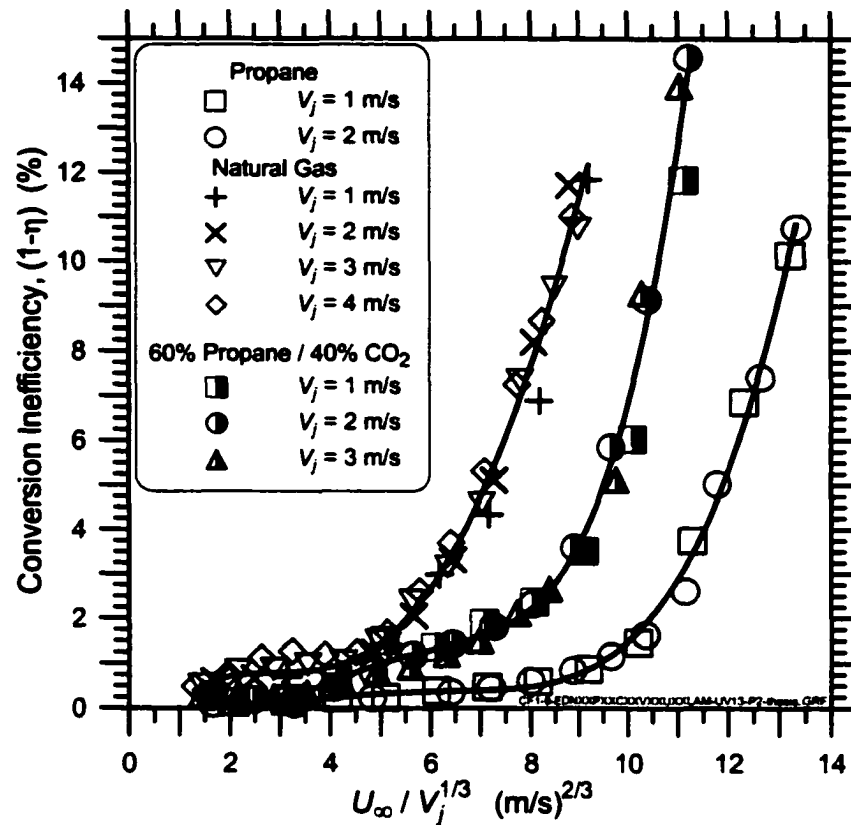
Figure 3.11: Inefficiency curves for propane, natural gas and propane/CO_2 flames where the parameter $U_\infty / V_j^{1/3}$ effectively correlates the relative importance of crosswind speed compared to exit velocity

More importantly, considering all the data in Figure 3.11 highlights a weakness in viewing the combustion efficiency in terms of the Richardson Number and the momentum flux ratio. While these two global parameters are successful at capturing many aspects of the flow field and mean flame characteristics, their characterization of the combustion efficiency is incomplete. Some physical properties that are specific to the fuel stream and are expected to play a role in the combustion processes avoid description within Ri and R. For example, if fuel stripping occurs across the non-reacting mixing layer (see Figure 3.7) or by interactions with wake vortices, the instantaneous location of

94

the flame and the formation of detached flame pockets become important. As a result, parameters like the premixed turbulent flame speed [20], the flammability limits of the fuel stream when mixed with air, and the extinction limits of under aerodynamic straining need to be included in any model.

3.4 CONCLUSIONS

The combustion efficiencies of low momentum propane, natural gas and propane/CO_2 diffusion flames in a crosswind have been measured experimentally using a closed-loop wind tunnel. Flames were established at the exit of a burner tube mounted vertically in the wind tunnel and perpendicular to the airflow, a configuration that is relevant to continuous gas flaring in the atmosphere. Results show that increased crosswind speed (U_∞) adversely affects the combustion efficiency, while increased jet exit velocity (V_j) makes the flame less susceptible to the effects of crosswind. Gas chromatographic analysis of the products of combustion showed that the inefficiencies result from fuel stripping, and photographic images link this process to the occurrence of the flame burning in detached pockets over its full length and the shortening of the flame tail.

Consideration of buoyancy and momentum forces as defined by a Richardson Number successfully predicted the velocity dependency of the combustion inefficiency as being $U_\infty / V_j^{1/3}$ and correlated data for each of the fuels. The density term in the Richardson number was unable in itself to bring together efficiency data from the different fuels. Further attempts to correlate the efficiency data using momentum flux ratio (R) or

95

velocity ratio between the two streams, parameters that were previously shown to be important in characterizing diffusion flames in crosswinds, did not work. Based on a fuel stripping mechanism the combustion efficiency could be expected to depend on fuel specific properties like flame speed, flammability limits or extinction limits. None of these fluid dynamic parameters contain this information and this was suggested to be the reason for their inability to correlate data from different fuels.

Photographic images of the propane and natural gas flames show qualitatively that the occurrence of a maximum mean flame length and the onset of downwash are related to R. Other features of the flame, like the flame burning in detached pockets and the disappearance of the flame tail, do not coincide at fixed values of R for the two fuels. These results suggest that R alone is not sufficient to account for the visual differences between the propane and natural gas flames.

3.5 REFERENCES

1. Energy Information Administration (1999) "International Energy Annual 1997", DOE/EIA-0219(97), Office of Energy Mines and End Use, U.S. Department of Energy, 254 pages.

2. Houghton, J.T., Meira Filho, L.G., Callander, B.A., Harris, N., Kattenberg, A., and Maskell, K. (1996) "Climate Change 1995: The Science of Climate Change", IPCC

(Intergovernmental Panel on Climate Change), Cambridge University Press, Cambridge, U.K., 572 pages.

3. Pohl, J.H., Lee, J., Payne, R., and Tichenor, B.A. (1986) "Combustion Efficiency of Flares", Combustion Science and Technology, 50, pp. 217-231.

4. Siegel, K.D. (1980) "Uber den Umsatzgrad von Facelgas in Raffinerie-Hochfackeln" (Degree of Conversion of Flare Gas in Refinery Flares), Ph.D. Dissertation, University of Karlsruhe, Germany.

5. Kuipers, E.W., Jarvis, B., Bullman, S.J., Cook, D.K. and McHugh, D.R. (1996) "Combustion Efficiency of Natural Gas Flares; Effect of Wind Speed, Flow Rate and Pilots", Internal Report, Shell Research and Technology Thorton and British Gas Research Centre, 13 pages.

6. Eiff, O.S. and Keffer, J.F. (1997) "On the Structures in the near-wake region of an elevated turbulent jet in a crossflow", Journal of Fluid Mechanics, 333, pp. 161-195.

7. Moussa, Z.M., Trischka, J.W. and Eskinazi, S. (1977) "The near field in the mixing of a round jet with a cross-stream", Journal of Fluid Mechanics, 80, pp. 49-80.

8. Strosher, M., (1996) "Investigation of Flare Gas Emissions in Alberta", Alberta Research Council Report to Environment Canada, Alberta Energy and Utilities Board, and Canadian Association of Petroleum Producers, 145 pages.

9. Kalghatgi, G.T. (1981) "Blow-out stability of gaseous jet diffusion flames. Part 1: In still air", Combustion Science and Technology, 26, pp.233-239.

97

10. Kalghatgi, G.T. (1981) "Blow-out stability of gaseous jet diffusion flames. Part 2: Effect of cross-wind", *Combustion Science and Technology*, 26, pp. 241-244.

11. Askari, A., Bullman, S.J., Fairweather, M. and Swaffield, F. (1990) "The Concentration Field of a Turbulent Jet in a Cross-Wind", Combustion Science and Technology, 73, pp. 463-478.

12. Birch, A.D., Brown, D.R., Fairweather, M. and Hargrave, G.K. (1989) "An Experimental Study of a Turbulent Natural Gas Jet in a Cross-flow", *Combustion Science and Technology*, 66, pp. 217-232.

13. Huang, R.F. and Chang, J.M. (1994) "The Stability and Visualized Flame and Flow Structures of a Combusting Jet in Cross Flow", *Combustion and Flame*, 98, pp. 267-278.

14. Huang, R.F. and Wang, S.M. (1999) "Characteristic Flow Modes of Wake-Stabilized Jet Flames in a Transverse Air Stream", Combustion and Flame, 117, pp. 59-77.

15. Gollahalli, S.R. and Nanjundappa, B. (1995) "Burner Wake Stabilized Gas Jet Flames in Cross-Flow", *Combustion Science and Technology*, 109, pp. 327-346.

16. Bourguignon, E., Johnson, M.R. and Kostiuk, L.W. (1999) "The Use of a Closed-Loop Wind Tunnel for Measuring the Efficiency of Flames in Cross-flow", *Combustion and Flame*, 119, pp. 319-334.

17. Ellzey, J.L., Berbee, J.G., Tay, Z.F., and Foster, D.E. (1990) "Total Soot Yield from a Propane Diffusion Flame in Cross-Flow", *Combustion Science and Technology*, 71, pp. 41-52.

18. Kalghatgi, G.T. (1983) "The Visible Shape and Size of a Turbulent Hydrocarbon Jet Diffusion Flame in a Cross-wind", *Combustion and Flame*, 52, pp. 91-106.

19. Gollahalli, S.R., Brzustowski, T.A., and Sullivan, H.F. (1975) "Characteristics of a Turbulent Propane Diffusion Flame in a Cross-wind", *Transactions of the Canadian Society for Mechanical Engineering*, Vol. 3, No.4, pp. 205-214.

20. Hasselbrink, E.F. and Mungal, M.G. (1998) "Observations on the stabilization Region of Non-Premixed Methane Transverse Jet Flames", *Twenty-Seventh Symposium (International) on Combustion*, The Combustion Institute, Pittsburgh, pp.1167-1173.

CHAPTER 4

AN INVESTIGATION OF PARAMETERS THAT AFFECT CONVERSION EFFICIENCY OF WAKE-STABILIZED DIFFUSION FLAMES

The information presented in this chapter is a blend of published and unpublished material by M.R. Johnson. Material from Sections 4.1 and 4.2 has been included as part of a collaborative paper under the citation L.W. Kostiuk, A.J. Majeski, P. Poudenx, M.R. Johnson, and D.J. Wilson, Proceedings of the Combustion Institute, Vol. 28, 2001. Much of the data from Sections 4.3 and 4.4 has appeared in technical reports and conference proceedings.

4.1 INTRODUCTION

In the paper presented in Chapter 3, the notion of a wake-stabilized flame was introduced and its carbon conversion inefficiency was examined in terms of the effects of crosswind velocity and fuel jet exit velocity. A preliminary model based on buoyancy and momentum flux successfully predicted the importance of the ratio $U_\infty / V_j^{1/3}$, but failed to correlate other important features of the data such as the displacement between the inefficiency curves for natural gas and propane. The failure of this simple modelling approach underscores the complexity of the problem and suggests that there are other

important parameters affecting the conversion inefficiency of these wake-stabilized flames.

Work by other researchers on wake-stabilized jet diffusion flames in crossflow is limited to a few publications (Huang and Chang, 1994 [1], Gollahalli and Nanjundappa, 1995 [2], Huang and Yang, 1996 [3], and Huang and Wang, 1999 [4]). None of these researchers specifically addressed the issue of emissions or conversion efficiencies of wake-stabilized flames. Huang and co-workers tested a single propane fueled burner (5.0 mm inside diameter and 6.4 mm outside diameter) and reported the existence of several characteristic flame modes described mostly in terms of their visual appearance. Transitions between these modes were gradual as increasing the crosswind velocity caused a greater portion of the fuel to be trapped and burned in the wake of the burner tube. When combustion was taking place in the wake of the burner tube, the flames were termed "never-lift" to reflect the fact that they did not separate from the stack prior to blowoff [1].

Gollahalli and Nanjundappa [2] used the same burner size as Huang *et al.* but did not follow their flame categorization into multiple distinct modes. Instead, as in this thesis, they identified three distinct regions within the flame: a recirculation zone directly downstream of the burner, an axisymmetric flame extending downstream from the recirculation zone, and a region at the junction between those two parts of the flame. They then classified the flames as either Type II (where combustion occurred in the axisymmetric tail) or Type I (where combustion existed only in the recirculation region).

101

By measuring the temperature and basic chemical composition within the flame, they suggested that combustion in this recirculating vortex was diffusion controlled while combustion in the downstream flammable region had similarities to partially premixed flames.

The data and discussions presented in Chapter 3 [5] support and further clarify the three-zone flames structure described in [2] even though the experiments were conducted on a much larger burner size (22.1 mm inside diameter, 24.7 mm outside diameter). Together, these references provide some foundation with which to begin a more detailed investigation into the conversion efficiencies of wake-stabilized jet diffusion flames in crossflow. The purpose of the chapter is to examine the effects of three general parameters: burner diameter, fuel composition, and turbulence in the crosswind, on the efficiency of these flames.

4.1.1 Experimental Facility

Flames were established at the exit of stainless-steel circular tubes with outside diameters (d_o) of 12.1, 18.6, 24.7, 37.2, and 49.8 mm. The outside of each burner tube was machined so the ratio of inside to outside diameter was fixed at 0.9. The height of the burner tubes in the wind tunnel was adjusted to allow the flame to be positioned outside the roof and floor boundary layers. A plug with a central orifice 30% of the inside tube diameter was placed eight inside diameters upstream of the burner exit to ensure that the mean and turbulence velocity profiles are similar to turbulent pipe flow for all burner

sizes and jet velocities tested. LDV measurements of the velocity and turbulence intensity profiles are published in [7]. For the data presented in sections 4.4 and 4.5, the burner tube used was constructed of quartz and matched the specifications of the 24.7 mm burner tube described above.

4.2 EFFECTS OF BURNER TUBE DIAMETER

An important observation by Johnson and Kostiuk [5] was that the structure and appearance of the visible flames had the same features as those on burners of 1/4 the diameter [1-4]. Flame structure similarities seen over a range of burner sizes from 5 to 22 mm in diameter suggest the possibility of developing geometric and fluid dynamic scaling functions for wake-stabilized flames. With the practical problem of flaring in mind, an understanding of the scaling relationships of these flames is crucial to allow laboratory scale experiments to be related to full-scale situations.

Figure 4.1 shows the conversion $inefficiency$ ($1-\eta$) of wake-stabilized propane flames as a function of U_∞. The data include four burner tube sizes at a single exit velocity ($V_j = 1$ m/s). The four curves have the same characteristic shape as those presented previously [5] and show that in a near quiescent environment these flames are very efficient (> 99.5%), but as the transverse air velocity increases there is a rapid increase in the mass of fuel not being fully converted to CO_2. The data show that the larger diameter burners are slightly more resistant to the effects of increased crosswind velocity. For

103

example, at a wind speed of 11 m/s, the 18.6 mm diameter propane flame operates at an inefficiency of 9% whereas the inefficiency of the 37.2 mm diameter burner is only 1%.
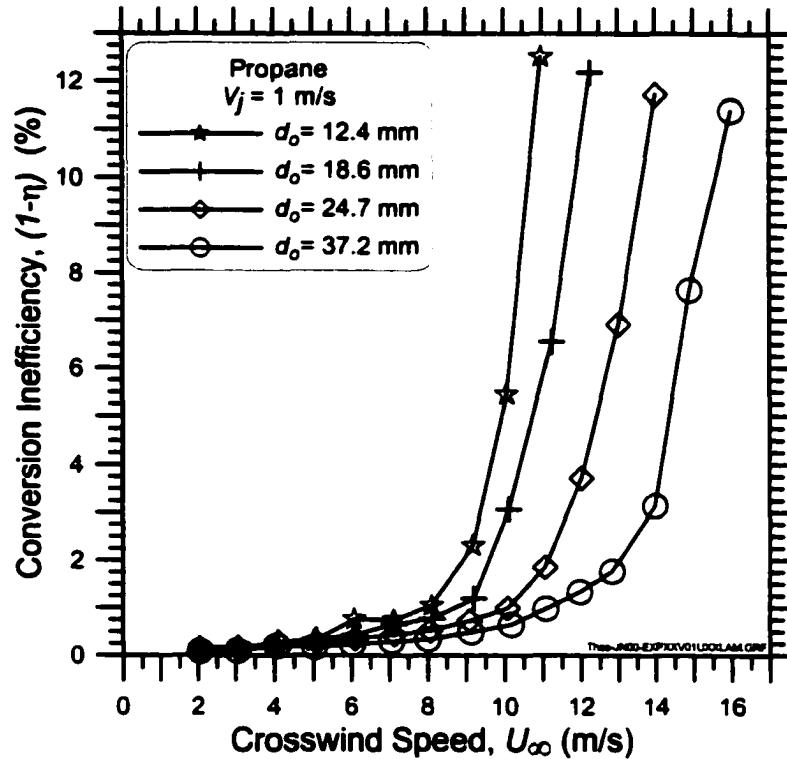
Figure 4.1: Measured combustion inefficiency of wake-stabilized propane flames with an exit velocity of 1 m/s for four different burner tube diameters. Larger burners are less susceptible to the effect of increased crossflow.

Similar data from experiments on natural gas fueled flames is shown in Figure 4.2. Because the natural gas flames were comparably smaller than the propane flames, it was possible to test a larger diameter (d_o = 49.8 mm) burner tube in the data. As well, the exit velocity of the fuel in this case was fixed at V_j = 2m/s. Both Figures 4.1 and 4.2 reveal that the effect of increased diameter is non-linear (i.e. as the diameter of the burner tube is increased linearly, the effect on the inefficiency diminishes).

104
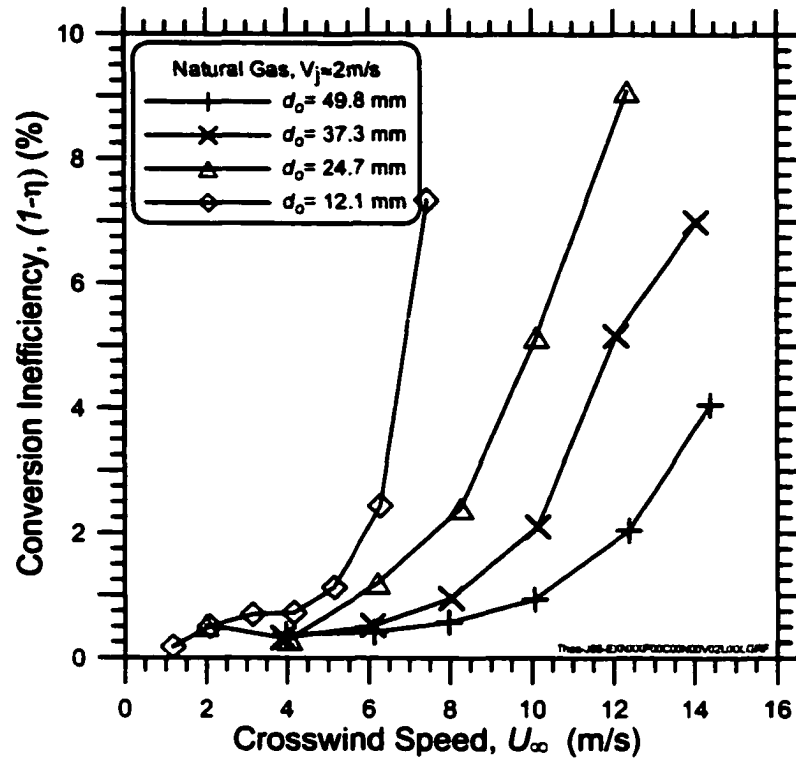
Figure 4.2: Conversion inefficiency of wake-stabilized natural gas flames with an exit velocity of 2 m/s for four different burner tube diameters.

In the previous work [5], the inefficiency was discussed in terms of fluid mechanics that resulted from the combination of momentum and buoyancy forces experienced by the flow through the development of a Richardson number. In those experiments the burner size was held constant while the jet exit velocity was varied and the data were shown to depend on $(U_\infty / V_j^{1/3})$. Including the gravitational constant, g, which appeared in the Richardson number development, one would then expect:

$$(1 - \eta) \propto \frac{U_\infty}{(g V_j)^{1/3}} d_o^n \tag{4.1}$$

where the value of n is derived from the experimental data. Figure 4.3 shows that data for propane flames are effectively collapsed when scaled by $1/d_o^{1/3}$, which also makes the

105

right-hand side of Equation 4.1 non-dimensional. Using this non-dimensional correlation, the collapse of the propane data onto a single curve is quite remarkable.

Unfortunately, the data for the natural gas curves are only partially collapsed by $d_o^{1/3}$ and are better correlated with the empirical exponent $d_o^{1/2}$ as shown in Figures 4.4 and 4.5. In a practical sense this difference of $d_o^{1/6}$ is slight, but nevertheless it is indicative of the complexity of the flow and points to the need for a broader understanding of the mechanism responsible for the measured inefficiencies.
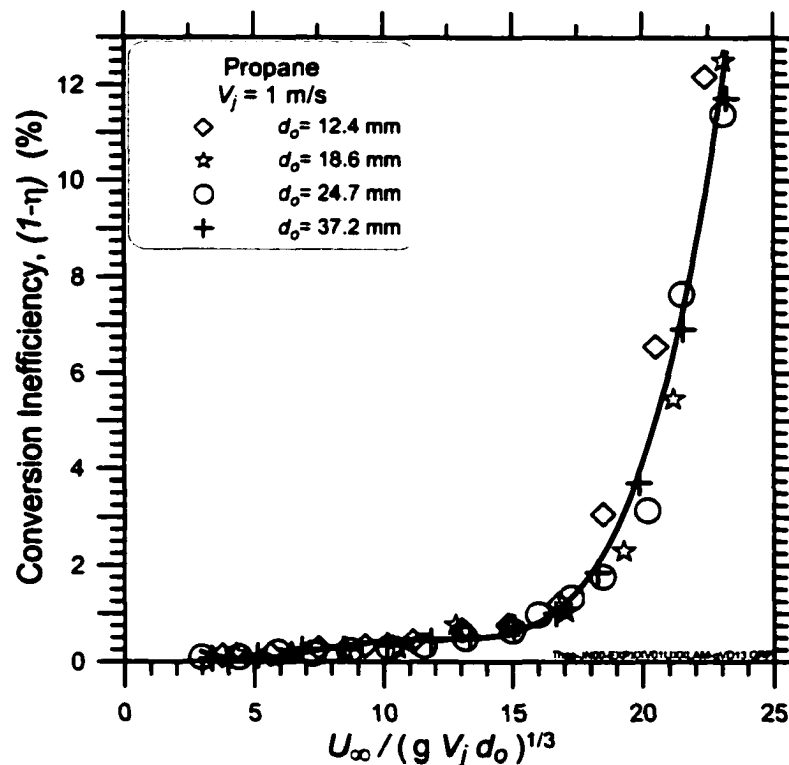
Figure 4.3: Dimensionless correlation of combustion inefficiency of wake-stabilized propane flames with varying burner tube diameter (d_o).

106
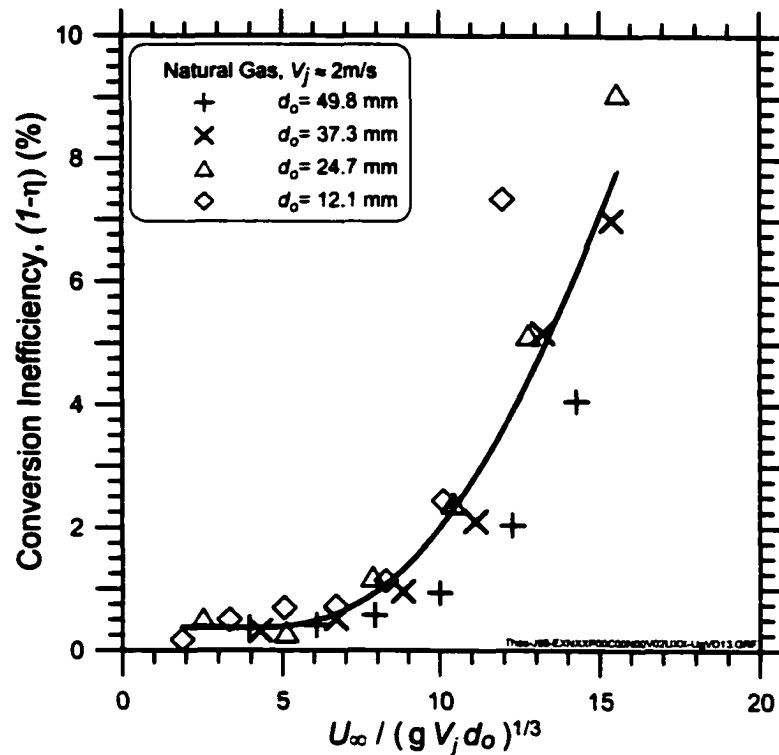
Figure 4.4: Dimensionless buoyancy based correlation with $d_o^{1/3}$ fails to collapse natural gas data for varied burner tube diameter
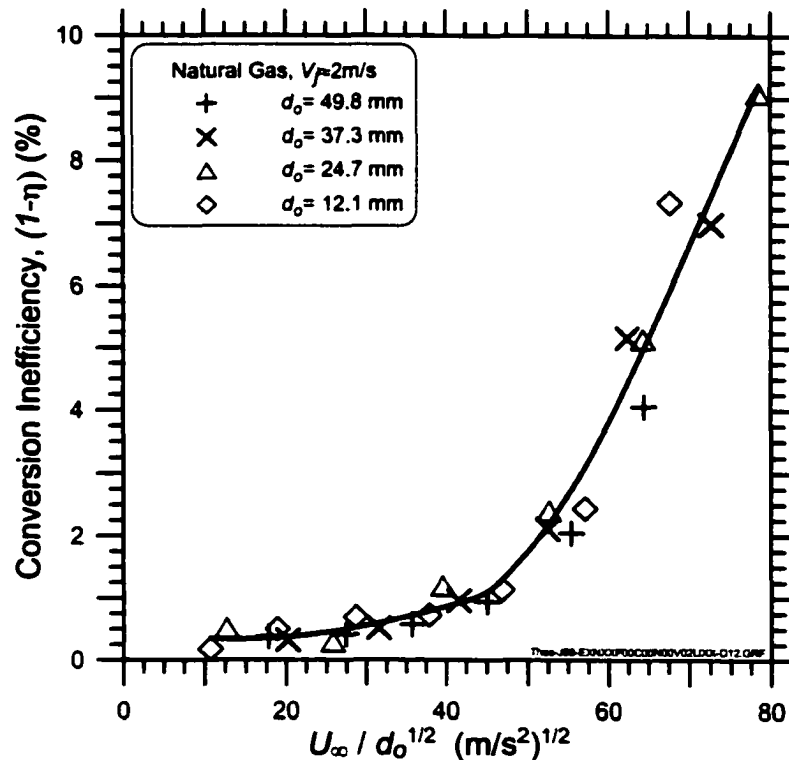
Figure 4.5: Dimensional empirical correlation with $d_o^{1/2}$ for wake-stabilized natural gas flames in crossflow with varied burner tube diameter

107

4.3 THE EFFECTS OF FUEL GAS COMPOSITION AND THE INCLUSION OF INERT DILUENTS

In the discussion section of Chapter 3, data from a few experiments were shown in which the efficiencies of flames burning a 60% / 40% blend of propane and carbon dioxide were measured. These data were used to illustrate the ultimate failure of the Richardson number based model to fully correlate the inefficiency phenomenon. What was not discussed, was the significant effect that addition of inert diluents had on the efficiency of the flames. As well, the inclusion of an inert diluent in the fuel is of practical importance to the problem of flaring in the energy industry where in certain types of gas plant installations, very high amounts of CO_2 may be present in the fuel.

4.3.1 Propane Based Fuel Mixtures

Figure 4.6 shows inefficiency curves for the 24.7 mm diameter burner with various mixtures of propane and CO_2 at an exit velocity of 2 m/s. Since both propane and CO_2 have molecular masses of approximately 44 g/mol, working with mixtures of these two gases allows the mass density to be held constant while other parameters including the energy density of the fuel are varied. The data show that increasing the amount of CO_2 in the fuel and consequently lowering its energy density has a strong, non-linear impact on the flare efficiency. Energy density can be reported as either the higher heating value (HHV) or the lower heating value (LHV) and is typically calculated on a volume basis at 15 C and 1 atm. Both values are shown on the graphs (i.e. HHV/LHV) although only the HHV is referred to in the text. As the fuel energy density is reduced, the flame becomes

108

much more susceptible to the crosswind, and the rapid rise in inefficiency begins at much lower wind speeds. For example, where the 94.5 MJ/m^3 flare burning pure propane has an inefficiency of less than 1% (>99 % efficient) at a wind speed of 10 m/s, the inefficiency of the same burner operating at 37.6 MJ/m^3 is approximately 18 % (~82 % efficient). For the minimum energy density mixture that was tested (18.7 MJ/m^3), the flare falls to below 80 % efficient before the wind speed reaches 5 m/s.
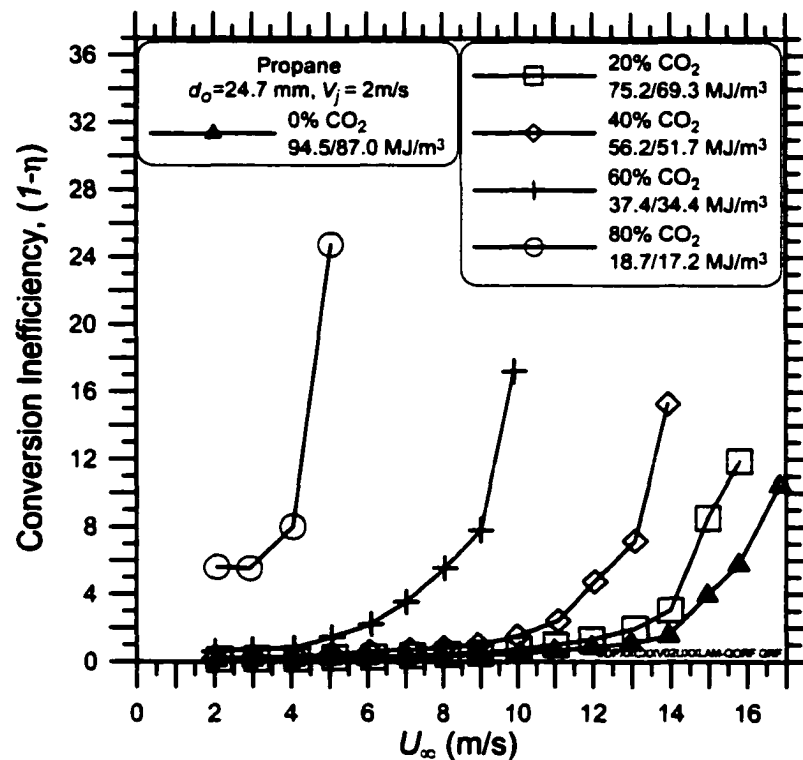
Figure 4.6: Inefficiency of Propane / CO_2 flames at V_j = 2 m/s and d_o = 24.7 mm. Reduced energy density has a significant, adverse effect on inefficiency

Changes in the visible appearance of the flames as energy density was reduced were also significant. At higher energy densities, the propane flames are a bright, luminous yellow-orange colour as the carbon-based solids within the flame emit visible radiation. As CO_2 is mixed into the fuel, there is an initial reduction in the luminosity of the flame. At this

109

time it is unclear if this reduction is due to a decrease in soot production, or due to a decrease in flame temperature which in turn may lead to lower radiative emission from the soot particles within the flame. As more CO_2 is added, the colour shifts from yellow toward blue until eventually all traces of yellow disappear and the flame becomes a deep blue colour that is different from the blue colour normally associated with pre-mixed natural gas or propane flames. Under these low energy density conditions, the flame also shows signs of instability and begins to flicker as if to blow off. If the energy density is reduced further the flames destabilize, separate from the stack and extinguish.

Figure 4.7 shows similar results for fuel mixtures of propane and N_2. In this case the molecular masses of fuel and diluent are not the same and the mass density will decrease as the energy density is reduced. Again the data show that as the amount of diluent in the fuel is increased, the conversion efficiency of the flame is adversely affected and the flame becomes more susceptible to the effects of increased crosswind. The axes in both Figures 4.6 and 4.7 have identical scales and inspection of the data reveals that the effect of added CO_2 is slightly greater than that of adding N_2 in equal volumes. For example, the 37.4 MJ/m^3 propane / N_2 flame exceeds 10 % inefficiency at a crosswind speed of approximately 11.1 m/s whereas the propane / CO_2 flame of the same volume fractions and hence energy density exceeds 10 % inefficiency at a crosswind speed of only 9.25 m/s. Reasons for this difference could include variations in the mass density and heat capacity of the two fuel mixtures. However, since multiple properties of the fuel mixture vary as the amount of diluent is increased, from this data alone it is not possible

110

to conclude what other parameters in addition to the energy density are important in setting the efficiency of the flame.
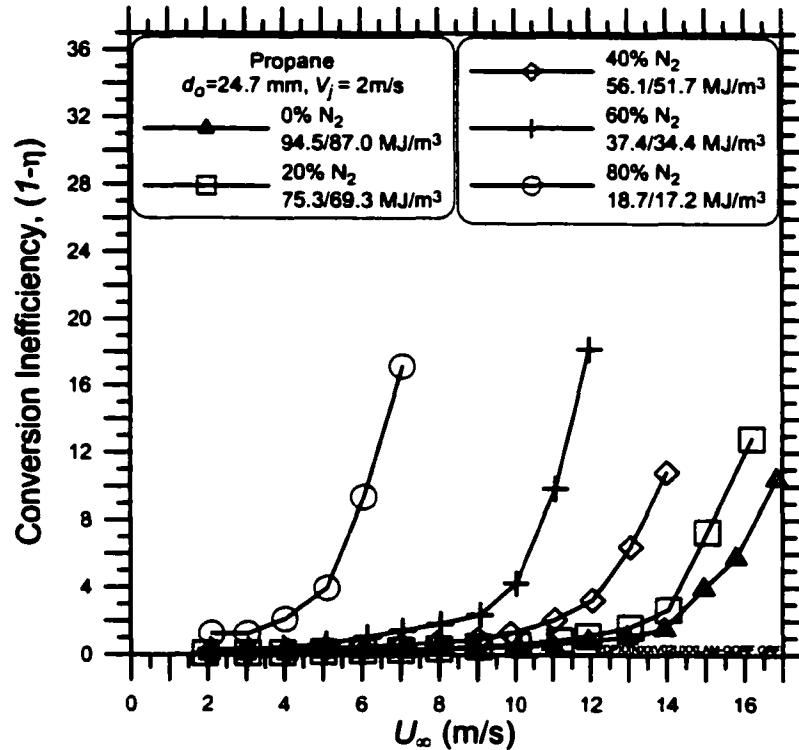
Figure 4.7: Inefficiency of Propane / N_2 flames at V_j=2 m/s and d_o= 24.7 mm. Effect of increased N_2 is strong, but less than that of added CO_2.

4.3.2   Natural Gas (Methane) Based Fuel Mixtures

In terms of the practical problem of solution gas flaring in crude oil production, the fuel stream would be based on methane or natural gas [8]. Figures 4.8 and 4.9 show the measured efficiencies of various blends of natural gas / CO_2 and natural gas / N_2 respectively as functions of the crosswind velocity. The same trends evident in the data

111

from the propane blends are again apparent as increasing the fraction of inert diluent causes the efficiency to decrease in a non-linear fashion. The implications of these results for industry have not gone unnoticed. In response to the data from the natural gas / CO_2 flames of Figure 4.8 as well as data contained in [9] and [10], the Alberta Energy and Utilities Board (AEUB) has raised the required minimum heating value of fuel that may be burned in a flare from 9 MJ/m^3 to 20 MJ/m^3. This change was implemented with AEUB Guide 60 [11] and became effective in January 2000.

The families of inefficiency curves of the natural gas blends exhibit a second trend that is more noticeable than it is in the propane based data. At high levels of inert diluent in the fuel stream, the inefficiency curves of natural gas based blends seem to shift upward as well as to the left. Although, this is apparent in the propane / CO_2 data of Figure 4.6, it is not as significant as in Figures 4.8 and 4.9. At lower wind velocities, extrapolation of the natural gas / CO_2 and natural gas / N_2 curves suggests that there would still be some differences in inefficiency at a crosswind velocity of 0 m/s. This secondary trend presents an added difficulty in modeling the experimental inefficiency data.

112
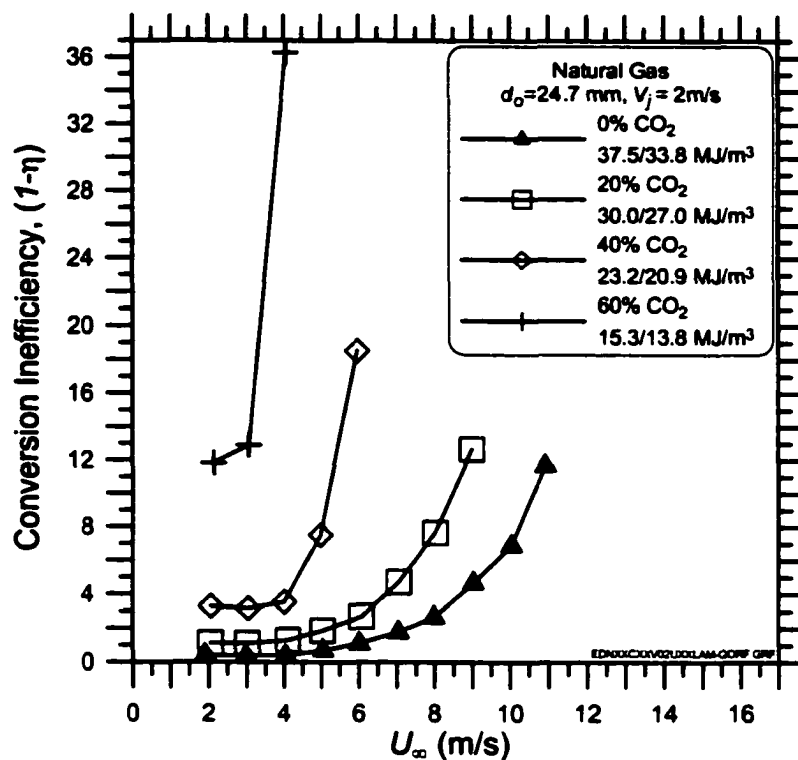
Figure 4.8: Inefficiency of Natural Gas / CO_2 flames at V_j=2 m/s and d_o = 24.7 mm. Curves are displaced vertically as well as to the left with increased diluent fraction.
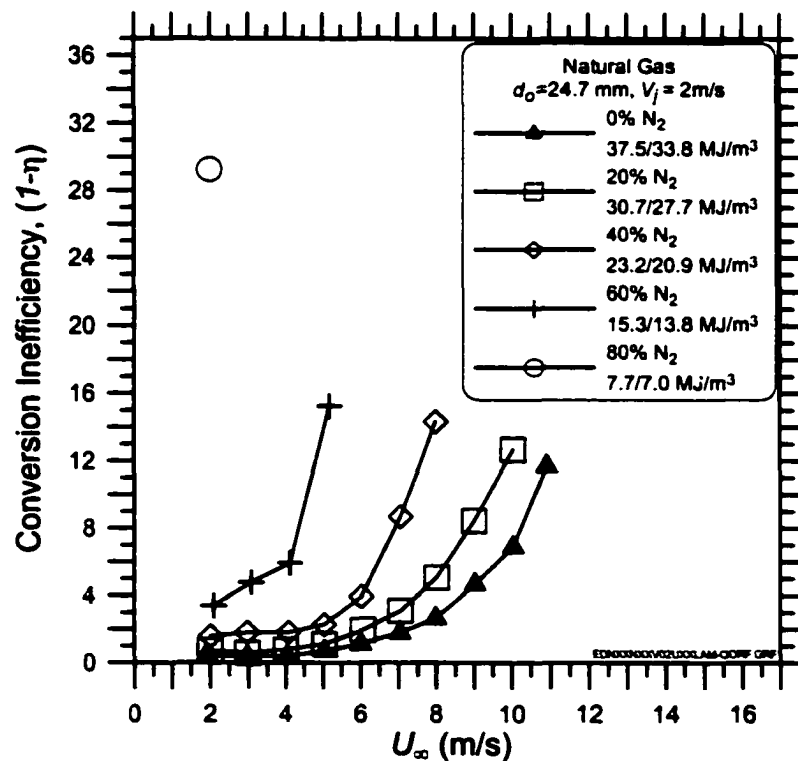
Figure 4.9: Inefficiency of Natural Gas / N_2 flames at V_j=2 m/s and d_o = 24.7 mm.

113

4.3.3 Understanding the Effects of Diluents in the Fuel

With the possible exception of the vertically displaced natural gas inefficiency curves noted in the previous section, it seems that all of the inefficiency curves in Figures 4.6 to 4.9 are sufficiently alike that they should be governed by the same physical processes. Unfortunately, the mechanism driving the inefficiencies seems to be exceedingly complex and at this point a general model to describe all of the data in Figures 4.6 to 4.9 has not yet been developed. The primary barrier to a deeper understanding of inefficiency phenomena in these wake-stabilized flames is the fact that it is nearly impossible to isolate the effects of individual parameters that may affect the flow. While experimental parameters such as the crosswind speed, exit velocity, and burner diameter are easily controlled on an individual basis, it is not so easy to isolate the effects of fuel mass density, energy density (heating value), heat capacity, and other more complex parameters. Even in the case of the constant density propane / CO_2 blends of Figure 4.6, as the amount of CO_2 in the fuel is increased, the energy density, heat capacity, thermal conductivity, flammability limits, etc. all vary.

Figure 4.10 shows inefficiency curves of four different fuel blends that have been chosen to have approximately the same energy density (calculated on a volume basis as the higher heating value). Although these four curves show the same general trend, the four curves are not coincident and therefore are a demonstration of the statements above that energy density alone does not determine the inefficiency. Table 4.1 lists the calculated values of various other parameters that may be important in determining the efficiency of these flames. Values of the mass density, constant pressure heat capacity, and thermal

114

conductivity are listed along with values of the maximum and minimum permissible dilutions with air for which the fuel mixture will remain flammable at 25 C and 1 atm. There are likely other parameters that may be important to the problem as well. Comparison of the four curves and the values of the listed parameters suggests that there is no simple monotonic dependency that will explain the differences in the inefficiency data.
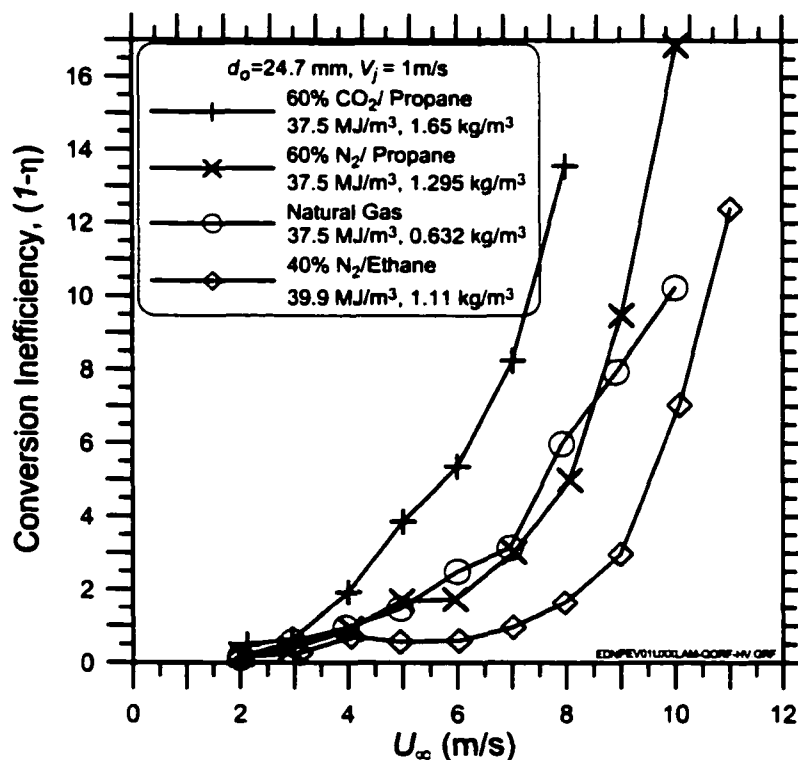
Figure 4.10: Comparison of inefficiency curves of four different fuel blends with similar energy densities.

Table 4.1: Property data for different fuel blends shown in Figure 4.10

Property @ 298 K and 1 atm (unless otherwise stated)	40% Propane / 60% CO_2	40% Propane / 60% N_2	Natural Gas	60% Ethane / 40% N_2
Energy Density (MJ/m^3) @15 C	37.5	37.5	37.5	39.9
Mass Density (kg/m^3)	1.65	1.30	0.63	1.11
Heat Capacity (J/mol-K)	51.7	46.7	35.7	43.3
Maximum Dilution	17.7	18.8	19.6	20.0
Minimum Dilution	5.3	5.5	6.6	5.8
Thermal Conductivity (W/mK)	0.0171	0.0224	0.0352	0.0231
Thermal Diffusivity (m^2/s)	0.803E-5	1.16E-5	2.42E-5	1.30E-5

115

Although a general model for the data has yet to be proposed, some limited success has been achieved in empirically correlating the inefficiency data for natural gas / CO_2 mixtures [9, 10]. This preliminary correlation used a dilution ratio derived from flammability limit data as well as the premixed laminar flame speed to crudely describe the natural gas / CO_2 data as a single function. While it is recognized that such empirical correlations have limited scientific value, such correlations satisfy the need for engineers and regulators to have some sort of tool to use in the making judgements about flaring.

Figure 4.11 shows an empirical correlation that uses the dimensionless $U_\infty / (g\ V_j\ d_o)^{1/3}$ on the horizontal axis and the cube of the mass based heating value (in this case the lower heating value) on the vertical axis. This correlation is slightly different than that of references [9] and [10]. The use of the mass based heating value could plausibly suggest the importance of specific heat release to support combustion but the choice of its cubic exponent is justifiable only because it makes the data collapse. Attempts to incorporate the heating value into the term on the horizontal axis instead of the vertical axis were less successful which suggests that the connection between the inefficiency and the $U_\infty /$ $(g\ V_j d_o)^{1/3}$ term is not a simple power-law relationship.

Figure 4.11 includes fuel streams based on natural gas, ethane, and propane that include CO_2 or N_2 as diluents although it must be noted that the burner tube diameter, d_o, is constant at 24.7 mm for all data. Apart from the potential (although limited) practical utility of this plot, what is most interesting is the fact that the propane and ethane based

116

data follow the same trend which is separate from that of the natural gas based data. This may suggest that the inefficiency mechanism(s) for natural gas are somewhat different than that of ethane and propane or simply that the empirical correlation is incomplete. Ultimately, more research will be necessary before an accurate experimental model for all of the data will be achievable.
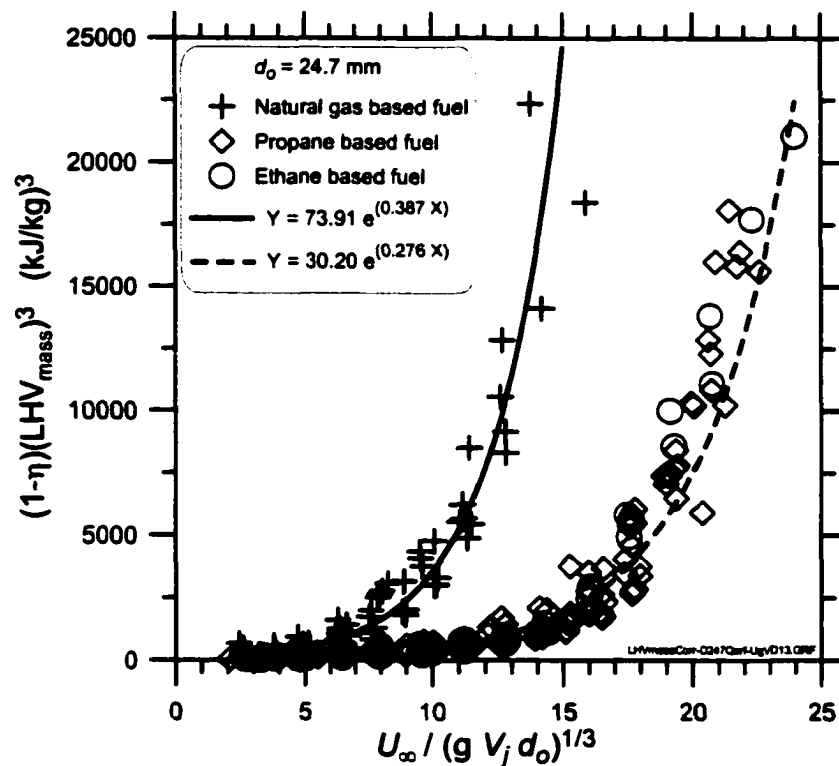
Figure 4.11: Empirical correlation for various fuel blends (hydrocarbon base plus either CO_2 or N_2) using mass-based lower heating value. Note that d_o is constant for all data. Propane and ethane based data follow the same trend where as natural gas based data is displaced.

Figure 4.12 shows the same data as Figure 4.11 but plotted on a semi-logarithmic scale. This figure is useful in estimating the accuracy of the correlation at different values of U_∞ / $(g\ V_j\ d_o)^{1/3}$. The data show that the percentage uncertainty is relatively constant along

117

full range of the data although the correlation is less accurate at low values of U_∞ / (g V_j d_o)$^{1/3}$ or alternatively at low values of $(1-\eta)*$LHV$_{mass}$^{3}. Since the data fall on a relatively straight line on the semi-logarithmic scale, the choice of the exponential fits seems justified. These same exponential fits have been transferred to Figure 4.11 for comparison with the data on a non-logarithmic scale.
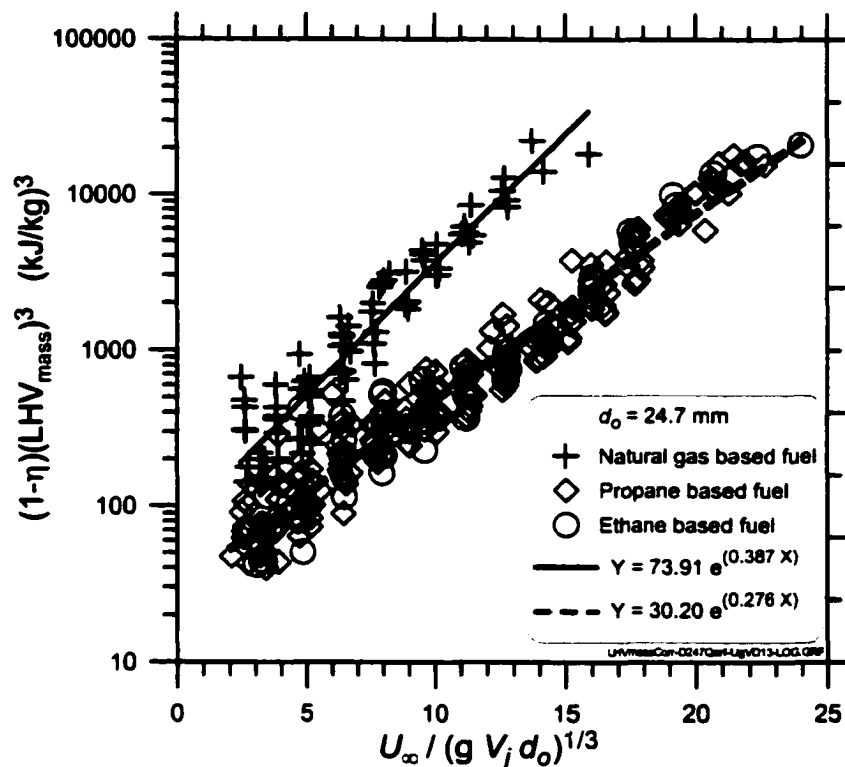
Figure 4.12: Empirical correlation of Figure 4.11 show on semi-logarithmic scale. Percentage error of data along fit is relatively consistent although somewhat higher at lower values of U_∞ / (g V_j d_o)$^{1/3}$. Note d_o is constant for all data.

Although in Section 4.2 it was shown that the inefficiency curves for the propane data scale very well with U_∞ / (g V_j d_o)$^{1/3}$, the natural gas data were better correlated with $d_o^{1/2}$. Since most practical flares burn natural gas based fuels [8], if one were to attempt to

118

apply these results to engineering problems related to flaring, a more appropriate practical correlation could be based on $d_o{}^{1/2}$ as shown in Figure 4.13. The data shown on this figure include the data for natural gas burners of Figure 4.2 in which the diameter was varied from 12.1 mm to 49.8 mm. While these results may prove to be a convenient tool to be applied to engineering problems, it is strongly urged that caution be used in their application. Although the correlations presented here are quite successful in collapsing the data, there are many important questions that will be answered only with further research into the mechanism responsible for the measured conversion inefficiencies. Chapter 5 presents data from a series of experiments designed to further understanding of the mechanism causing the measured inefficiencies in wake-stabilized flames. Results from these experiments ultimately lead to the proposal of a fuel stripping mechanism that appears to be driving the measured inefficiencies in wake-stabilized natural gas flames.
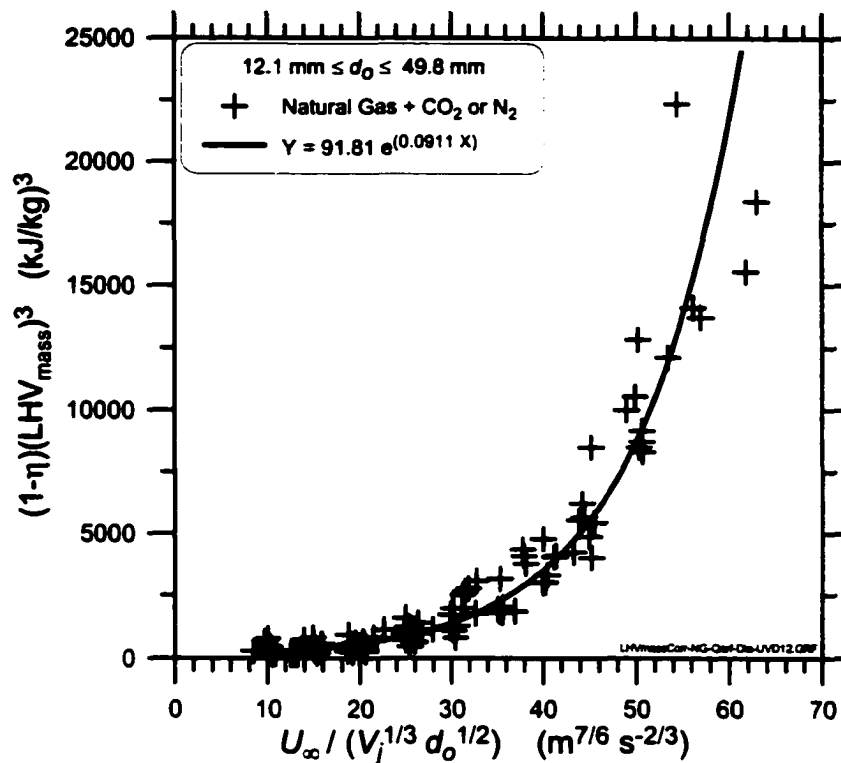
Figure 4.13: Practical empirical correlation for natural gas based flares with a $d_o^{1/2}$ dependency. Fuel mixtures include blends of natural gas and CO_2 and natural gas and N_2 and d_o varies from 12.1 to 49.8 mm.

4.4   INFLUENCE OF CROSSWIND TURBULENCE

In all of the experiments presented thus far, the crosswind has been uniform with very low turbulence. Hot-wire anemometer measurements have show the turbulence intensity in the core flow of the test section is less than 0.4 % in almost all cases. In the real world application of gas flaring, the crosswind imposed on a flare would be expected to be turbulent. While a full investigation of the effects of turbulence in the crossflow are

120

beyond the scope of this thesis, it was desired to run a few experiments to estimate the potential importance of this effect.

To generate turbulence in the crossflow, a rectangular grid was placed in the test section of the wind tunnel, 5.4 m upstream of the flare. The dimensions of the grid are shown in Figure 4.14. Hot wire anemometer measurements showed that the average turbulence intensity in the core flow of the test section at the location of the burner was approximately 5%. The characteristic length scale of the turbulence (i.e. integral length scale) was about 20 cm.
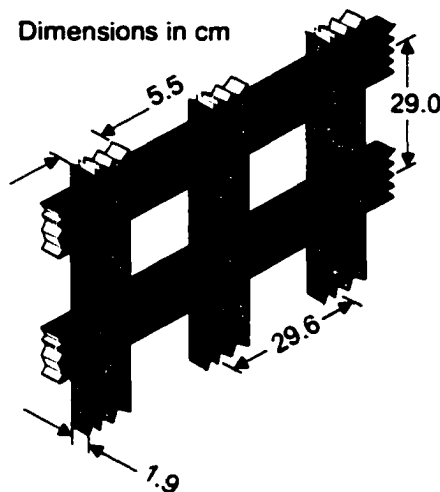
Figure 4.14: Portion of the 2.4 x 1.2 m rectangular grid used to generate ambient turbulence in the crossflow

With the grid in place the flames were strongly buffeted by the turbulence although the general three-zone structure of the flames was unchanged. Figure 4.15 shows the results of efficiency tests for a natural gas flame at an exit velocity of 3 m/s with and without ambient turbulence. Although there is a measurable difference between the curves, the effects of adding ambient turbulence to the crossflow were relatively small in comparison

121

to the effects induced by other parameters such as exit velocity, diameter, and energy density. Also important is the fact that the added ambient turbulence did not alter the shape of the inefficiency curves. This result is not unexpected given the time scales of ambient turbulence and those of the combustion. Combustion time scales are much shorter than those associated with changes in the flow velocity and direction experienced by the flame and hence the flame might be expected to be able to respond to these changes in a quasi-steady manner.

Based on these time-scale arguments, if the ambient turbulence is assumed to act only to increase and decrease the windspeed in a quasi-steady but random fashion, it is possible to predict the inefficiency curve in the presence of ambient turbulence from the inefficiency curve without added turbulence. This can be achieved by piecewise fitting the non-turbulent in data in Figure 4.15 with a polynomial function and solving Equations 4.2 and 4.3 numerically.

$$\eta_T|_{\overline{U_\infty},\sigma} = \int_{-\infty}^{\infty} P(U_\infty)|_{\overline{U_\infty},\sigma}\, \eta(U_\infty)\, dU_\infty \qquad (4.2)$$

where U_∞ = *wind speed at the flare stack*

$\overline{U_\infty}$ = *mean wind speed at the flare stack*

σ = *standard deviation of the turbulent wind speed about the mean wind speed*

$\eta_T|_{\overline{U_\infty},\sigma}$ = *the efficiency of the flame in ambient turbulence at a fixed $\overline{U_\infty}$ and σ*

$\eta(U_\infty)$ = *the efficiency of the flame as a function of wind speed without ambient turbulence*

$P(U_\infty)|_{\overline{U_\infty},\sigma}$ = *probability distribution function of wind speed given by Eq. 4.3*

122

$$P(U_\infty) = \frac{1}{\sqrt{2\pi}\sigma} \exp\left[-0.5\left(\frac{U_\infty - \overline{U_\infty}}{\sigma}\right)^2\right]$$

(4.3)
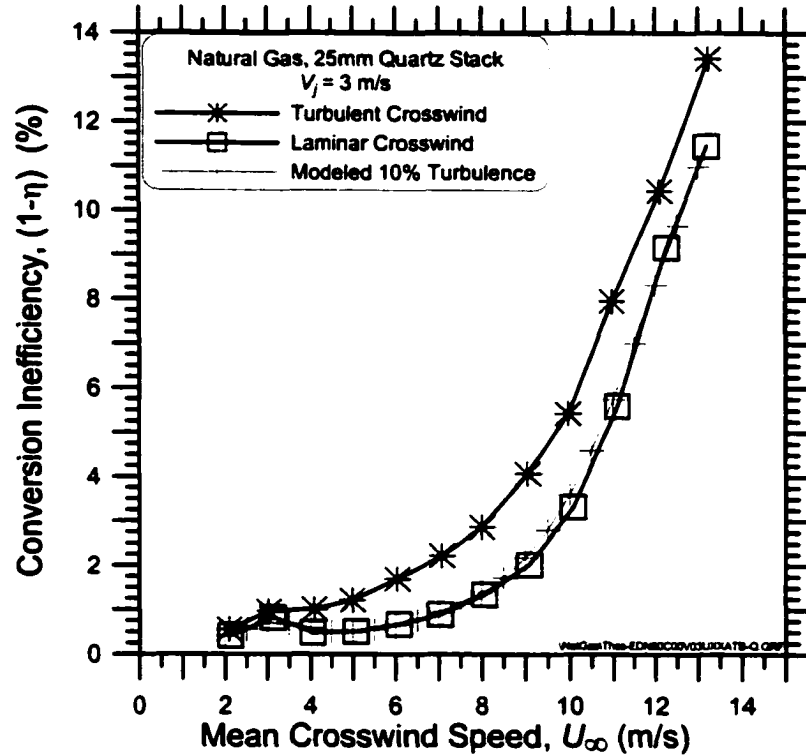
Figure 4.15: Effect of ambient turbulence in the crossflow on the inefficiency of a natural gas flame

Figure 4.15 shows the predicted inefficiency curve for the $V_j=3$ m/s natural gas flame in the presence of 10 % intensity ambient turbulence and the predicted curve differs only slightly from the measured curve without turbulence. A calculation based on 10 % and not 5 % turbulence intensity was used on the graph because the displacement of the curve at 5 % turbulence intensity was barely noticeable. This result suggests that the ambient turbulence has an effect on the flame that cannot be accounted for by simply increasing and decreasing the crosswind speed in a quasi-steady manner. Clarification of this effect

123

will require further experimentation and will require a clearer understanding of the mechanism responsible for the measured inefficiencies. However, the purpose of this section was to try to quantify the overall effect of added turbulence which based on these results appears to be less important than other primary variables.

4.5 CONCLUSIONS

The experiments presented in this chapter reveal that the mechanism governing the conversion efficiency of wake-stabilized diffusion flames in crossflow is complex. The data show that each of three general parameters – burner diameter, fuel composition, and ambient turbulence in the crosswind – affect the measured inefficiency of the flame.

Measurements of the inefficiency $(1-\eta)$ for undiluted propane flames showed that the data scaled with the non-dimensional parameter $\dfrac{U_\infty}{\left(gV_j d_o\right)^{1/3}}$, which was developed out of the Richardson number based arguments presented in Chapter 3. Unfortunately, the data for the natural gas curves were only partially correlated by $d_o^{1/3}$ and were better correlated with $d_o^{1/2}$. In a practical sense this difference of $d_o^{1/6}$ is small, but nevertheless it is indicative of the complexity of the flow and points to the need for a broader understanding of the mechanism responsible for the measured inefficiencies.

124

Experiments to evaluate the importance of fuel composition revealed that increasing the amount of inert diluent in the fuel has a profound, adverse effect on the conversion inefficiency. By adding either CO_2 or N_2 to the methane or propane fuel stream, the energy density of the fuel was reduced and the flames became much more susceptible to the effects of increased crosswind. The implications of these results for industry have led to an increase in the required minimum heating value of fuel that may be burned in a flare in Alberta from 9 MJ/m^3 to 20 MJ/m^3.

Although the effects of adding inert diluents to the fuel are not fully understood, some success was achieved in empirically correlating the data using the lower heating value of the fuel calculated on a mass basis. Using this correlation, data from propane based and ethane based fuel mixtures were effectively collapsed onto a single curve. Data from natural gas / CO_2 and natural gas / N_2 curves were also collapsed by the same parameters but followed a different curve than the propane and ethane based data. At this point the reasons for this difference are not understood and they may imply that the inefficiency mechanism(s) for natural gas are somewhat different than that of ethane and propane or simply that the empirical correlation is incomplete. Despite these shortcomings, with this new empirical model it is now possible to make predictions about the performance of flares in the field. However, any attempts to apply these results to engineering problems must be done with extreme caution indicative of the empirical nature of the correlations.

The third parameter that was investigated in this chapter was the addition of turbulence to the crossflow. Simple experiments showed that the addition of ambient turbulence in the

125

crossflow caused a measurable increase in the conversion inefficiency of the flames. However the net effect was relatively small in comparison to the effects induced by other parameters such as exit velocity, diameter, and energy density. More important was the fact that the added turbulence did not alter the general shape of the inefficiency curves, which suggests that the mechanism driving the inefficiencies was the same as that in the low-turbulence case.

In summary, the results of all of the experiments in this chapter point to the need for a broader understanding of the mechanism(s) responsible for the measured conversion inefficiencies in wake-stabilized diffusion flames. Although significant progress has been made in understanding the influence of various parameters on the flame inefficiecy, many of the questions raised will require further study. The following chapter will present results from a series of experiments designed to help discover and describe the origins of these inefficiencies.

4.6 REFERENCES

1. Huang, R.F. and Chang, J.M. (1994) "The Stability and Visualized Flame and Flow Structures of a Combusting Jet in Cross Flow", *Combustion and Flame*, 98, pp. 267-278.

2. Gollahalli, S.R. and Nanjundappa, B. (1995) "Burner Wake Stabilized Gas Jet Flames in Cross-Flow", *Combustion Science and Technology*, 109, pp. 327-346.

3. Huang, R.F. and Yang, M.J. (1996) "Thermal and concentration fields of burner attached jet flames in cross-flow", *Combustion and Flame*, 105, pp.211-224.

4. Huang, R.F. and Wang, S.M. (1999) "Characteristic Flow Modes of Wake-Stabilized Jet Flames in a Transverse Air Stream", Combustion and Flame, 117, pp. 59-77.

5. Johnson, M.R. and Kostiuk, L.W. (2000) "Efficiencies of low momentum jet diffusion flames in crosswinds", *Combustion and Flame*, 123, pp. 189-200.

6. Bourguignon, E., Johnson, M.R. and Kostiuk, L.W. (1999) "The Use of a Closed-Loop Wind Tunnel for Measuring the Efficiency of Flames in Cross-flow", *Combustion and Flame*, 119, pp. 319-334.

7. Majeski, A.J. (2000) "Size and Shape of Low Momentum Jet Diffusion Flames in Cross Flow", *M.Sc. Thesis*, University of Alberta, p. 126.

8. Johnson, M.R., Spangelo, J.L., and Kostiuk, L.W. (2001) "A Characterization of Solution Gas Flaring in Alberta", *Journal of the Air and Waste Management Association*, in press.

9. Johnson, M.R. and Kostiuk, L.W. (1999) "Effects of a Fuel Diluent on the Efficiency of a Jet Diffusion Flame in a Crosswind", *presented at The Combustion Institute, Canadian Section, 1999 Spring Technical Meeting*, Edmonton, Alberta, May 16-19.

10. Kostiuk, L.W. and Johnson, M.R. (2001) "University of Alberta Flare Research Project Interim Report November 1996 - June 2000", University of Alberta, December 2000, p. xxii, 149.

11. Alberta Energy and Utilities Board (1999) "GUIDE 60: Upstream Petroleum Industry Flaring Requirements", *Alberta Energy and Utilities Board Guide Series*, 1st Ed., July, p. 75.

CHAPTER 5

A FUEL STRIPPING MECHANISM FOR WAKE-STABILIZED JET DIFFUSION FLAMES IN CROSSFLOW

This paper was co-authored by my two supervisors and myself. This work
was solely my work, while the writing of the manuscript was conducted
jointly.

5.1 INTRODUCTION

A diffusion flame burning in a crossflow of air is a basic combustion problem that has many applications. A common example occurs in the energy and petrochemical industries where this configuration is relevant to gas flaring – the process of disposing of unwanted flammable gases by combusting them in a flame in the open atmosphere. Other applications include cross-stream fuel injection in some types of furnaces and gas turbine combustors.

Depending on the relative magnitudes of the momentum fluxes of the fuel and the crossflow, the appearance of the flame can be quite different. At high momentum flux ratios ($R = \rho_j V_j^2 / \rho_\infty U_\infty^2$ where ρ is the density, V and U are velocity, and subscripts j and ∞ denote the fuel jet and crossflow respectively), the flame exists as a lifted diffusion flame bent over by the crossflow and has been studied by several researchers [c.f. 1-4]. At low momentum flux ratios, the flame is "wake-stabilized" by a standing vortex that exists on the leeward side of the burner tube as shown in Figure 5.1. The transition between these two regimes is hysteretic and has been shown to depend on the ignition conditions of the fuel jet [5]. This paper focuses on flames in this low-momentum regime (R of the order of 1 or less), which have been the subject of a few recent publications [5-9].
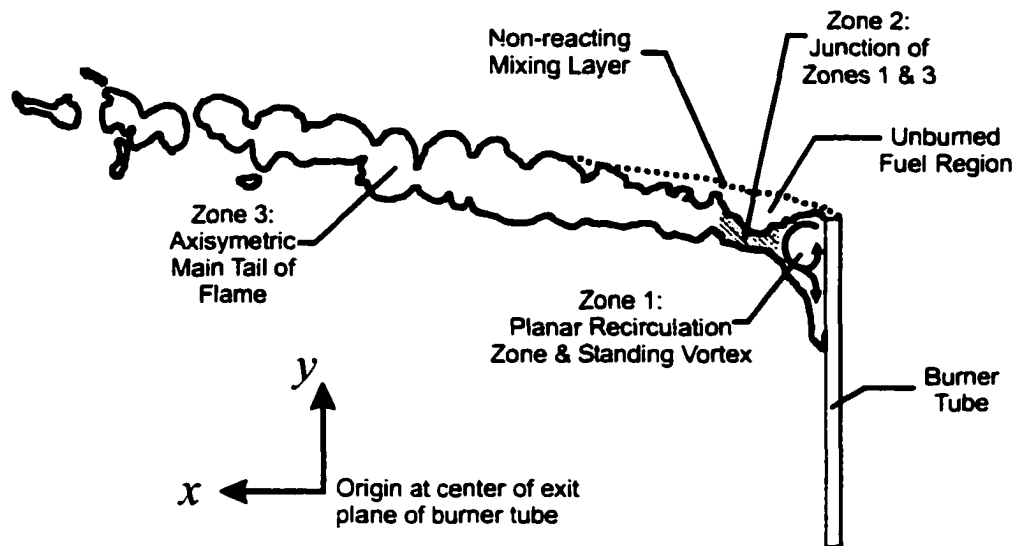
Figure 5.1: Three-zone flame structure of a wake-stabilized jet diffusion flame in crossflow

Important to this paper are the reported emissions characteristics of low-momentum flames which have been examined in terms of a carbon conversion efficiency, η [9]. The

130

carbon conversion efficiency is a measure of the ability of the flame to fully convert the fuel to carbon dioxide and defined according to

$$\eta = \frac{\text{mass rate of carbon in the form of } CO_2 \text{ produced by the flame}}{\text{mass flow rate of carbon entering the flame in the form of hydrocarbon fuel}} \qquad (5.1)$$

Figure 5.2 shows the overall inefficiency $(1-\eta)$ as a function of crossflow speed, U_∞, of a natural gas flame exiting from a 24.7 mm diameter burner tube at a velocity, V_j, of 1 m/s. By plotting the conversion inefficiency $(1-\eta)$, the fractional increase of fuel not being burned is emphasized. The methodology used to measure the efficiency has been previously described in detail [10].
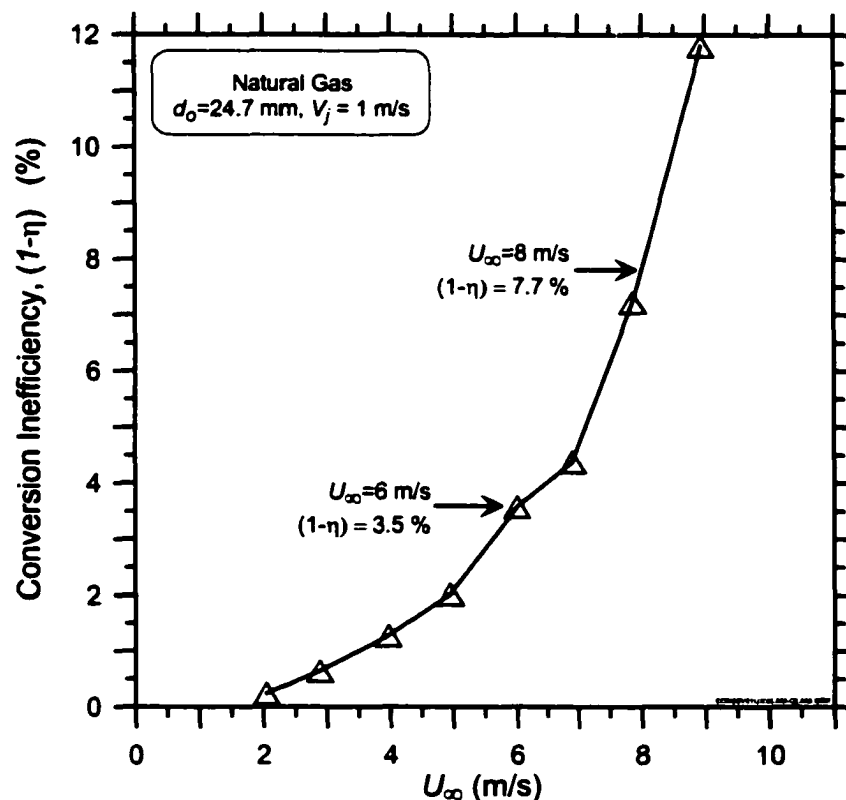
Figure 5.2: Carbon conversion inefficiency of a low-momentum natural gas jet diffusion flame in crossflow

131

The shape of the inefficiency curve in Figure 5.2 demonstrates a non-linear dependence of the mass of incomplete combustion products on crossflow speed. At low crossflow speeds, the inefficiency is quite low, but as the air speed is increased to greater than 5 m/s, the inefficiency rises rapidly. Previous work has also reported the effects of changing exit velocity, V_j, fuel type, and stack diameter on the measured inefficiency [9,8] and shown that $\eta \propto U_\infty / V_j^{1/3}$. The rapid rise in inefficiency has been found to correspond with the flame existing in a wake-stabilized mode in which the flame consists of three distinct zones as shown in Figure 5.1. As well, photographic data suggested links between the drop in efficiency with the formation of discrete pockets of combustion in the main tail of the flame [9].

Analysis of the combustion products has shown that the inefficiencies are primarily in the form of unburned hydrocarbons along with some carbon monoxide and not pyrolitic compounds. A gas chromatograph analysis of the hydrocarbons in the products of natural gas flames has shown that the hydrocarbons have essentially the same compositional make-up as the fuel. Although, these results suggested that the observed inefficiencies could be a result of "fuel stripping" from the fuel jet before any combustion [9], a mechanism for this was not described. This paper reports on experiments that indicate that measured inefficiencies are indeed a result of a fuel "leakage" or "stripping" mechanism that is related to coherent structures in the flow field.

132

5.2 POTENTIAL PATHS FOR FUEL LEAKAGE

Given that unburned fuel is present in the combustion products, the fuel must originate at the exit of the burner tube and ultimately be transported away from the flame without burning. Figure 5.3 shows a sketch of the wake-stabilized flame in side and end views. As indicated on the figure, there are a five possible paths along which fuel could be exiting a control volume surrounding the burner / jet / flame system. One possibility is that there could be some upward dispersion of unburned fuel from the non-reacting mixing layer that exists on the upper surface of the flame. Alternatively, given that the wake-stabilized flame is known to burn as a series of discrete flame pockets [9], it is possible that some unburned fuel exists between these flame pockets and is subsequently ejected from the tip of the flame.
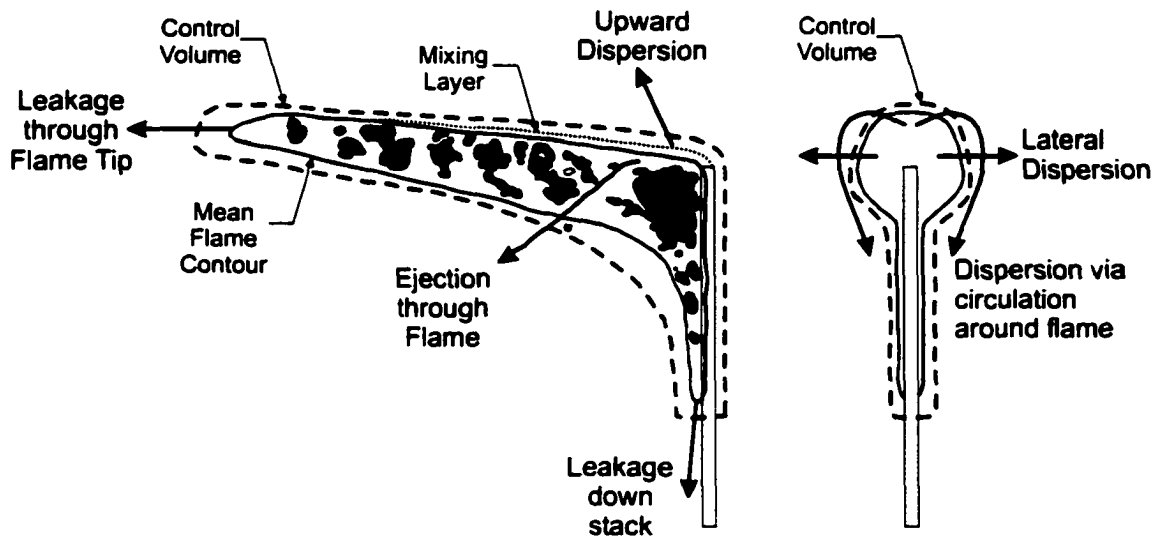
Figure 5.3: Potential paths for fuel leakage or stripping from a wake-stabilized flame

A third path for fuel leakage could entail lateral dispersion out the sides of the flame or involve some sort of circulation around the outside of the flame which might draw

133

unburned fuel from the mixing layer around the outside of the flame. A fourth possibility is that fuel could be emitted from the recirculation region in zone 1 of the flame and leak down the leeward side of the burner tube. Finally, it is possible that unburned fuel from the fuel stream could be drawn down through gaps between the flame pockets to the underside of the flame where it is then transported away from the flame by the mean flow. The experiments that follow were designed to investigate these five possibilities to first identify the path the fuel takes in being stripped and then consider the fluid dynamic mechanism that drives the flow in that path.

5.3   EXPERIMENTAL SETUP AND METHODOLOGY

Experiments to discover the origins and mechanism of the inefficiencies were conducted in a closed-loop wind tunnel which has been described in detail in [9]. The test section is 2.44-m wide and 1.22-m high and the internal volume of the tunnel is approximately 350-m^3. For the range of wind speeds considered here, the root mean square turbulent velocity fluctuation in the core flow of the tunnel where the flame was positioned was less than 0.4%. The boundary layer on the tunnel walls, floor, and roof had grown to 0.12-m at the location where the fuel is injected so that the core flow was 2.20-m wide and 0.98-m high.

Flames burning natural gas (95.2% CH_4, 2.1% C_2H_6, 1.7% N_2, 0.8% CO_2, 0.2% other) were established at the exit of 24.7-mm o.d. (22.1-mm i.d.) quartz tube that protruded 70-cm into the test section of the wind tunnel. The burner tube was constructed of quartz to

134

withstand direct flame impingement on its leeward side at low values of R, while its low coefficient of thermal expansion prevents it from deflecting due to uneven heating. The burner tube was mounted vertically (y-direction) and the crossflowing air blew horizontally (x-direction) across the tube. Mass flow controllers were used to control the flow rate of fuel to the burner tube. The characteristic exit velocity of the fuel, V_j, is the volume flow rate of fuel at ambient conditions divided by the inside area of the burner tube. For the data presented here, V_j was fixed at 1 m/s.

To provide insight into the origins of the stripped fuel, a fast flame ionization detector (FFID) probe was mounted on a three-dimensional traversing system in the wind tunnel. The detector was used to record "instantaneous" hydrocarbon concentrations above, below, and beside the flame at several different locations downstream of the burner tube. The FFID was capable of responding to changes in hydrocarbon concentration on the order of 1 millisecond with a minimum resolution of 4.1 ppm. To avoid aliasing effects, the signal from the FFID was sent through a low-pass Butterworth analog filter with a cut-off frequency of 1000 Hz before being sampled at 3600 Hz. At each measurement location, a series of 131072 (2^{17}) data points was collected over a 36.4-second period. Figure 5.4a shows a typical plot of the instantaneous hydrocarbon signal from a measurement location beneath the flame. Figure 5.4b shows an expanded view of the FFID output with individual data points noted with crosshairs (+) and illustrates the temporal resolution of the signal.

135
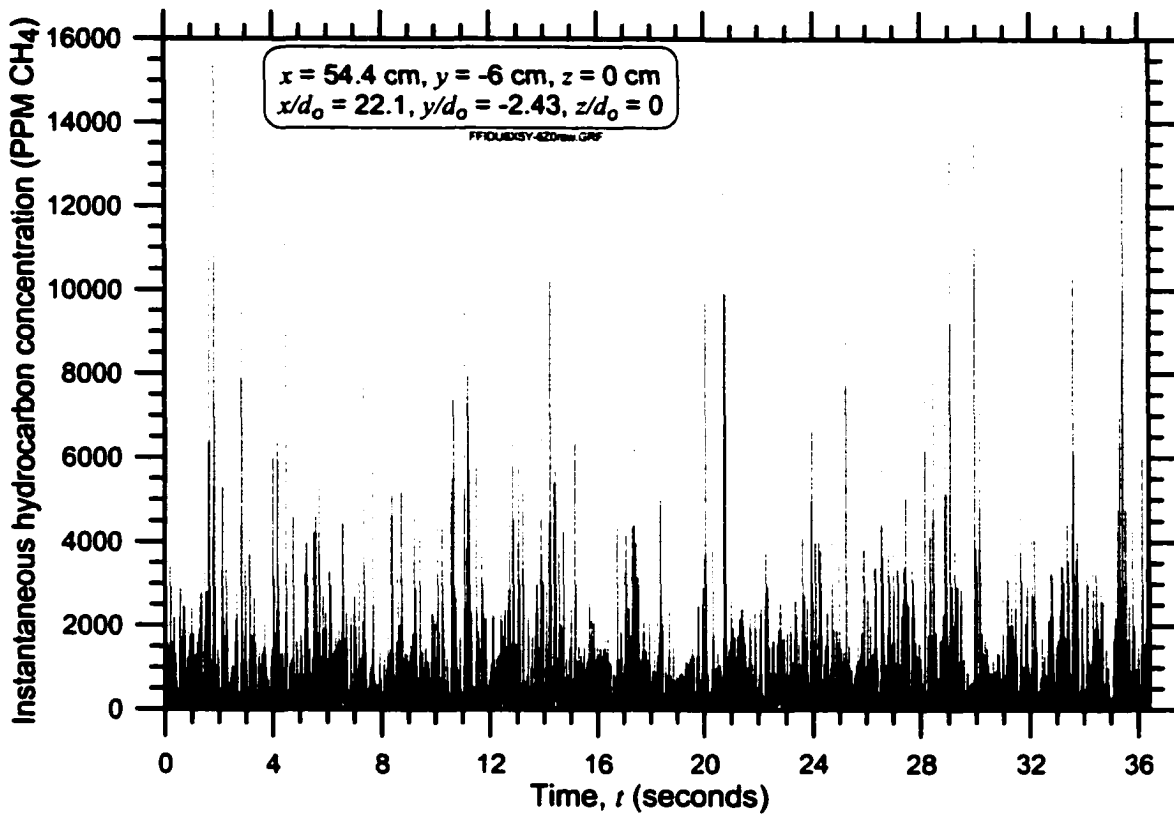
Figure 5.4a: Typical instantaneous hydrocarbon signal for a measurement location beneath the flame.
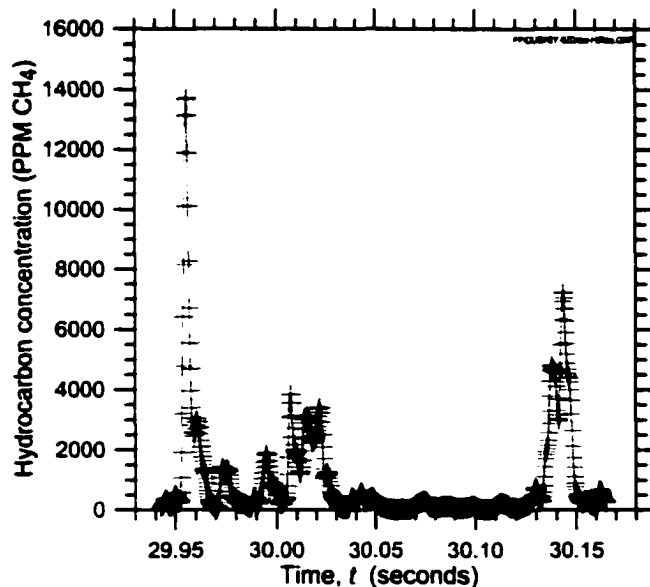
Figure 5.4b: Magnification of hydrocarbon signal from Fig. 3a. Crosshairs denote individual data points and illustrate the time resolution of the signal.

136

The raw signal shown in Figure 5.4 was processed in several steps. Since the combustion occurred in a closed-loop wind tunnel, it was necessary to account for any slight increases in background hydrocarbon concentrations during the sampling period. This was achieved by fitting background concentration data with a least-squares best-fit line that was then subtracted from the signal. In the data shown in Figure 5.4, the background concentration of HC rose from 47 to 51 ppm during the measurement so the effect of changing background concentration is negligible.

To isolate the peaks of hydrocarbon concentration in the FFID signal, a noise threshold was applied to the time series concentration data. Several ways of setting the cut-off threshold were investigated and a simple noise band criteria proved to be the most reliable. The noise band was determined by measuring the fluctuations in steady state background readings of the FFID probe. Depending on the gain setting of the FFID, these fluctuations were consistently within 3 to 5 digital counts on the 12-bit (4096 count) A/D board used to read the signals. A threshold of 3 times the background fluctuations was applied to the data during analysis to identify and isolate any bursts of emitted hydrocarbons. Although this choice was arbitrary, choosing higher or lower thresholds did not influence the data in any significant way. Once the threshold was applied to the data, occurrences of hydrocarbon peaks were determined by noting local maxima in the concentration signals. The probability density function of the time spacing between these peaks was determined by tracking the time periods between successive maxima.

137

5.4 RESULTS

FFID measurements were conducted on natural gas flames with $V_j = 1$ m/s at crossflow air speeds of $U_\infty = 6$ m/s and $U_\infty = 8$m/s. Figures 5.5 and 5.6 show the FFID measurement locations in the symmetry planes (i.e. $z = 0$) of the two flames. The outlines of the flames were traced from long-exposure (>10 s) photographs taken of the flames and represent a mean flame shape and position. The shaded regions within the outline were traced from instantaneous short-exposure images (~1/1000 s) of the flames and serve to highlight the differences between the mean flame and its instantaneous structure.

The series of plots on Figures 5.5 and 5.6 show the mean concentration profiles of hydrocarbons in the symmetry plane of the flow along the streamwise direction. For all of the profiles, the mean concentration is maximum at the underside of the mean flame and decreases as the probe is moved vertically downward in the negative y-direction. By contrast, on the upper side of the flame, the mean concentrations are essentially negligible. This strongly suggests that the unburned hydrocarbons being emitted are either originating on the underside of the flame or are being transported laterally from the top or sides of the fuel flow around the outside of the flame as indicated in Figure 5.2.

138

Figure 5.5: Mean concentration profiles of hydrocarbons in the symmetry plane of the flow above and below the flame at U_∞ = 6 m/s. Crosshairs around flame image denote specific measurement locations. Angled cross-hairs (×) indicate locations where significant numbers of hydrocarbon peaks were observed. Vertically aligned crosshairs (+) indicate locations where no peaks were observed.

Also interesting is the observation that for both the U_∞ = 6 m/s and U_∞ = 8 m/s flames, the mean concentration profiles in the near field of the stack ($x \leq 25$ cm) show negligible rise over the background concentration. Thus, fuel does not appear to be leaking from zone 1, the recirculating vortex region of the flame (see Figure 5.1), and hence unburned fuel is not escaping down the leeward side of the stack. Instead, the mean concentration profiles rise sharply near zone 2 of the flame suggesting that the source of unburned hydrocarbons is only available or the removal mechanism only activates as the flow moves past the recirculation region, zone 1. The data for U_∞ = 6 m/s shows that the

139

magnitudes of the mean profiles increase along the streamwise direction until the probe is moved past the end of the mean flame. The $U_\infty = 8$ m/s data shows a similar trend but the maximum mean concentration actually drops at $x = 55$ cm, which is upstream of the tip of the flame. Directly downstream of the visible flame tip, the mean profile data for $U_\infty = 6$ m/s show a second peak in the hydrocarbon profile. This peak may be indicative of some additional fuel leakage through the tip of the flame or it may simply have been caused by placing the probe too close to the reaction zone. This second peak is not apparent in the $U_\infty = 8$ m/s data, where the probe was placed slightly further downstream of the mean flame tip.
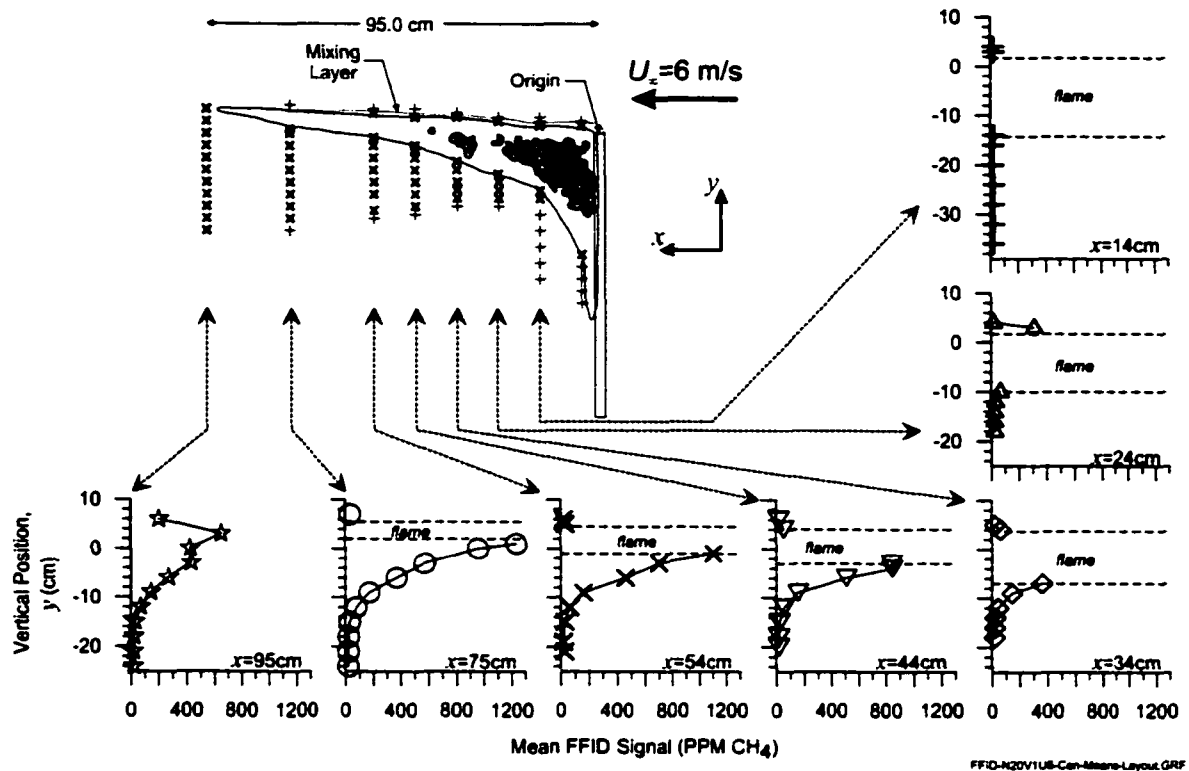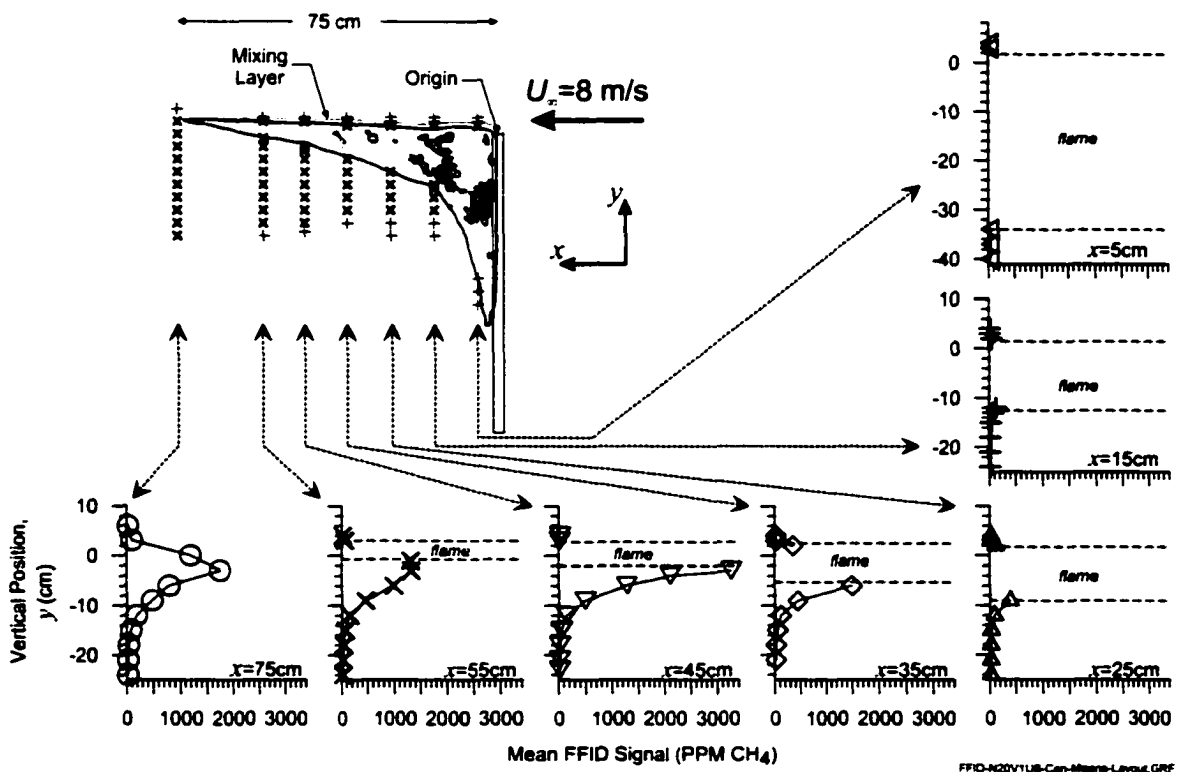

Figure 5.6: Mean concentration profiles of hydrocarbons in the symmetry plane of the flow above and below the flame at $U_\infty = 8$ m/s. Crosshairs are as in Figure 5.5.

140

To examine the possibility of lateral dispersion or circulation of unburned fuel around the flame, the cross-stream spread of the hydrocarbons beneath the flame was investigated. Figures 5.7 and 5.8 show profiles of the mean concentration below the flame in the z-direction at a fixed vertical location of $y = -6$ cm. The data show that, downstream of zone 2, the hydrocarbons are distributed over an approximately 8 cm span in the cross-stream direction. (In making these measurements, the probe traversing mechanism was observed to cause a small shift 2-cm) in the horizontal (z) position of the mean flame. The data shown in Figures 5.7 and 5.8 have been plotted with the origin aligned with the maximum concentration.) The profiles are essentially symmetric about a single peak and decrease sharply on either side of that peak. This evidence counters the possibility that fuel is being circulated around the sides of the flame. Moreover, additional measurements along the sides of the flame have verified the lateral dispersion of hydrocarbons is not happening. The shape of the mean concentration profiles under the mean flames is consistent with the observation that the unburned hydrocarbons originate within the mean flame and their concentrations decrease as the probe is moved farther from the mean flame surface.

141
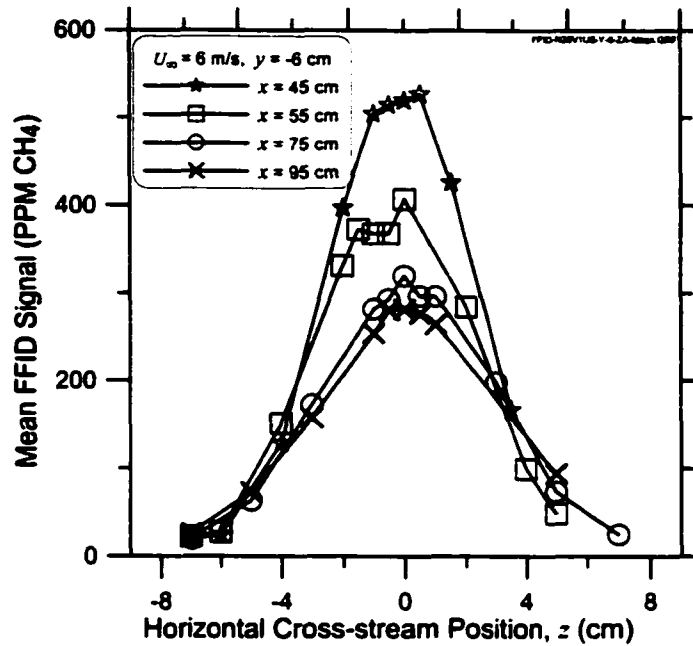
Figure 5.7: Mean hydrocarbon concentration profiles in the z-direction for various downstream locations along the $U_\infty = 6$ m/s flame. Concentrations are maximum beneath the flame.
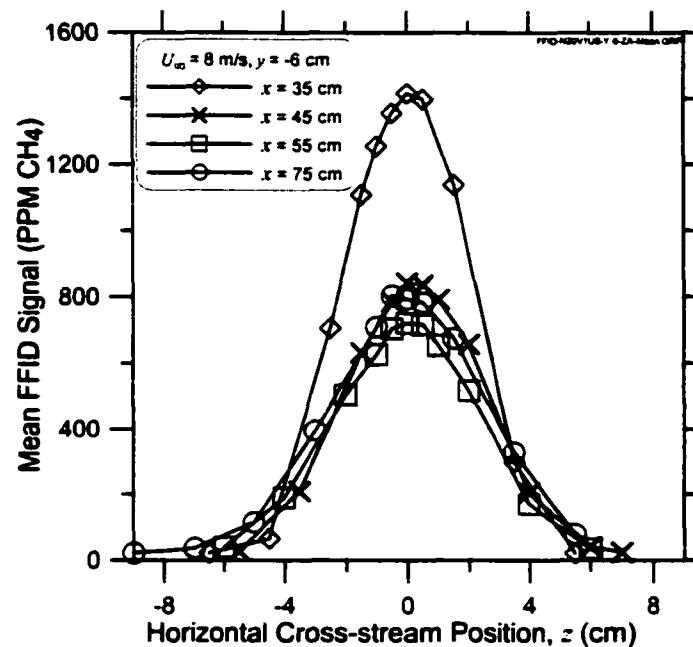
Figure 5.8: Mean hydrocarbon concentration profiles in the z-direction for various downstream locations along the $U_\infty = 8$ m/s flame. Concentrations are maximum beneath the flame.

142

While the mean concentration results in Figure 5.5 through 5.8 clearly indicate that the stripped hydrocarbons are being emitted from the underside of the flame downstream of zone 2, the instantaneous signals provide insight as to the probable removal mechanism. The instantaneous hydrocarbon signal shown in Figure 5.4 is typical of measurement locations beneath the flame and downstream of zone 2. The presence of sharp peaks in the data indicates that hydrocarbons are being ejected from the flame in a highly intermittent process. These measured "bursts" of hydrocarbons suggest that coherent flow structures containing unburned fuel are advecting past the FFID probe. The angled crosshairs (x) in Figures 5.5 and 5.6 indicate measurement locations where significant peaks of hydrocarbon signal were observed in the FFID signals. The vertically aligned crosshairs (+) indicate points where no significant peaks were observed. From the distribution of angled and vertically aligned crosshairs in Figures 5.5 and 5.6, it is apparent that unburned hydrocarbons exist over a much wider area beneath the flame than above the flame.

Above the flame, the transition between having very large peaks to no peaks in the FFID signal was apparent over distances as small as one centimetre. These show the location of a non-reacting mixing layer of unburned fuel and air just above the upper surface of the mean visible flame. Measurement points inside this layer showed bursts of hydrocarbon concentration as high as 80%, whereas points just 1 or 2 cm above showed no concentration peaks. With these extremely sharp gradients it might be expected that upward dispersion of unburned fuel could be taking place, but as verified by the mean concentration data this does not seem to be happening.

143

For measurement locations beneath the flame, the magnitude of the peaks was greatest for points directly below the flame and decreased slowly as the probe was moved downward in the negative y-direction. The region of measurable hydrocarbon peaks extends further downward as the flow moves downstream. This result is consistent with the mean concentration profile data and supports the idea that unburned fuel is being transported away from the flame. For measurement locations downstream of the flame tip, the hydrocarbon peaks were characteristic of points beneath the flame and were not associated with fuel leakage from the upper mixing layer.

5.5 DISCUSSION

Collectively, the presence of unburned hydrocarbons beneath the flame, their first appearance at zone 2, the intermittency of the hydrocarbon signals, and apparent vertical transport of hydrocarbons away from the flame, suggest that unburned fuel is being drawn out of the underside of the mean flame and is being transported in coherent flow structures. To further understand the flow mechanism that could be responsible for this path, it is worth considering the literature on non-reacting jets in crossflow since several similar flow characteristics appear to exist.

The present data show fuel in discrete structures beneath the flame. By analogy, several recent publications have identified jet fluid in discrete structures beneath the mean cold flow jet. Experiments on wall jets by Smith and Mungal [11] present sheet laser images

144

of high-momentum wall jets in crossflow ($R = 400$) which clearly show that jet fluid is contained in the wake vorticies shed from the jet. Similar observations were made by Kelso et al. [12] for experiments on wall jets in a water channel at $R = 16$. Eiff et al. [13] used temperature measurements on a slightly heated jet issuing from a stack at $R = 9$ and also demonstrated that fluid from the jet was shed in the wake vorticies. Eiff et al. [13], Eiff and Keffer [14], and Moussa et al. [15] have also demonstrated phase locking of wake vortices shed from the strong jet and those shed from the stack. For a combusting jet in crossflow, Hasselbrink and Mungal [4] present a mie scattering image of a piloted methane flame in crossflow ($R = 79.2$) seeded with alumina particles that showed particles deposited beneath the jet. Unfortunately, since alumina particles survive the combustion process, it is not possible to conclude whether they represent unburned fuel or combustion products beneath the flame.

The momentum flux ratio of the present experiments on wake-stabilized flames is significantly different from the high velocity jets quoted above ($R = 0.016$ and 0.010 compared to $R \approx 1$ to 625) and as such there are important differences in the flow field. The most notable difference is the presence of the standing vortex on the leeward side of the stack (zone 1), which is a dominant feature of the flow. Wake vortices shed from the jet itself are not expected to be present in this wake-stabilized regime. However, other basic structures such as the shear layer vortices on the upper surface of the jet [16, 9] (also referred to as ring-vortices to reflect their origins on the inside of the stack) and Kármán wake vortices shed from the stack [17] are expected to be present in both regimes. Thus, it is expected that the relevant flow structures in the wake-stabilized

145

flame would be the recirculating vortex on the lee-side of the stack (zone 1), the shear layer vortices in the mixing layer above the flame, and the wake vortices shed from the stack.

For the wake-stabilized flames presented here, the unburned hydrocarbons found beneath the flame appear in "bursts". To better understand the origins of the "bursts" and the mechanism of their creation, the measured hydrocarbon signals for points beneath the flame were considered in more detail. Initially it was thought that Fourier Transform analysis of the FFID time signal could reveal characteristic frequencies that governed this bursting process. Unfortunately, this was not the case. The frequency spectra for the instantaneous hydrocarbon signal showed that a large, essentially continuous range of frequencies were present in the hydrocarbon signals and no clear or consistent peaks were apparent in the data. However, by tracking the time between adjacent hydrocarbon peaks (peak spacing) in the time domain, some insight can be gained. Figure 5.9 shows a typical histogram of the peak spacings in the hydrocarbon signal for a measurement location beneath the flame. This shape of this distribution could be a result of several processes. Assuming the bursts of hydrocarbons are occurring randomly in space, they would pass by a fixed Eulerian probe with a Poisson distribution in time. Alternatively, if the fixed probe was failing to detect some of the hydrocarbon peaks (i.e. some of the bursts were not passing over the probe) the distribution would be biased in the manner shown in Figure 5.9.

146
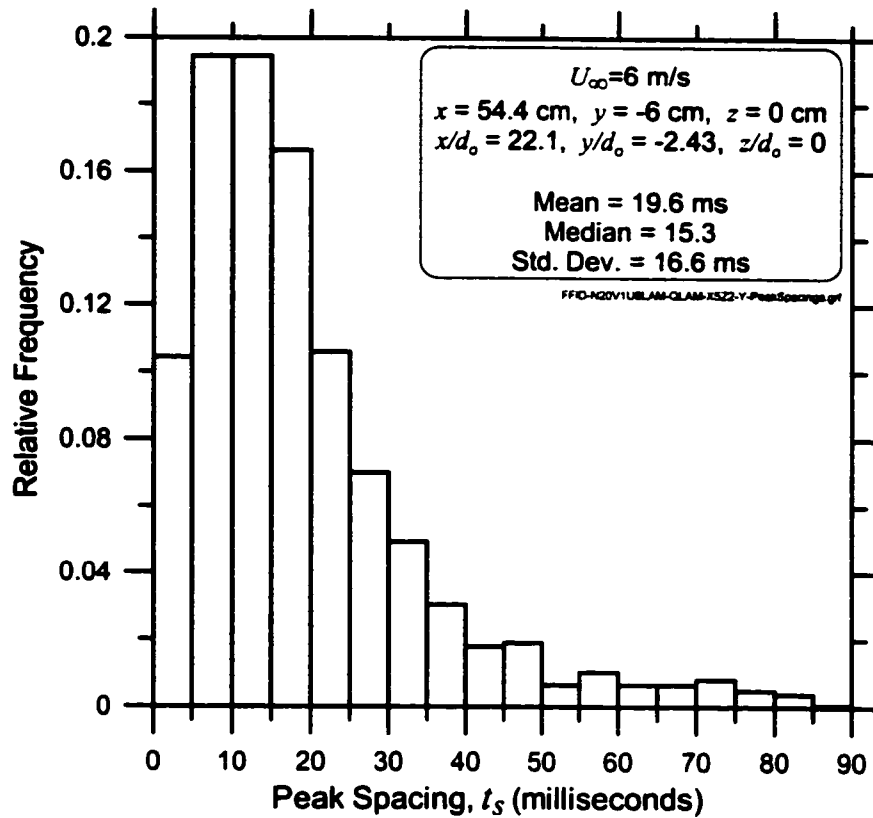
Figure 5.9: Typical histogram of the mean time between adjacent hydrocarbon peaks in the instantaneous hydrocarbon signal.

Using the mean peak spacing, $\overline{t_s}$, the outer diameter of the stack, d_o, and the free stream

crosswind velocity, U_∞, a mean Strouhal number ($\overline{St}$) for the hydrocarbon bursts can be

calculated as $\overline{St} = \dfrac{d_o}{U_\infty \overline{t_s}}$. Figure 5.10 shows profiles of Strouhal number for several

measurement locations beneath the $U_x = 6$ and 8 m/s flames. There is a consistent trend

in the plots that shows that the Strouhal number decreases as the probe is moved farther

beneath the flame. Assuming that the measured bursts of hydrocarbons represent

hydrocarbons bound up in coherent flow structures passing the probe, this trend is

consistent with the notion that farther beneath the flame these structures may be moving

147

over a wider cross-stream area and thus may cross the fixed probe less often. Since the mean concentration profiles suggest that the hydrocarbons originate along the centerline of the underside of the flame, the drop in Strouhal number could also reflect the limited penetration of the bursts of hydrocarbons into the region beneath the flame. As the probe is moved along the streamwise direction downstream of zone 2, the mean peak spacings are closer and the Strouhal number increases.
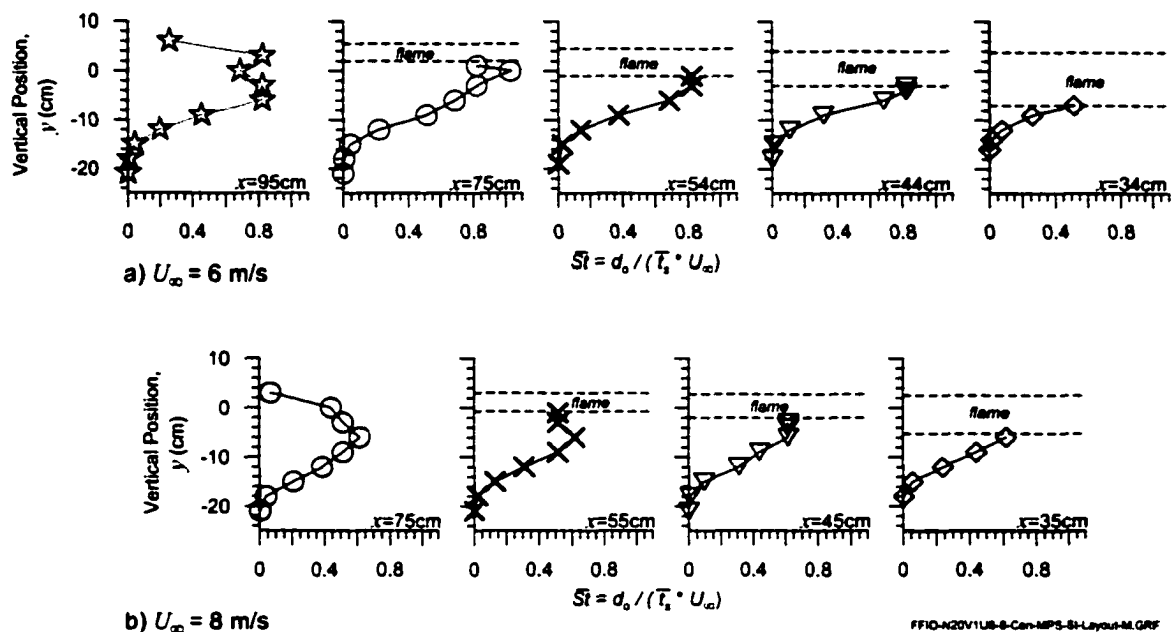
Figure 5.10: Mean Strouhal number profiles for hydrocarbon peaks beneath the flame at a) $U_\infty = 6$ m/s and b) $U_\infty = 8$ m/s.

Directly beneath the flame the Strouhal number was measured to be as high as 0.9. By comparison the Strouhal number for the shedding of wake vortices from a 24.7 mm cylinder in an 6 or 8 m/s crossflow is typically quoted as 0.2, which represents vortex shedding from one half of the Kármán vortex street [18]. However, the relevant

148

comparison Strouhal number value for wake vortices from a simple cylinder is 0.4 since a probe placed in the centerline of the cylinder wake would tend to sense vortices from both sides of the Kármán vortex street. The fact that the measured Strouhal number data directly beneath the flame are significantly higher than that of the comparable cold flow case is significant. This suggests that the observed bursts of hydrocarbons are likely not contained in wake vortices shed from the stack. This is an important difference from cold flow studies at high R where the wake vortices from the stack have been shown to be phase-linked to fluid being shed from the jet [13-15]. Moreover, the mean concentration profiles demonstrate that the hydrocarbon bursts are only present downstream of zone 2. Thus, if the unburned hydrocarbons are contained within wake vortices, the mean concentration profiles suggest that this fluid does not enter the vortices as they are shed from the stack through the recirculation zone.

It is also interesting to note that the peak Strouhal numbers for the $U_\infty = 6$ m/s case are slightly higher than those for the $U_\infty = 8$ m/s case. This suggests that there is some non-linearity of the fuel stripping with U_∞, which is apparent in the inefficiency curve of Figure 5.2.

In light of all the evidence, a fuel-stripping mechanism for wake-stabilized diffusion flames is proposed which is shown schematically in Figure 11. The three numbered images represent a time sequence of events to illustrate the evolution of an unburned fuel packet as it escapes combustion. The process begins as the mean recirculating vortex on the lee-side of the stack draws fluid from the fuel stream down into the junction region of

149

the mean flame. Discussions by Gollahalli and Nanjundappa [6] and images presented by Johnson and Kostiuk [9] identify this junction region (zone 2 in Figure 1) as an area of local extinctions of the flame, which causes the flame to burn in a series of detached pockets. These "instantaneous flame pockets" are illustrated schematically in Figure 11. While most of the fuel is drawn into the flame and ultimately burns either in the recirculation zone or the tail of the flame, sporadic fuel packets are instead drawn through the mean flame zone without reacting and emerge on the underside of the flame. The path of the fuel packet indicated on Figure 11 is just one of many such paths that could be drawn through the mean flame zone. Unburned fuel between the flame pockets emerges from the underside of the flame as shown in Figure 11 or further downstream as the buoyancy assisted trajectory of the mean flame rises away from the unburned fuel packets. With this concept in mind, leakage of unburned fuel directly out of the flame tip would be less important than the ejection unburned fuel beneath the flame, an observation which is verified by the experimental data presented here. The apparent structure of the unburned fuel bursts is most likely related to its origins in the ring vortices of the upper shear layer which are stretched and contorted as they are pulled by the mean recirculating vortex (shown in Figure 11) through the flame. Although wake vortices shed from the stack are expected to be present and influence the flow field, their importance is believed to be secondary with respect to the stripping of fuel in these flows.
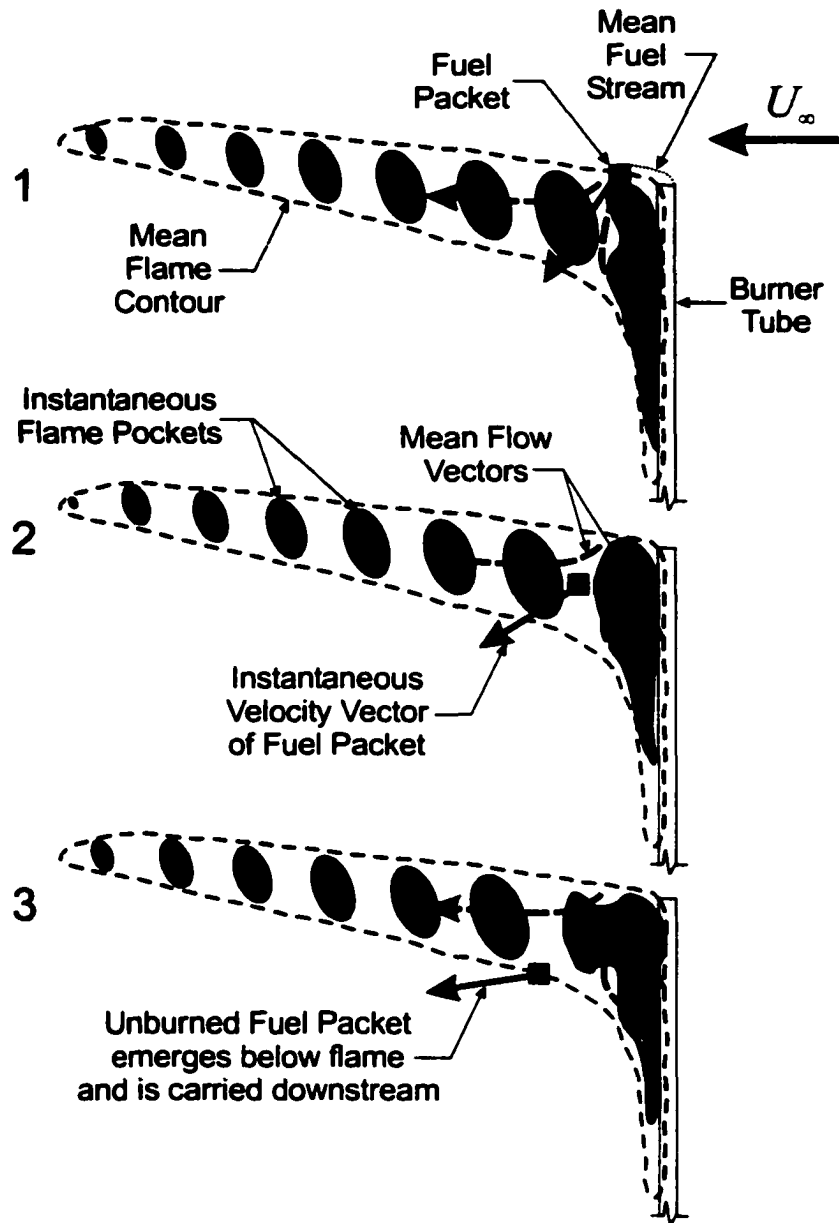
Figure 5.11: Schematic showing a time sequence of events that illustrate the proposed fuel stripping mechanism for wake-stabilized diffusion flames in crossflow.

151

5.6   CONCLUSIONS

Experiments were conducted to reveal the origins of measured inefficiencies in low-momentum jet diffusion flames in crossflow. The inefficiencies have been shown to consist primarily of unburned fuel and the measurements with a single point fast flame ionization detector show that these hydrocarbons are ejected from the flame in a highly intermittent and spatially variable process. Several potential paths for fuel leakage from the flame were systematically investigated. It was shown that bursts of unburned hydrocarbons appear on the underside of the flame and disperse somewhat as they move away from the flame. Although strong gradients in mean hydrocarbon concentration were observed in the mixing layer on the upper surface of the flame, measurements established that hydrocarbons were not being stripped from this region.

Significant bursts of hydrocarbons are only present beneath the flame downstream of the region in which local extinctions of the flame have been identified. It is proposed that the mean flow induced by the standing vortex that exists on the leeward side of the stack transports and stretches the ring vortices from the upper shear layer and ejects them on the underside of the flame creating the observed bursts of hydrocarbons that are stripped away from the jet without burning.

152

5.7 REFERENCES

1. Kalghatgi, G.T. (1981) "Blow-out stability of gaseous jet diffusion flames. Part 2: Effect of cross-wind", *Combustion Science and Technology*, 26, pp. 241-244.

2. Gollahalli, S.R., Brzustowski, T.A., and Sullivan, H.F. (1975) "Characteristics of a turbulent propane diffusion flame in a cross-wind", *Transactions of the Canadian Society for Mechanical Engineering*, Vol. 3, No.4, pp. 205-214.

3. Botros, P.E. and Brzustowski, T.A. (1978) "An experimental and theoretical study of the turbulent diffusion flame in cross-flow", *Seventeenth Symposium (International) on Combustion*, The Combustion Institute, Pittsburgh, pp. 389-398.

4. Hasselbrink, E.F. and Mungal, M.G. (1998) "Observations on the stabilization region of non-premixed methane transverse jet flames", *Twenty-Seventh Symposium (International) on Combustion*, The Combustion Institute, Pittsburgh, pp.1167-1173.

5. Huang, R.F. and Chang, J.M. (1994) "The stability and visualized flame and flow structures of a combusting jet in cross flow", *Combustion and Flame*, 98, pp. 267-278.

6. Gollahalli, S.R. and Nanjundappa, B. (1995) "Burner wake stabilized gas jet flames in cross-flow", *Combustion Science and Technology*, 109, pp. 327-346.

7. Huang, R.F. and Chang, J.M. (1994) "Coherent structure in a combusting jet in crossflow", *AIAA*, Vol. 32, No. 6, pp. 1120-1125.

8. Kostiuk, L.W., Majeski, A.J., Poudenx, P., Johnson, M.R., and Wilson, D.J. (2001) "Scaling of wake-stabilized jet diffusion flames in a transverse air stream", *accepted for publication at the Twenty-Eighth International Symposium on Combustion*, The Combustion Institute.

9. Johnson, M.R. and Kostiuk, L.W. (2000) "Efficiencies of low momentum jet diffusion flames in crosswinds", *Combustion and Flame*, 123, pp. 189-200.

10. Bourguignon, E., Johnson, M.R., and Kostiuk, L.W. (1999) "The use of a closed-loop wind tunnel for measuring the combustion efficiency of flames in a cross flow", *Combustion and Flame*, 119, pp. 319-334.

11. Smith, S.H. and Mungal, M.G., (1998) "Mixing, structure and scaling of the jet in crossflow", *Journal of Fluid Mechanics*, 357, pp. 83-122.

12. Kelso, R.M., Lim T.T., Perry, A.E. (1996) "An experimental study of round jets in a cross-flow", *Journal of Fluid Mechanics*, 306, pp. 111-144.

13. Eiff, O.S., Kawall, J.F., and Keffer, J.F. (1995) "Lock-in of vorticies in the wake of an elevated round turbulent jet in a crossflow", *Experiments in Fluids*, 19, pp. 203-213.

14. Eiff, O.S. and Keffer, J.F. (1997) "On the structures in the near-wake region of an elevated turbulent jet in a crossflow", *Journal of Fluid Mechanics*, 333, pp. 161-195.

15. Moussa, Z.M., Trischka, J.W. and Eskinazi, S. (1977) "The near field in the mixing of a round jet with a cross-stream", *Journal of Fluid Mechanics*, 80, pp. 49-80.

154

16. Huang, R.F. and Wang, S.M. (1999) "Characteristic flow modes of wake-stabilized jet flames in a transverse air stream", *Combustion and Flame*, 117, pp. 59-77.

17. Williamson, C.H.K. (1996) "Vortex dynamics in the cylinder wake", *Annual Review of Fluid Mechanics*, 28, pp. 477-539.

18. White, F.M. (1999) *"Fluid Mechanics"*, McGraw-Hill, 4th Ed., 826 pages.

CHAPTER 6

SUMMARY AND CONCLUSIONS

The discussions in Chapters 1 through 5 represent a detailed investigation of wake-stabilized diffusion flames in crosswind, which are fundamental to the applied problems of solution gas flaring. With over 1.4 billion m^3 of solution gas being flared and vented in Alberta annually and much more being flared worldwide, the relevance of this research is clear. Surprisingly, prior to the commencement of this work, very little scientific data had been published on the problems of flaring, particularly with reference to pollutant emissions. Of this limited amount of work, most researchers had studied high-momentum diffusion flames in little or no crosswind, a flow regime that is considerably different from the low-momentum, wake-stabilized flames that are discussed here. The background data in Chapter 1 outline the complexities of the practical problem flaring and highlight the need to represent and understand solution gas flaring as a general class of flows.

Open diffusion flames in a crosswind can be particularly difficult to study especially in the case of emissions measurement. The lack of a confined flow makes sampling difficult and problems with dilution can severely limit experimental accuracy. To overcome these problems, a new measurement technique was developed. Flames were established at the exit of a burner tube that was mounted vertically in the test section of a

156

closed-loop wind tunnel. The methodology relied on experimentally tracking the accumulation rates of the major carbon containing species in the products of combustion, which are contained within the closed-loop wind tunnel. In the case of flames that produce little or no soot, these major species are limited to CO_2, CO and hydrocarbons. Problems of leakage of material from the tunnel and reburning of combustion products within the tunnel were accounted for by extracting accumulation rate data from the start of the experiment where both of these terms were shown to be negligible. With this technique, combustion completion and the emissions of unburned fuel and carbon monoxide can be very accurately characterized by the measured carbon conversion efficiency.

The closed-loop wind tunnel methodology was used to conduct a large number of efficiency measurements under a variety of conditions. Natural gas, propane, ethane, and blends of these gases with N_2 and CO_2 were all used as fuels. The results show that for any given fuel, increased crosswind speed (U_∞) adversely affects the combustion efficiency, while increased jet exit velocity (V_j) makes the flame less susceptible to the effects of crosswind. Photographic images of the propane and natural gas flames show that at low momentum flux ratios, R, the flame can be described in terms of three distinct zones. Zone 1 is the planar recirculating vortex that exists on the leeward side of the burner tube and acts as a stabilizing anchor for the flame. Zone 3 is the long, approximately axisymmetric main tail of the flame. Zone 2 is the highly strained junction region of Zones 1 and 3.

157

Although photographic images showed qualitatively that the occurrence of a maximum mean flame length and the onset of downwash were related to R, other features of the flame, like the flame burning in detached pockets and the disappearance of the flame tail, did not coincide at fixed values of R for different fuels. These results suggested that R alone is not sufficient to account for the visual differences between the propane and natural gas flames. Consideration of buoyancy and momentum forces as defined by a Richardson Number successfully predicted the velocity dependency of the combustion inefficiency as being $U_\infty / V_j^{1/3}$ and correlated data for each of the fuels. Although the density term in the model failed to explain the differences in the natural gas and propane inefficiency curves, this approach was successful in predicting effects of varied burner tube diameter on the propane flames. Measurements showed that the inefficiency of undiluted propane flames emanating from various diameter burners scaled with the non-dimensional parameter $\dfrac{U_\infty}{\left(g V_j d_o\right)^{1/3}}$. Unfortunately, the data for the natural gas curves were only partially correlated by $d_o^{1/3}$ and were better correlated with $d_o^{1/2}$. In a practical sense this difference of $d_o^{1/6}$ is nominal, but nevertheless it is indicative of the complexity of the flow. The ultimate failure of this Richardson number approach demonstrated that other parameters are important to the mechanism responsible for the measured inefficiencies and pointed to the need for a broader understanding of the mechanism responsible for the measured inefficiencies.

Experiments to evaluate the importance of other parameters on the conversion efficiency of wake-stabilized flames included an evaluation of the effects of fuel composition and

158

ambient turbulence in the crossflow. While adding turbulence to the crosswind was found to have a comparatively minor effect on efficiency, the effect increasing the amount of inert diluent in the fuel was profound. By adding either CO_2 or N_2 to the methane or propane fuel stream, the energy density of the fuel was reduced and the flames became much more susceptible to the effects of increased crosswind leading to increased inefficiencies. With high levels of CO_2 or N_2 in the fuel stream, the stability of the flames was affected and the inefficiencies could surpass 20 % at even modest crosswind speeds. The implications of these results for industry have not gone unnoticed and have lead to an increase in the required minimum heating value of fuel that may be burned in a flare in Alberta from 9 MJ/m^3 to 20 MJ/m^3.

Although the effects of adding inert diluents to the fuel are not fully understood, some success was achieved in empirically correlating the data using the lower heating value of the fuel calculated on a mass basis. With this approach, data from propane based and ethane based fuel mixtures were effectively collapsed onto a single curve. Data from natural gas / CO_2 and natural gas / N_2 curves were also collapsed by the same parameters but followed a different curve than the propane and ethane based data. At this point the reasons for this difference are not understood and they may imply that the inefficiency mechanism(s) for natural gas are somewhat different than that of ethane and propane or simply that the empirical correlation is incomplete. Despite these shortcomings, with this new empirical model it is now possible to make predictions about the performance of flares in the field. However, any attempts to apply these results to engineering problems must be done with necessary caution indicative of the empirical nature of the correlations.

159

The results of all of these experiments pointed to the need for a broader understanding of the mechanism(s) responsible for the measured conversion inefficiencies in wake-stabilized diffusion flames. Analysis of the combustion products has shown that the inefficiencies are primarily in the form of unburned hydrocarbons along with some carbon monoxide and not pyrolitic compounds. A gas chromatograph analysis of the hydrocarbons in the combustion products of natural gas and propane flames has shown that the hydrocarbons have essentially the same compositional make-up as the fuel. Combined with the photographic data which show the link between flame burning in detached pockets and the measured inefficiencies, these results suggested that the observed inefficiencies could be a result of "fuel stripping" from the fuel jet before any combustion

A series of experiments were conducted to investigate the importance of fuel stripping in the flow and to determine the mechanism responsible for the measured inefficiencies. Measurements with a single point fast flame ionization detector showed that when the flame was burning in an inefficient mode, unburned hydrocarbons were ejected from the flame in a highly intermittent and spatially variable process. Several potential paths for fuel leakage from the flame were systematically investigated. It was shown that bursts of unburned hydrocarbons appeared on the underside of the flame and dispersed somewhat as they moved away from the flame. Although strong gradients in mean hydrocarbon concentration were observed in the mixing layer on the upper surface of the flame, measurements established that hydrocarbons were not being stripped from this region.

Significant bursts of hydrocarbons were only present beneath the flame downstream of Zone 2, the region in which local extinctions of the flame have been identified. Based on the experimental data, it was proposed that the recirculating vortex in Zone 1 draws fluid from the non-reacting mixing layer down through Zone 2. The local extinctions in this region allow this fuel to pass through the mean flame zone without reacting. The mean flow induced by the standing vortex transports and stretches the ring vortices from the upper shear layer and ejects them on the underside of the flame creating the observed stochastic or random bursts of hydrocarbons beneath the flame. Although wake vortices shed from the stack are expected to be present and influence the flow-field, their importance is believed to be secondary with respect to the stripping of fuel in these flows. It is proposed that this fuel-stripping mechanism is responsible for creating the measured carbon conversion inefficiencies in these flows.

6.1 FUTURE WORK

With the identification and discovery of this fuel-stripping mechanism, several opportunities for extending this research arise. Full field laser sheet imaging techniques are currently being used to further clarify the details of the mechanism and to elucidate what parameters are important in allowing this fuel-stripping to take place. It is speculated that momentum effects may be important in determining whether fuel is trapped within the rotating flow structures or whether the fuel may escape these structures to mix with air and react. An extensive series of ongoing efficiency

161

measurements with constant mass density fuel mixtures of Ethane / Nitrogen and Propane / CO_2 will help clarify this hypothesis by attempting to isolate the effects of changing the energy density of the fuel.

Preliminary experiments presented here have shown a measurable effect on the measured efficiency with the addition of ambient turbulence to the crossflow air. Further tests suggest that the scale of the turbulence might be a key factor in setting the mechanism that strips fuel from the flame. With a better understanding of the mechanism causing the measured inefficiencies, opportunities also arise for developing methods to suppress the fuel-stripping as a means to improving flare performance. Considering the practical problem of flaring, it will also be important to test the limits of the current research by investigating other aspects of the flaring problem such as the inclusion of entrained liquids in the fuel stream and the production of soot and other undesirable compounds in the combustion products.

From a fundamental research perspective, the data presented here represent a very small part of the exciting new opportunities for more general investigations of combusting jets in crossflow. Links between the internal structure of the flames themselves and their stability and emissions are emerging as important areas of fundamental research. These problems present significant scientific challenges since aerodynamics, turbulence, heat transfer, and chemistry are all important in creating these complex flows.

APPENDIX A

IMPLEMENTATION AND EXTENSIONS TO THE METHODOLOGY FOR MEASURING CONVERSION EFFICIENCY

The methodology for measuring efficiency presented in Chapter 2 was developed with the assumption that at the start of an experiment when the flame is ignited, effects of leakage from the tunnel and reburning of products within the tunnel are negligible. While this is certainly true, there are some important nuances in the successful implementation of this methodology that must be considered. In order to measure the accumulation rates of the major carbon containing species at the start of a test, the slopes of the concentration curves need to be calculated. However, since there is a mixing transient at the start of each experiment, concentration data shortly after the flame is ignited can not be used for this calculation. Instead, data from later in the experiment when the mixing transient has died off must be used. This was not a problem for the data from methane flames shown in Chapter 2 where the concentration versus time curves during the experiment were almost perfectly linear. In this case, the rates of accumulation of each of the major carbon containing species remained constant throughout the experiment and the choice of what segment of data to use in the calculations of efficiency became irrelevant. However, in practice this is not always the case.

163

In some experiments, especially in the case of very large propane flames or for experiments at very high wind velocities, the effects of being in a closed-loop wind tunnel can become apparent. In these cases, the concentration data may have some slight non-linearity. Figure A.1 shows plots of CO_2, CO, and hydrocarbon concentrations divided by temperature during a test in which these slight non-linearities are present. (The curvature is most apparent in the CO_2 and hydrocarbon plots.) To provide the best possible experimental accuracy, this non-linearity is accounted for mathematically. This can be accomplished by fitting data from later in the experiment with a curve and projecting that curve back to the start of the experiment where the slope can be calculated at a time where assumptions of negligible leakage and reburning effects are proven to be valid. However, it is important to use an appropriate functional form for the curve fit used to project the data back to the start of the experiment.

Figure A.2 is a simple control volume diagram of the closed-loop wind tunnel. Arrows on the diagram indicate leakage of species i into and out of the tunnel (infiltration and exfiltration) as well as the emission of species i from the flare. During an experiment, the mole fraction of species i (Y_i) in the tunnel, the temperature in the tunnel (T), and the density of species i in the tunnel (ρ_i) will vary with time. Effects of reburning are not included in the diagram because the assumption of low hydrocarbon concentrations near the start of the experiment is still valid as shown in Chapter 2.
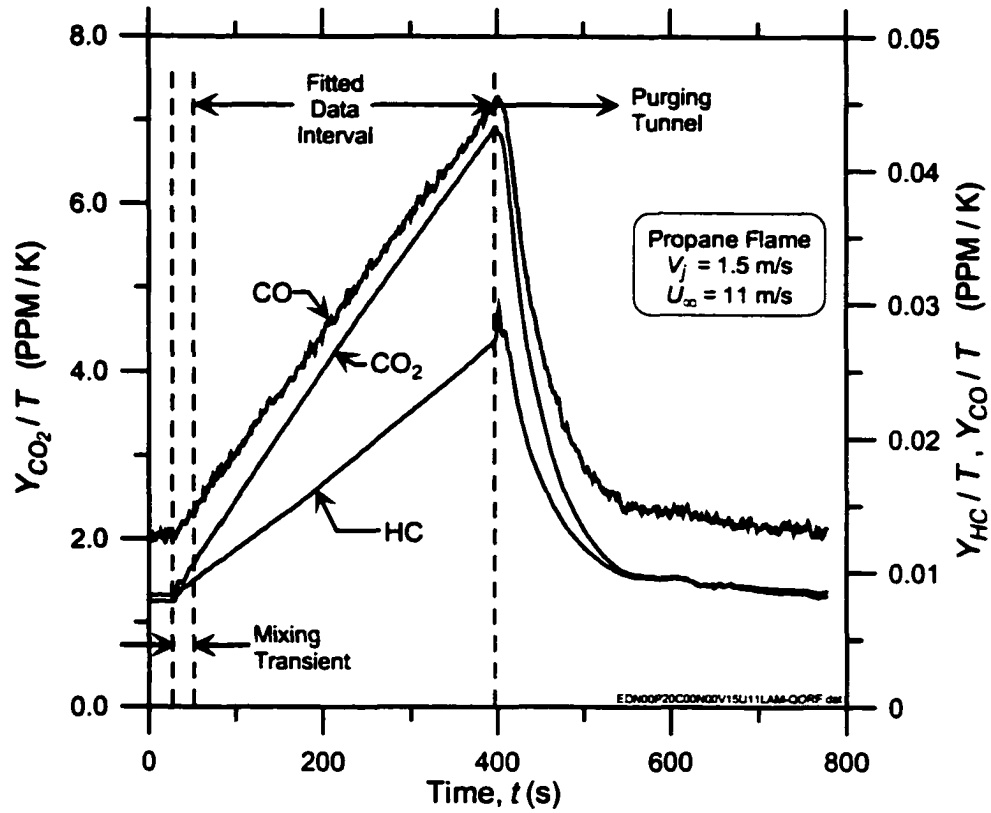
Figure A.1: Concentration versus time curves for major carbon containing species during an efficiency experiment. Slight curvature in plots can be seen during fitted data interval.
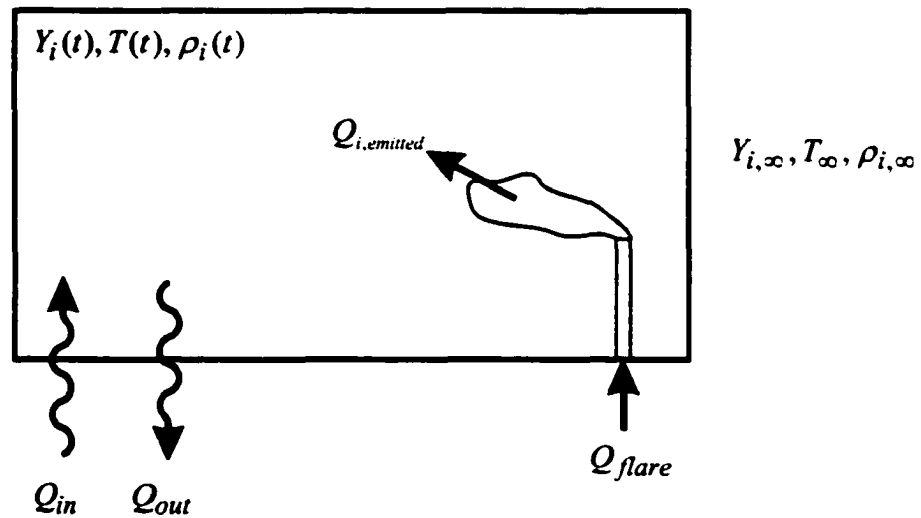
Figure A.2: Simple control volume diagram of the wind tunnel.

165

From this diagram, a mass balance can be constructed as shown in Equation A.1:

$$\frac{d}{dt}(\rho_i Y_i V) = \rho_{i,\infty} Y_{i,\infty} Q_{in} - \rho_i Y_i Q_{out} + \rho_\infty Q_{i,emitted}$$
(A.1)

where Y_i = mole fraction of species i in the tunnel

$Y_{i,\infty}$ = mole fraction of species i in the ambient air

ρ_i = density of species i in the tunnel

ρ_i = density of species i in ambient air

Q_{in} = volume flow rate of ambient air leaking into the tunnel

Q_{out} = volume flow rate of air leaking out of the tunnel

$Q_{i,emitted}$ = mass flow rate of species i emitted by the flare

$Q_{CO_2,inert}$ = volume flow rate of CO_2 into tunnel as part of flare gas

V = internal volume of the windtunnel

Using the ideal gas law, equation A1 can be re-written as follows:

$$V\frac{d}{dt}\left(\frac{Y_i}{T}\right) = \frac{Y_{i,\infty}}{T_\infty}Q_{in} - \frac{Y_i}{T}Q_{out} + \frac{Q_{i,emitted}}{T_\infty}$$

Finally, substituting $X = \frac{Y_i}{T}$ and letting A, B, and C represent arbitrary constants yields:

$$\frac{dX}{dt} = A - BX + CQ_{i,emitted}$$
(A.2)

By solving Equation A.2, the appropriate general form of the equation for the concentration rise in the tunnel during an experiment can be derived. However, the term $Q_{i,emitted}$ has an unknown time dependency. Ideally, $Q_{i,emitted}$ would remain constant throughout the experiment. This would indicate that the effects of changes in the ambient

166

air in the tunnel (e.g. changes in temperature and oxygen concentration) would be negligible. If this was true, and if the effects of leakage from the tunnel were also negligible, then the entire right side of Equation A.2 would remain constant and the mole fraction / temperature (X) curves would rise linearly in time. This was the case with the data from the methane experiments shown in Chapter 2 where the concentration curves were linear for several minutes after the ignition of the flame.

If the effects of leakage from the tunnel are not negligible, but $Q_{i,emitted}$ is still assumed to remain constant, then Equation A.2 must be solved by integration to yield a solution of the form:

$$X = D + Ee^{Ft} \tag{A.3}$$

where D, E, and F are arbitrary constants. This situation might occur during experiments at very high wind velocities where the infiltration and exfiltration from the tunnel would be more apparent.

For very large flames, it is possible that $Q_{i,emitted}$ might vary during the experiment. This might occur at what would be regarded as the limits of the facility, where effects of changes in the air composition in the tunnel start to become relevant. The complexity of the problem precludes predicting the time dependency $Q_{i,emitted}$ in this situation. As a first order approximation, it could be assumed that $Q_{i,emitted}$ would vary linearly with time. This again would be a valid assumption near the beginning of an experiment. With this first order approximation, Equation A.2 can be re-written as:

167

$$\frac{dX}{dt} = A - BX + Ct \tag{A.4}$$

where A, B, and C are arbitrary constants.

By writing Equation A.4 in standard form, it is recognizable as a first order, linear ordinary differential equation that can be solved analytically with the use of the integrating factor $e^{\int Bdt}$ as follows:

$$\frac{dX}{dt} + BX = A + Ct \tag{A.5}$$

$$e^{\int Bdt}\left(\frac{dX}{dt} + BX\right) = e^{\int Bdt}(A + Ct) \tag{A.6}$$

$$\frac{d}{dt}\left(Xe^{Bt}\right) = e^{Bt}(A + Ct) \tag{A.7}$$

$$Xe^{Bt} = A\int e^{Bt}dt + C\int te^{Bt}dt \tag{A.8}$$

$$Xe^{Bt} = \frac{A}{B}e^{Bt} + \frac{1}{B^2}(Bt - 1)e^{Bt} + C \tag{A.9}$$

168

$$X = \frac{A}{B} + \frac{1}{B^2}(Bt - 1) + Ce^{-Bt} \qquad\qquad (A.10)$$

Finally, collecting all of the constants in Equation A.10 together and redefining A, B, C, and D as new arbitrary constants yields a general solution in the form of:

$$X = A + Bt + Ce^{Dt} \qquad\qquad (A.11)$$

This equation can then be fit to the experimental concentration data to accurately capture any slight curvature that might be present in some experiments as a result of leakage and changing air composition. The results presented in Chapters 3 through 5 used this procedure to accurately measure the accumulation rates of the major carbon containing species at the start of an experiment.

IMPLEMENTATION

With this extension to the methodology in place, the choice of when to start using data after the mixing transient is no longer critical. Nevertheless, an analytical procedure was developed both to aid in making this decision and to speed data collection. This procedure was programmed into the data acquisition computer using LabVIEW software.

At the start of an experiment, before the flame is lit, the concentrations of the major carbon containing species exist at their background levels. The data acquisition system

tracks these species as well as 28 other parameters on a continual basis with a sampling rate of 1 Hz. After the flame is ignited, combustion products are aggressively mixed into the wind tunnel air with 6 large mixing fans and the accumulation process begins. The data acquisition program focuses on the CO_2 concentration and records the time at which the signal first begins to rise. This time becomes t_o, the start time of the experiment at which the accumulation slopes of all of the major species are evaluated to calculate the conversion efficiency.

With the experiment underway, the computer program continues to follow the CO_2 concentration / temperature curve (X_{CO_2}) to determine when the initial mixing transient has finished. This is accomplished by having the computer fit successive 100 second data intervals (or windows) starting from t_o. For each 100 second window, the computer applies a linear regression routine and evaluates the uncertainty of the linear fit. Curvature of the data is not a problem during this stage of the test so the linear fit is an effective tool. If the uncertainty of the fit does not fall below a given threshold, then the computer waits while more data is collected and repeats this process at successive, partially overlapping time intervals until the mixing transient is found to be finished. An appropriate linear fit threshold of 0.1 % was determined by evaluating several data sets by hand until a repeatable threshold value was found. While it is recognized that this was a somewhat arbitrary decision, since the final calculation uses the advanced curve fit routine developed above, the decision of when to start using data in the efficiency calculation is not critical.

170

Once the computer has determined that the mixing transient has completed, the program then starts the process of calculating the carbon conversion efficiency. The computer begins by fitting the combined linear-exponential function developed above ($X = A + Bt + Ce^{Dt}$) to the CO_2, CO and HC curves over the 100 second data window for which the mixing transient was declared to be complete. The fit is performed using a Levenberg-Marquardt fit routine. Initial guess coefficients are derived from a second order polynomial fit to the same data. The three curves are then differentiated and the projected back to t_o where the accumulation rates of each species are evaluated. These slopes are used to calculate the initial value of the efficiency (Equation 2.17). This process is then repeated over successively longer time intervals as more data is collected during the experiment. With every 15 seconds of new data, the fit routines and efficiency calculation are repeated. The change in successive calculations of the efficiency are tracked until convergence is achieved. Typically, the efficiency converges to within 0.025 % after no more than 300 seconds. Convergence would take less time except for the fact that the signal from the CO analyzer used in these experiments was very noisy. This very tight tolerance on the efficiency convergence is an indicator of the accuracy of this methodology.

171